

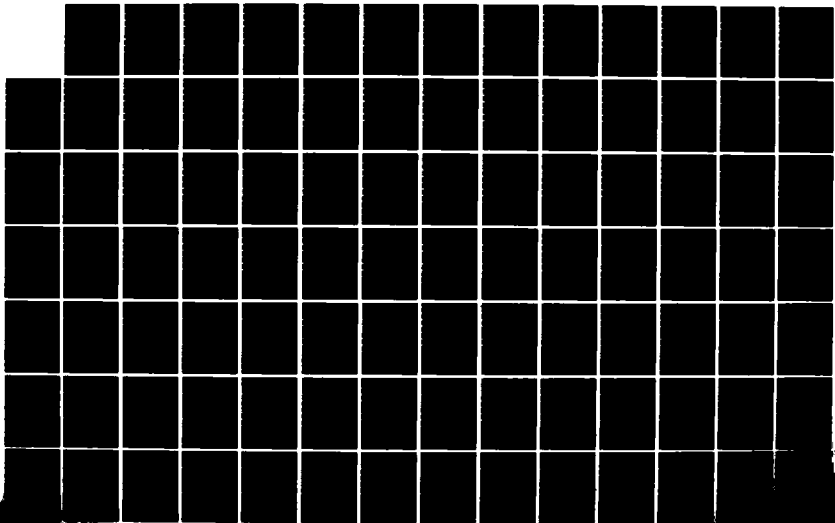
AD-A141 174

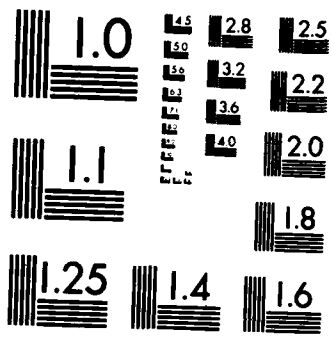
THE DETERMINATION OF THE BODNER MATERIAL COEFFICIENTS  
FOR INDIUM 718 AND (U) AIR FORCE INST OF TECH  
WRIGHT-PATTERSON AFB OH SCHOOL OF ENGI... R L BERMAN  
MAR 84 AFIT/GAE/AA/84M-1 F/G 11/6

1/2

UNCLASSIFIED

NL





MICROCOPY RESOLUTION TEST CHART  
NATIONAL BUREAU OF STANDARDS-1963-A

AFIT/GAE/AA/84M-1



AD-A141 174

THE DETERMINATION OF THE BODNER MATERIAL  
COEFFICIENTS FOR IN 718 AND THEIR EFFECTS  
ON CYCLIC LOADING

THESIS

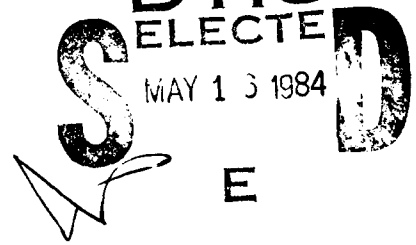
Rebecca L. Beaman  
First Lieutenant, USAF

AFIT/GAE/AA/84M-1

DTIC FILE COPY

DTIC  
ELECTE

MAY 13 1984



UNCLASSIFIED

Approved for public release: IAW AFR 190-17.

LYNN E. WOLLAVER

Dean for Research and Professional Development

Air Force Institute of Technology (AFIT)

Wright-Patterson AFB OH 45433

84 05 14 116

AFIT/GAE/AA/84M-1

THE DETERMINATION OF THE BODNER MATERIAL COEFFICIENTS FOR  
IN 718 AND THEIR EFFECTS ON CYCLIC LOADING

THESIS

Presented to the Faculty of the School of Engineering  
of the Air Force Institute of Technology  
Air University  
In Partial Fulfillment of the  
Requirements for the Degree of  
Master of Science

Rebecca L. Beaman

First Lieutenant, USAF

Graduate Aerospace Engineering

March 1984

UNCLASSIFIED

Approved for public release: IAW AFR 190-17.

Lynn E. WOLAVER  
Dean for Research and Professional Development  
Air Force Institute of Technology (AFIT)  
Wright-Patterson AFB OH 45433

Accession For	
NTIS/GA&I	*
FBI	
Department of Justice	
Library	
Requester/	
Availability Codes	
and/or	
Special	
A-1	



84 05 14 110

### Acknowledgements

I wish to express my gratitude to Dr. A. N. Palazotto for his guidance and support throughout the course of this work. Thanks also to Dr. T. Nicholas, of the Air Force Wright Aeronautical Laboratories (Materials Laboratory) for not only his technical assistance but also his patience and quiet good humor. I also wish to thank A. M. Rajendran of the University of Dayton Research Institute for the computer programs he provided in support of this study. Without the help of these individuals this work would never have been completed.

Table of Contents

	Page
Acknowledgements . . . . .	ii
List of Figures . . . . .	iv
List of Tables . . . . .	vii
List of Symbols . . . . .	viii
Abstract . . . . .	x
I. Introduction . . . . .	1
II. Theory . . . . .	5
General Theory . . . . .	5
Applications for Evaluating Coefficients . . . . .	11
III. Applications to IN 718 . . . . .	26
IV. Load Cycling Effects Using the Bodner Coefficients As Evaluated . . . . .	56
V. Conclusions . . . . .	72
Appendix A: Discussion of the Coefficients . . . . .	74
The Coefficient D . . . . .	74
The Coefficients $n$ and $Z_1$ . . . . .	74
The Coefficients $m$ and $Z_0$ . . . . .	77
The Coefficient A . . . . .	83
The Coefficient $Z_2$ . . . . .	87
The Coefficient $r$ . . . . .	93
Appendix B: Determination of $n$ and $Z_1$ . . . . .	97
Appendix C: Determination of $m$ and $Z_0$ . . . . .	103
Appendix D: Computer Programs . . . . .	117
Bibliography . . . . .	129
Vita . . . . .	132

List of Figures

Figure		Page
1	Variation of $n$ and $Z_1$ . . . . .	15
2	Variation of $m$ . . . . .	16
3	Variation of $Z_0$ . . . . .	17
4	Variation of $m$ and $Z_0$ . . . . .	18
5	Strain Rate Versus Stress Curve: A Guide to the Information . . . . .	22
6	Variation of $A/D_0$ . . . . .	23
7	Variation of $r$ . . . . .	24
8	Variation of $Z_2$ . . . . .	25
9	Experimental Data Base; IN 718, 1200°F . . . . .	28
10	Determination of $n$ and $Z_1$ . . . . .	29
11	Experimental Stress-Strain Curve . . . . .	32
12	Stress Versus Plastic Strain, IN 718, 1200°F, $\dot{\epsilon} = 1.3 \times 10^{-5} \text{ sec}^{-1}$ . . . . .	33
13	Determination of $m$ and $Z_0$ , $n = 2.5$ . . . . .	34
14	Determination of $m$ and $Z_0$ , $n = 3.0$ . . . . .	35
15	Determination of $m$ and $Z_0$ , $n = 3.125$ . . . . .	36
16	Determination of $m$ and $Z_0$ , $n = 3.211$ . . . . .	37
17	Fit of Bodner Model to High Strain Rate Data, $n = 2.5$ . . . . .	39
18	Fit of Bodner Model to High Strain Rate Data, $n = 3.0$ . . . . .	40
19	Fit of Bodner Model to High Strain Rate Data, $n = 3.125$ . . . . .	41
20	Fit of Bodner Model to High Strain Rate Data, $n = 3.211$ . . . . .	42

Figure		Page
21	Determination of $m$ and $Z_0$ : Fit of Model to Stress Strain Data . . . . .	44
22	Creep Curves: Comparison of Bodner Model With Data . . . . .	46
23	Creep Curves: Comparison of Bodner Model With Data . . . . .	47
24	Parametric Study Used to Evaluate A . . . . .	50
25	Parametric Study Used to Evaluate $Z_2$ . . . . .	51
26	Parametric Study Used to Evaluate $r$ . . . . .	52
27	Fit of the Bodner Model to Data, All Coefficients Evaluated . . . . .	54
28	Procedure for Evaluating Coefficients . . . . .	55
29	Experimental Cyclic Loading Data, IN 718, 1200°F (Strain Control, $\pm .8\%$ ) . . . . .	57
30	Experimental Cyclic Loading Data, IN 718, 1200°F (Stress Control, $\pm 120$ KSI) . . . . .	58
31	Bodner Model Prediction of Cyclic Loading Behavior: Strain Control, $q = 1$ . . . . .	60
32	Bodner Model Prediction of Cyclic Loading Behavior: Strain Control, $q = 0$ . . . . .	61
33	Behavior of $Z^t$ and $Z^c$ During Application of a Cyclic Load . . . . .	63
34	Bodner Model Prediction of Cyclic Loading Behavior: Strain Control, $q = -.05$ . . . . .	65
35	Bodner Model Prediction of Cyclic Loading Behavior: Strain Control, $q = -.1$ . . . . .	66
36	Bodner Model Prediction of Cyclic Loading Behavior: Stress Control, $q = 1$ . . . . .	67
37	Bodner Model Prediction of Cyclic Loading Behavior: Stress Control, $q = 0$ . . . . .	68
38	Bodner Model Prediction of Cyclic Loading Behavior: Stress Control, $q = -.05$ . . . . .	69



Figure		Page
39	Bodner Model Prediction of Cyclic Loading Behavior: Stress Control, $q = -.1$ . . . . .	70
40	Variation of $n$ , All Other Coefficients Constant . . . . .	76
41	Variation of $n$ . . . . .	78
42	Variation of $n$ . . . . .	79
43	Variation of $m$ Times $Z_1$ , All Other Coefficients Constant . . . . .	81
44	Variation of $m$ , All Other Coefficients Constant . . . . .	82
45	Variation of $m-Z_0$ Pairs, As Indicated by Figure 14 . . . . .	84
46	Variation of $Z_0$ , All Other Coefficients Constant . . . . .	85
47	Variation of $A/D_0$ , All Other Coefficients Constant . . . . .	86
48	Variation of $A$ at a High Strain Rate . . . . .	88
49	Variation of $A$ at a Low Strain Rate . . . . .	89
50	Variation of $Z_2/Z_1$ . . . . .	90
51	Variation of $Z_2$ at a High Strain Rate . . . . .	91
52	Variation of $Z_2$ at a Low Strain Rate . . . . .	92
53	Variation of $r$ . . . . .	94
54	Variation of $r$ at a High Strain Rate . . . . .	95
55	Variation of $r$ at a Low Strain Rate . . . . .	96
56	Experimental Data Base; IN 718, 1200°F . . . . .	99
57	Determination of $n$ and $Z_1$ . . . . .	100
58	Experimental Stress Strain Curve; IN 718, 1200°F . . . . .	104

List of Tables

Table		Page
I	Nominal Coefficient Values Used in Bodner Equations For Stress-Strain Curves . . . . .	13
II	Nominal Coefficient Values Used in the Bodner Equations For Strain-Rate Versus Stress Curves . . . . .	19
III	Experimental Data Base; IN 718, 1200 <sup>o</sup> F . . . . .	27
IV	Coefficient Values for the Bodner Model, IN 718, 1200 <sup>o</sup> F . . . . .	49
V	Experimental Data, Constant Strain Rate Tensile Tests . . . . .	97
VI	Experimental Data, Formatted to Allow Determination of n and Z <sub>1</sub> . . . . .	98
VII	Values Computed for n and Z <sub>1</sub> . . . . .	101
VIII	Experimental Data From Figure 58 . . . . .	105
IX	Computation of Plastic Strain . . . . .	106
X	Determination of the Elastic Strain Rate $\dot{\epsilon}^e$ . . . . .	109
XI	Determination of Plastic Strain Rate $\dot{\epsilon}^p$ . . . . .	110
XII	Computation of Ln(Z <sub>1</sub> -Z): n = 2.5, Z <sub>1</sub> = 1992.878 MPa . .	111
XIII	Computation of Ln(Z <sub>1</sub> -Z); n = 3.0, Z <sub>1</sub> = 1794.672 MPa . .	112
XIV	Computation of Ln(Z <sub>1</sub> -Z); n = 3.125, Z <sub>1</sub> = 1756.858 MPa .	113
XV	Computation of Ln(Z <sub>1</sub> -Z); n = 3.211, Z <sub>1</sub> = 1732.871 MPa .	114

### List of Symbols

$(\dot{\quad})$	Time rate of change
$\epsilon, \epsilon^e, \epsilon^p$	Total strain; elastic strain; plastic strain
$e, e^e, e^p$	Total deviatoric strain: elastic, plastic deviatoric strains
$\lambda$	Scalar material function of $T, Z_k, J_2$
$S_{ij}$	Deviatoric stress
$D_2^p$	Second invariant of the deviatoric plastic strain rate $e_{ij}^p$
$J_2$	Second invariant of the deviatoric stress $S_{ij}$
$Z_k$	Internal state variables
$T$	Temperature, absolute scale
$D_0$	Limiting value for the plastic strain rate in shear
$n$	State variable describing strain rate sensitivity
$\sigma, \sigma_x$	Stress; uniaxial stress
$W_p$	Plastic work
$Z$	Material hardness parameter
$Z_{rec}, Z_{wh}$	Hardness due to recovery/work hardening
$Z_0$	Initial value of material hardness $Z$
$Z_0$ (mean)	A value for $Z_0$ computed a particular way (see Appendix C)
$Z_1$	Saturation (maximum) value of $Z$
$Z_2$	Minimum recoverable value of $Z$
$A$	Hardening recovery coefficient
$r$	Hardening recovery exponent
$m$	State variable describing rate of work hardening
$m$ (mean)	A value for $m$ computed a particular way (see Appendix C)

List of Symbols

E	Elastic modulus
a	$Z/\sigma$
x	$\sigma/Z_1$
y	$\dot{\epsilon}^p/D_0$
v	Dislocation velocity
v*	Limiting value of dislocation velocity
$P_{\square}$	Probability function associated with dislocation velocity
$\sigma_s$	Shear stress
D	Drag stress constant
q	Parameter describing isotropic/directional nature of work hardening
$Z^t, Z^c$	Hardness parameter Z used in cyclic loading cases for tension loading ( $Z^t$ ) and compression loading ( $Z^c$ )
$Z_{eff}$	$Z^t$ when loading is tensile; $Z^c$ when loading is compressive
$U_a$	$\frac{\sigma}{ \sigma }$

## Abstract

Development and use of new materials and technologies for use in high temperature environments are dependent on the availability of a material model appropriate for such applications. The Bodner-Partom constitutive model shows promising flexibility in modeling materials under such conditions. Evaluation of the model's adequacy and range of application has thus far been hampered by a lack of physical understanding of the model's coefficients and the lack of a systematic method for evaluating them.

This study uses experimental data for IN<sup>(INDIUM)</sup>718 at 1200°F to establish a systematic approach to the evaluation of the Bodner coefficients. Parametric studies were used to develop a comprehensive description of each coefficient and its impact on the material model. A simple extension of the Bodner constitutive equations to model cyclic loading situations was carried out.

Results show that systematic evaluation of the Bodner coefficients from experimental data is achievable although somewhat subjective in nature. Cyclic load studies revealed that the Bodner model is capable of modeling isotropic and directional strain hardening as well as strain softening.

## I. Introduction

The continued and growing use of high performance gas turbine engines on military aircraft has placed the United States Air Force in a position where more information is needed on material behavior under the conditions of these applications [1]. High temperature engine operation is typified by complex material behavior where time dependence and temperature effects interact with a varying load spectra [2,3]. An analytical technique to model material behavior under these conditions is required to allow further development and use of materials and technology.

Development of an appropriate analytical model has been a slow process. A model is proposed; then it must be evaluated, compared to experimental data, and revised. As technology advances, new materials and new applications require changes in the models. Today's constitutive models have evolved from classical plasticity over a period of many years.

Early material models were based on the assumptions of classical plasticity. These models are time independent. They are thus unable to adequately describe high temperature material behavior where time and rate dependence are significant.

The classical elasto-viscoplastic models followed. They corrected some, but not all, of the deficiencies of the classical plasticity models. Classical elasto-viscoplastic theories allow for strain rate dependent plastic flow, but rely on a strain rate independent yield criterion [21] (e.g. von Mises). Thus, they too inadequately describe

high temperature material behavior.

Several non-classical elasto-viscoplastic constitutive models have been proposed to allow analysis of the behavior of rate sensitive materials. Each attempts to model the mechanism of rate dependence, temperature dependence, creep and relaxation behavior, and each predicts a slightly different material response because the mechanisms are modeled differently. A brief look at some of the models serves to point out some of the differences between them. This is by no means a comprehensive overview. It is merely intended to provide a rudimentary understanding of some of the model types in use today.

Cernocky and Krempl [24] proposed a constitutive model that relies on an overstress mechanism (a variation on that proposed by Malvern in 1951 [27]) and an equilibrium material stress-strain response. The difference between the flow stress and the equilibrium stress is called the overstress. The model is non-linear in stress and strain and linear in stress and strain rates. It does not use a yield surface. This model incorporates stress-rate history effects but not strain-rate history effects [17], and is thus unable to model observed material behavior.

Lin and Wu [23] developed constitutive equations based on the endochronic theory attributed by Valanis. In the endochronic theories of viscoplasticity, a transformation is used to move from the absolute time measured by a clock to a subjective time scale that is essentially a material property. Thus the current value of stress is determined by "the memory of the material with respect to the endochronic time" [23]. Endochronic theories are most often used in the study of brittle

materials, such as concrete. This model does not rely on a yield surface. It models creep behavior, but does not predict relaxation behavior [17]; thus it is unable to model observed material response.

The model proposed by Wu and Yip [25] is also an endochronic theory. Unlike that of Lin and Wu, this model predicts both creep and relaxation behavior. However, where most endochronic theories do not require use of a yield surface, this one does; the internal measure of time depends on the plastic strain rate. Thus, use of this model requires that a yield criterion be established.

The Bodner-Partom model for plastic flow [22] does not depend on a yield surface. It predicts creep and relaxation behavior; it incorporates time, rate and temperature effects. Both stress and strain rate history effects are modeled. And it can be used to model material behavior during application of cyclic loads as well as monotonic loading conditions.

Because the Bodner-Partom flow law appears to incorporate mechanisms for modeling these important parameters of material behavior, it has a great potential as an analytical tool. At this time, however, there is no established method for determining the eight material coefficients used in this model. Efforts to evaluate the adequacy and flexibility of the model and to use it effectively have been hampered by the non-availability of the required material parameters.

D. C. Stouffer [9] evaluated the coefficients used in the Bodner flow law to model Inconel 100. The data base he used for this work consisted of twenty experiments, including both tensile and creep tests. Although he did develop appropriate values for the coefficients, he did



so without developing much physical understanding of them. It was not known how sensitive the model may be to small variations in the values of the various coefficients. There was little guidance as to what data should be used to evaluate which coefficients, and no guidance as to how sensitive the model is to small deviations from the "best fit" values at any given point.

This thesis provides a systematic method for evaluating the coefficients of the Bodner model from experimental data. The work done by Stouffer [9] is used as a starting point; some guidance is given regarding what constitutes an adequate data base for the evaluation process. A comprehensive discussion of the coefficients and their characteristic effects on the Bodner model provides additional insight into the model. A study of the Bodner model under conditions of cyclic loading establishes the validity of such uses of this model and suggests additional characteristics that must be incorporated into the cyclic formulation to allow adequate representation of material behavior under such conditions.

## II. Theory

### General Theory

The Bodner-Partom plastic flow model is based on the assumption that the total deformation rate tensor consists of elastic (reversible) and inelastic (non-reversible) components at every stage of the loading history. In the case of small strains, this is written

$$\dot{\epsilon}_{ij} = \dot{\epsilon}_{ij}^e + \dot{\epsilon}_{ij}^p \quad (1)$$

where the elastic and inelastic components are both non-zero for all non-zero values of stress. Anelastic stresses and strains are neglected in this formulation.

The elastic strain rate  $\dot{\epsilon}_{ij}^e$  is related to the stress rate by the time derivative of Hooke's Law. The inelastic strain rate  $\dot{\epsilon}_{ij}^p$  is taken to follow the Prandtl-Reuss flow law of classical plasticity [29],

$$\dot{\epsilon}_{ij}^p = \dot{e}_{ij}^p = \lambda S_{ij} \quad (2)$$

where  $\dot{e}_{ij}^p$  is the deviatoric plastic strain rate and  $S_{ij}$  the deviatoric stress. If both sides of Equation (2) are squared and divided by two, the result is

$$\frac{1}{2} \dot{e}_{ij}^p \dot{e}_{ij}^p = D_2^p = \frac{1}{2} \lambda^2 S_{ij} S_{ij} = \lambda^2 J_2 \quad (3)$$

where  $D_2^p$  is the second invariant of the deviatoric plastic strain rate and  $J_2$  is the second invariant of the deviatoric stress. It is assumed in this formulation that the plastic deformations are described by the functional relationship

$$D_2^P = D_2^P (J_2, T, Z_k) \quad (4)$$

where  $D_2^P$  is written explicitly as a function of the deviatoric stress  $J_2$ , absolute temperature  $T$  and a set of internal state variables  $Z_k$ . The current values of the  $Z_k$  are meant to reflect all the pertinent effects of any prior inelastic deformations. Thus, we can write

$$\lambda = \left( D_2^P (J_2, T, Z_k) / J_2 \right)^{1/2} \quad (5)$$

The form chosen by Bodner and Partom [22] for expressing  $D_2^P$  ( $J_2, T, Z_k$ ), motivated by the equations of dislocation dynamics, is

$$D_2^P = D_0^2 \exp \left[ - \left[ \frac{Z^2}{3J_2} \right]^n \frac{n+1}{n} \right] \quad (6)$$

where  $D_0$  is a limiting value for the plastic strain rate in shear and  $n$  is a temperature dependent state variable which describes strain rate sensitivity. The variable  $Z$  is a material hardness parameter indicating in some sense the material's internal resistance to plastic flow, and is discussed in greater detail subsequently.

Some insight into the form of Equation (6) may be gained from a brief look at dislocation dynamics. Dislocation velocity cannot increase without limit as stress increases; it must approach some limiting value. Quite generally the velocity may be written

$$v = v^* P_m^*(\sigma_s) \quad (7)$$

where  $v$  is the dislocation velocity,  $v^*$  the limiting value of dislocation velocity,  $\sigma_s$  the shear stress between slip planes and  $P_m^*$  the average probability of  $v$  taking on the value  $v^*$  at a given instant. Whatever

functional form is chosen for  $P_m(\sigma_s)$ , it must satisfy two conditions:  $P_m(\sigma_s)$  must be zero at  $\sigma_s = 0$ , and  $P_m(\sigma_s)$  must approach unity asymptotically for high values of  $\sigma_s$ . The form proposed by Gilman [13] which satisfies both these conditions is

$$P_m = e^{-D/\sigma_s} \quad (8)$$

where  $D$  is a drag stress constant, sometimes called the dislocation drag term. Note the similarity between the resulting expression

$$v = v^* \exp \left[ -\frac{D}{\sigma_s} \right] \quad (9)$$

and Equation (6).

If Equations (2), (3), (5), and (6) are combined, the resulting expressions are found, considering a uniaxial stress  $\sigma_x$ :

$$\begin{aligned} \dot{\epsilon}_x^p &= \lambda s_x = \lambda \sigma_x \\ &= \frac{\sigma_x}{\sqrt{J_2}} D_0^2 \exp \left( - \left[ \frac{Z^2}{3J_2} \right]^n \frac{n+1}{n} \right)^{\frac{1}{2}} \\ \dot{\epsilon}_x^p &= \frac{2}{\sqrt{3}} \frac{\sigma_x}{|\sigma_x|} D_0 \exp \left( - \frac{1}{2} \left[ \frac{Z}{\sigma_x} \right]^{2n} \frac{n+1}{n} \right) \end{aligned} \quad (10)$$

The hardness parameter  $Z$  consists of two terms, as does the time rate of hardening,  $\dot{Z}$ . The first term represents hardening due to plastic work,  $W_p$ , while the second incorporates the effects of thermal recovery of the hardening generated by plastic work. By examining the mechanics of strain hardening and recovery on a microscopic scale, some insight into the forms of these two terms can be found.

The softer a material is, the easier it is for dislocations to

propagate through the material lattice. It is the result of this propagation of dislocations that is called "plastic strain." Dislocations scattered through the material are one of many mechanisms that serve to impede the propagation of mobile dislocations. Strain hardening is the multiplication of dislocations in the material in such a way as to impede dislocation motion.

A material containing these "impedance" dislocations has a higher internal energy than the same material without the dislocations. The higher the dislocation density, the higher the internal energy [11]. Over time, the material will tend toward a lower internal energy state. The material reduces its dislocation density and hence its internal energy by eliminating or relocating impedance dislocations. This reduction in dislocation density is what is called recovery, and the result is a softer material.

In Bodner's formulation, [22], the work hardening expression is written in terms of  $\dot{Z}$ :

$$\dot{Z}_{wh} = \frac{\partial Z_{wh}}{\partial W_p} \frac{\partial W_p}{\partial t} \quad (11)$$

The change in hardness  $Z$  with respect to plastic work  $W_p$  (per unit volume) is

$$\frac{\partial Z_{wh}}{\partial W_p} = m (Z_1 - Z) \quad (12)$$

where  $m$  is a material constant describing the rate of work hardening and  $Z_1$  is the saturation (maximum) value of  $Z$ . Note also that

$$\frac{\partial W_p}{\partial t} = \sigma \dot{\epsilon}^p \quad (13)$$

The thermal recovery term is postulated by Bodner [1] to have the form

$$\dot{Z}_{\text{rec}} = -A Z_1 \left[ \frac{Z - Z_2}{Z_1} \right]^r \quad (14)$$

where  $Z_2$  is the non-work hardened value of  $Z$  at a given temperature, and  $A$  and  $r$  are temperature dependent material coefficients. The complete expression for the rate of hardening then becomes

$$\dot{Z} = m (Z_1 - Z) \sigma \dot{\epsilon}^p - A Z_1 \left[ \frac{Z - Z_2}{Z_1} \right]^r \quad (15)$$

Equations (10) and (15) together are assumed to provide sufficient information to model the material behavior. For test conditions where there is no load reversal, a forward integration technique may be used to incrementally describe material behavior. When there is a load reversal, however, proper application of the constitutive equations is considerably more complex.

Under cyclic loading the hardness parameter  $Z$  develops directional characteristics. Strain hardening caused by tensile loading affects the material's subsequent behavior under compressive loads. Separate values of the hardness  $Z$  would thus be indicated for use in Equation (10), depending on the sign of the applied stress. When the applied stress is tensile, the applicable  $Z$  is called  $Z^t$ ; when the applied stress is compressive, the applicable  $Z$  is called  $Z^c$ . A simple model [7] incorporating isotropic and directional hardening allows  $Z^t$  and  $Z^c$  to be incrementally computed from the initial value  $Z_0$  according to a few basic principles.

Initially,

$$Z^t = Z^c = Z_0 \quad (16)$$

Changes from this state are computed according to

$$\dot{Z}^t = q \dot{Z} + (1 - q) \dot{Z} U_\alpha \quad (17a)$$

$$\dot{Z}^c = q \dot{Z} - (1 - q) \dot{Z} U_\alpha \quad (17b)$$

where  $U_\alpha = \frac{\sigma}{|\sigma|}$  depends on the sign of the applied stress, and

$$\dot{Z} = m (Z_1 - Z_{\text{eff}}) \sigma \dot{\epsilon}^p - A Z_1 \left[ \frac{Z_{\text{eff}} - Z_2}{Z_1} \right]^r \quad (18)$$

where

$$Z_{\text{eff}} = Z^t \text{ or } Z^c \quad (19)$$

depending on  $U_\alpha$ . Using these computed values of  $\dot{Z}^t$  and  $\dot{Z}^c$ , values of  $Z^t$  and  $Z^c$  are determined incrementally over time using the relationships

$$Z^t = Z^t + \dot{Z}^t \Delta t \quad (20a)$$

$$Z^c = Z^c + \dot{Z}^c \Delta t \quad (20b)$$

Thus, at the end of the first incremental time step, there are two values of hardness,  $Z^t$  and  $Z^c$ . The parameter  $q$  is a significant feature of this formulation, and its value corresponds to the nature of the hardening process. If the hardening is purely isotropic,  $q = 1$ ; for this case  $Z^t = Z^c$ . A value of  $q = 0$  indicates that the hardening is purely directional. This model also allows for situations where hardening is partly isotropic and partly kinematic; in this case some positive fractional value is assigned to  $q$ . In general work related to strain

hardening it has been proposed [7] that these constitutive equations can also be associated with strain softening; in this case a value of  $q < 0$  is used. In the subsequent discussion it is this phenomenon of strain softening that will be dealt with. The Bodner constitutive model is capable of modeling both hardening and softening; this is very rare.

#### Applications for Evaluating Coefficients

The preceding paragraphs briefly present a technique whereby Equations (10) and (15) can be used to describe material behavior under cyclic loading. Under certain other loading conditions, these two equations can be simplified to facilitate the evaluation of some of the coefficients.

When both strain rate and stress are constant, as is the case when saturation is reached, Equation (10) indicates that the hardness parameter  $Z$  must also be constant. Furthermore, for tests of short duration (with no recovery) the material must be in a fully work hardened state at saturation "to obtain the maximum value of stress" [9], so that  $Z = Z_1$ . For these steady flow conditions,

$$\begin{aligned} \dot{\epsilon}^P &= \frac{2}{\sqrt{3}} D_0 \exp \left[ - \frac{n+1}{2n} \left( \frac{Z_1}{\sigma} \right)^{2n} \right] \\ \frac{\sqrt{3}\dot{\epsilon}^P}{2D_0} &= \exp \left[ - \frac{n+1}{2n} \left( \frac{Z_1}{\sigma} \right)^{2n} \right] \\ -\ln \frac{\sqrt{3}\dot{\epsilon}^P}{2D_0} &= + \frac{n+1}{2n} \left( \frac{Z_1}{\sigma} \right)^{2n} \\ \ln \left[ -\ln \frac{\sqrt{3}\dot{\epsilon}^P}{2D_0} \right] &= \ln \left[ \frac{n+1}{2n} \left( \frac{Z_1}{\sigma} \right)^{2n} \right] \\ \ln \left[ -\ln \frac{\sqrt{3}\dot{\epsilon}^P}{2D_0} \right] &= -2n \ln \sigma + \left[ 2n \ln Z_1 + \ln \left( \frac{n+1}{2n} \right) \right] \end{aligned} \quad (21)$$



From this form it is seen that  $\ln(-\ln(\frac{\sqrt{3}\epsilon^p}{2D_o}))$  is linearly related to  $\ln \sigma$ . Characterization of appropriately plotted experimental data will allow determination of  $n$  from the slope of the line. Once  $n$  is determined,  $Z_1$  can be deduced mathematically.

For test conditions such as high strain rate situations which preclude recovery, Equation (15) can be written

$$dZ = m (Z_1 - Z) dW_p \quad (22)$$

This can be integrated to give

$$\ln (Z_1 - Z) = \ln (Z_1 - Z_0) - mW_p \quad (23)$$

where  $Z_0$  is defined as the initial value of hardness  $Z$ . This shows that a linear relationship exists between  $\ln (Z_1 - Z)$  and the plastic work  $W_p$ . The value of  $Z$  for each data point of interest can be computed from an inversion of Equation (10) which reduces to

$$Z = \sigma \left[ \frac{2n}{n+1} \ln \frac{2D_o}{\sqrt{3}\epsilon^p} \right]^{\frac{1}{2}n} \quad (24)$$

Plotting  $\ln (Z_1 - Z)$  against plastic work  $W_p$  allows the determination of a value for  $Z_0$  from the linearly extrapolated value of  $\ln (Z_1 - Z)$  at  $W_p = 0$ . The slope of this line defines a value for  $m$ . Once the initial value of hardness  $Z_0$  and the rate of work hardening  $m$  are known, stress-strain curves can be generated using a forward integration technique on Equations (10) and (15). This allows comparison of the high strain rate analytical predictions with the data.

Based on the values determined for  $n$ ,  $m$ ,  $Z_0$  and  $Z_1$ , stress-strain curves are generated using forward integration. This procedure is

insensitive to the values chosen for A, r, and  $Z_2$  (as they appear only in the recovery term) so the fact that these coefficients have not yet been determined exactly does not impact these curves. Comparison of these curves with appropriate experimental data allows refinement of the values chosen for n, m,  $Z_0$  and  $Z_1$  to best model experimental data.

A parametric study of the coefficients and their impact on the resulting stress-strain curves provides some guidance for the refinement process. The results of this study are contained in Figures 1 through 4. The nominal values used for the coefficients are given in Table I: deviations from these values are annotated on the individual figures.

TABLE I  
Nominal Coefficient Values Used in Bodner Equations  
For Stress-Strain Curves

Variable	Description	Value
n	Strain Rate Sensitivity Parameter	3.0
m	Rate of Work Hardening	.219 MPa <sup>-1</sup>
$Z_0$	Initial Value of Material Hardness Z	1669 MPa
$Z_1$	Saturation (Maximum) Value of Z	1795 MPa
$Z_2$	Minimum Recoverable Value of Z	718 MPa
A	Hardening Recovery Coefficient	.001 sec <sup>-1</sup>
r	Hardening Recovery Exponent	7.0
$D_0$	Limiting Value, Plastic Strain Rate in Shear	10 <sup>6</sup> sec <sup>-1</sup>
E	Elastic Modulus	162.5 x 10 <sup>3</sup> MPa
$\dot{\epsilon}$	Strain Rate	1.3 x 10 <sup>-5</sup> sec <sup>-1</sup>

Figure 1 shows the impact of varying  $n$  and  $Z_1$  at a strain rate of  $1.3 \times 10^{-5} \text{ sec}^{-1}$ . (This strain rate is one of those for which experimental data exists). The four stress-strain curves overlay one another quite closely. Any  $n$  value in the range from  $n = 2.5$  to  $n = 3.211$  clearly predicts material behavior quite similar to that predicted by any other  $n$  value in the range.

Figure 2 shows the impact of varying  $m$  plus and minus ten percent of its mean experimental value ( $.219 \text{ MPa}^{-1}$ ), again at a strain rate of  $1.3 \times 10^{-5} \text{ sec}^{-1}$ . Again, the four curves overlay one another closely, but this time the effect is to change the shape of the stress-strain curve slightly (increasing  $m$  causes higher saturation stress over the domain shown).

Figure 3 shows the impact of varying  $Z_0$  plus and minus ten percent of its mean experimental value ( $1669 \text{ MPa}$ ), at a strain rate of  $1.3 \times 10^{-5} \text{ sec}^{-1}$ . Changes in  $Z_0$  are much more readily seen than changes in  $m$  in these figures. Increasing  $Z_0$  is equivalent to increasing the initial hardness of the material without changing the saturation hardness  $Z_1$ . Thus the nature of the hardening portion of the curve is affected. Higher values of  $Z_0$  correspond to a flatter appearance of the stress-strain curve.

Figure 4 shows the impact of varying  $m$  and  $Z_0$  at a strain rate of  $1.3 \times 10^{-5} \text{ sec}^{-1}$ . The shape of the stress-strain curve can clearly be changed significantly by different choices of values for  $m$  and  $Z_0$ .

A procedure for determining appropriate values for the remaining material coefficients ( $A$ ,  $Z_2$  and  $r$ ) requires use of the full equations (equations (10) and (15)). To demonstrate more vividly the character

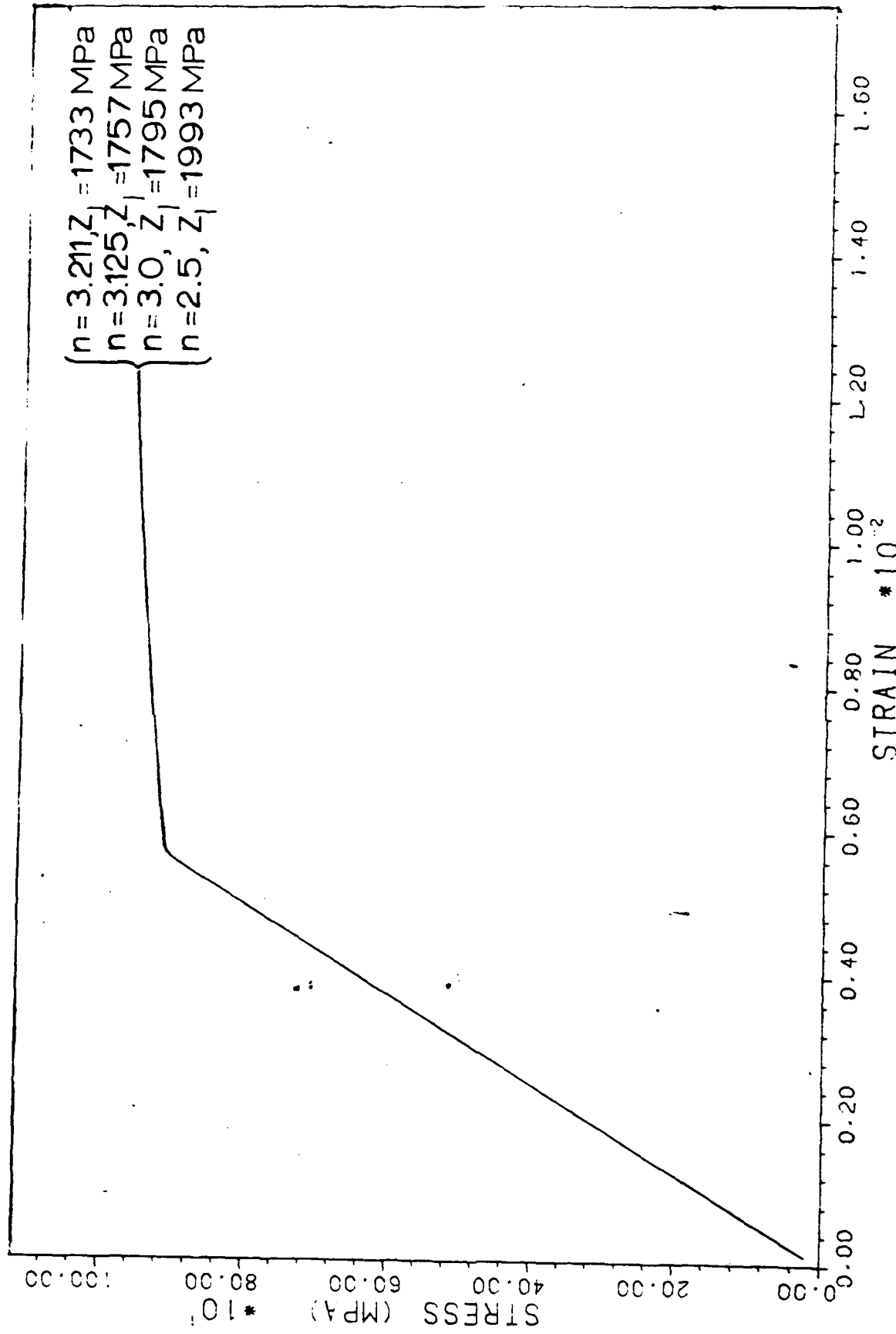


Figure 1. Variation of  $n$  and  $Z_1$

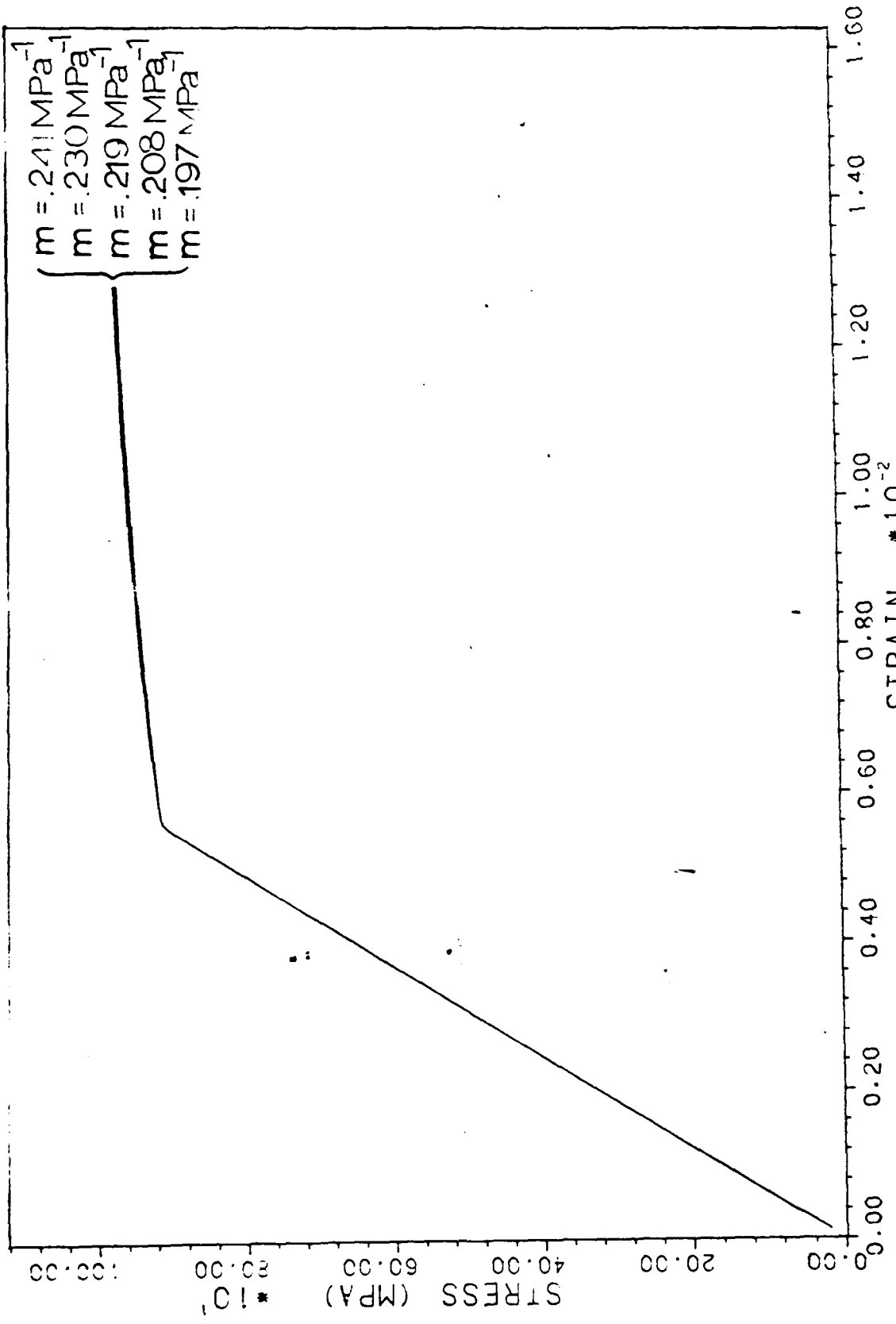


Figure 2. Variation of m

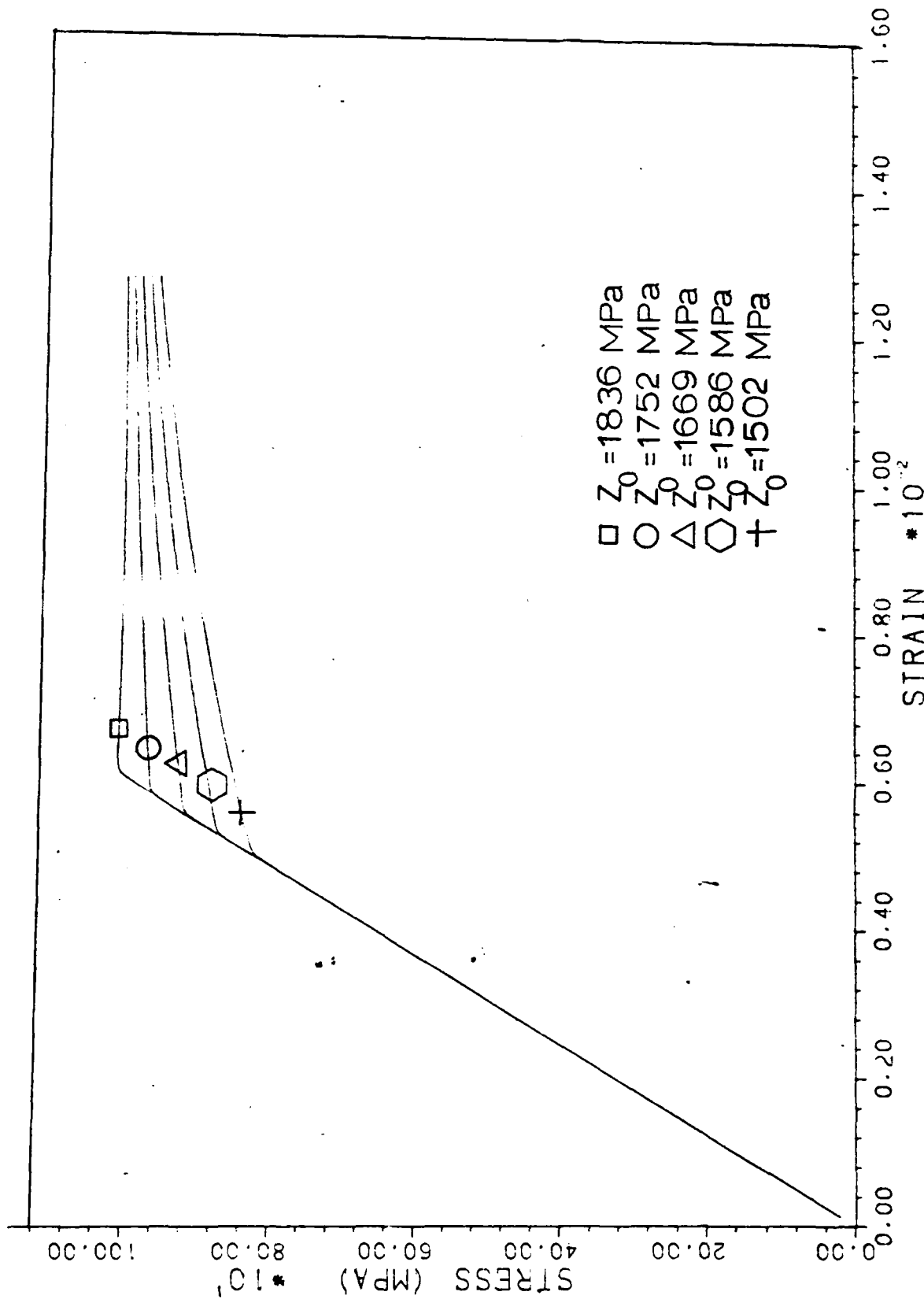


Figure 3. Variation of  $Z_0$

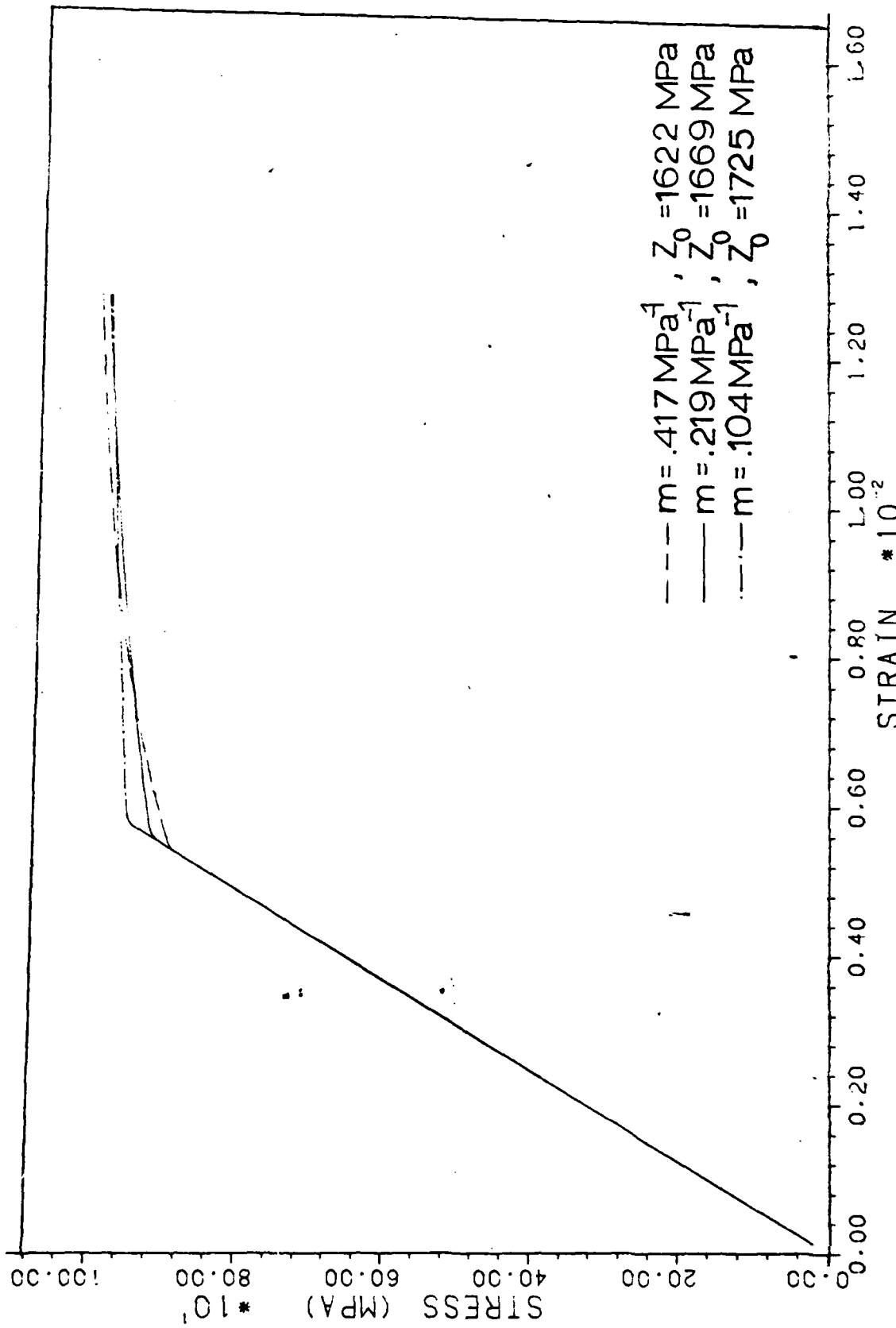


Figure 4. Variation of  $m$  and  $Z_0$

of the various coefficients, a parametric study was undertaken. The information contained in Equations (10) and (15) can be graphed as a non-dimensionalized strain rate versus a non-dimensionalized stress to allow for a more general presentation. In this study, nominal values were selected for all coefficients but one, and various values for this coefficient of interest were selected to illustrate the impact of varying that parameter. The nominal values used in this study are presented in Table II.

TABLE II  
Nominal Coefficient Values Used in the Bodner Equations  
For Strain-Rate Versus Stress Curves

Variable	Description	Value
n	Strain Rate Sensitivity Parameter	5.0
m times Z <sub>1</sub>	Dimensionless Form of m	1000.
Z <sub>2</sub> /Z <sub>1</sub>	Dimensionless Form of Z <sub>2</sub>	.1
A/D <sub>o</sub>	Dimensionless Form of A	.000001
r	Hardening Recovery Exponent	3.0

Equation (10) was non-dimensionalized as follows:

$$\exp \left[ \frac{1}{2} \left( \frac{Z}{\sigma} \right)^{2n} \frac{n+1}{n} \right] = \frac{2D_o}{\sqrt{3}\dot{\epsilon}^p}$$

$$\left[ \frac{1}{2} \left( \frac{Z}{\sigma} \right)^{2n} \frac{n+1}{n} \right] = \ln \left[ \frac{2D_o}{\sqrt{3}\dot{\epsilon}^p} \right]$$

$$\left( \frac{Z}{\sigma} \right)^{2n} = \frac{2n}{n+1} \ln \left[ \frac{2D_o}{\sqrt{3}\dot{\epsilon}^p} \right]$$



$$\alpha = \frac{Z}{\sigma} = \left[ \frac{2n}{n+1} \ln \left[ \frac{2D_o}{\sqrt{3}\epsilon^{\cdot P}} \right] \right]^{\frac{1}{2}n} \quad (25)$$

where  $\alpha$  is defined as  $\frac{Z}{\sigma}$ . For this study, the condition of saturation was assumed, meaning that

$$\dot{Z} = 0$$

Substituting this into Equation (15) leads to the following:

$$m(Z_1 - Z)\sigma\epsilon^{\cdot P} = A Z_1 \left[ \frac{Z - Z_2}{Z_1} \right]^r \quad (26)$$

Note again that  $\frac{Z}{\sigma} = \alpha$ . Then Equation (26) can be written

$$m(Z_1 - \sigma\alpha)\sigma\epsilon^{\cdot P} = A Z_1 \left[ \frac{\sigma\alpha - Z_2}{Z_1} \right]^r$$

$$mZ_1 \left(1 - \frac{\sigma\alpha}{Z_1}\right) \frac{\sigma}{Z_1} \frac{\epsilon^{\cdot P}}{D_o} = \frac{A}{D_o} \left[ \frac{\sigma\alpha - Z_2}{Z_1} \right]^r$$

Let  $x = \frac{\sigma}{Z_1}$  and  $y = \frac{\epsilon^{\cdot P}}{D_o}$ . Then

$$mZ_1(1-\alpha x)xy = \frac{A}{D_o} \left( \alpha x - \frac{Z_2}{Z_1} \right)^r$$

$$mZ_1(1-\alpha x)xy - \frac{A}{D_o} \left( \alpha x - \frac{Z_2}{Z_1} \right)^r = 0 \quad (27)$$

Using an iterative procedure, a value for  $x$  (or  $\frac{\sigma}{Z_1}$ ) can be computed for each value of  $y$  (or  $\frac{\epsilon^{\cdot P}}{D_o}$ ). Using Equations (25) and (27), an initial estimate of the proper value for  $x$  is made. Equation (25) is substituted into Equation (27) and the left hand side of Equation (27) is calculated.

As this will not be zero unless the value for  $x$  is guessed exactly, the difference between this calculated value and zero serves as a guide to the next approximation of  $x$ . At high strain rates, where there are no significant recovery effects,  $Z = Z_1$ . Under these conditions, with  $Z_1$  substituted into Equation (25), a value for  $x$  can be found directly from this equation alone.

Graphing the dimensionless strain rate  $\frac{\dot{\epsilon}^p}{D_0}$  versus the dimensionless stress  $\frac{\sigma}{Z_1}$  illustrates the impact of  $A$ ,  $r$ , and  $Z_2$  on the predicted material behavior. Figure 5 serves as a guide to the information contained in this type of figure; it is based on the studies contained in Appendix A. Figures 6, 7, and 8 and the following discussion serve to clarify the behavior of  $A$ ,  $r$ , and  $Z_2$ .

$A/D_0$  is the dimensionless form of the coefficient in the expression for thermal recovery of work hardening (Equation (27)). The "branching" effect in the lower left of Figure 6 shows that the primary effect of changes in  $A/D_0$  is to extend the predicted recovery regime of the material. The onset of the dominance of thermal recovery is described by this variable. For larger values of  $A/D_0$ , thermal recovery dominates at higher strain rates; for lower values of  $A/D_0$ , thermal recovery remains a negligible phenomenon until relatively slower strain rates occur. Changes in  $A/D_0$  have no significant influence at strain rates faster than that at which recovery becomes significant. As a part of the equation descriptive of thermal recovery,  $A/D_0$  does not effect material behavior at higher strain rates where recovery is negligible.

The coefficient  $r$  appears as an exponent in the expression for thermal recovery of work hardening (Equation (27)). If  $A$  (or  $A/D_0$ )

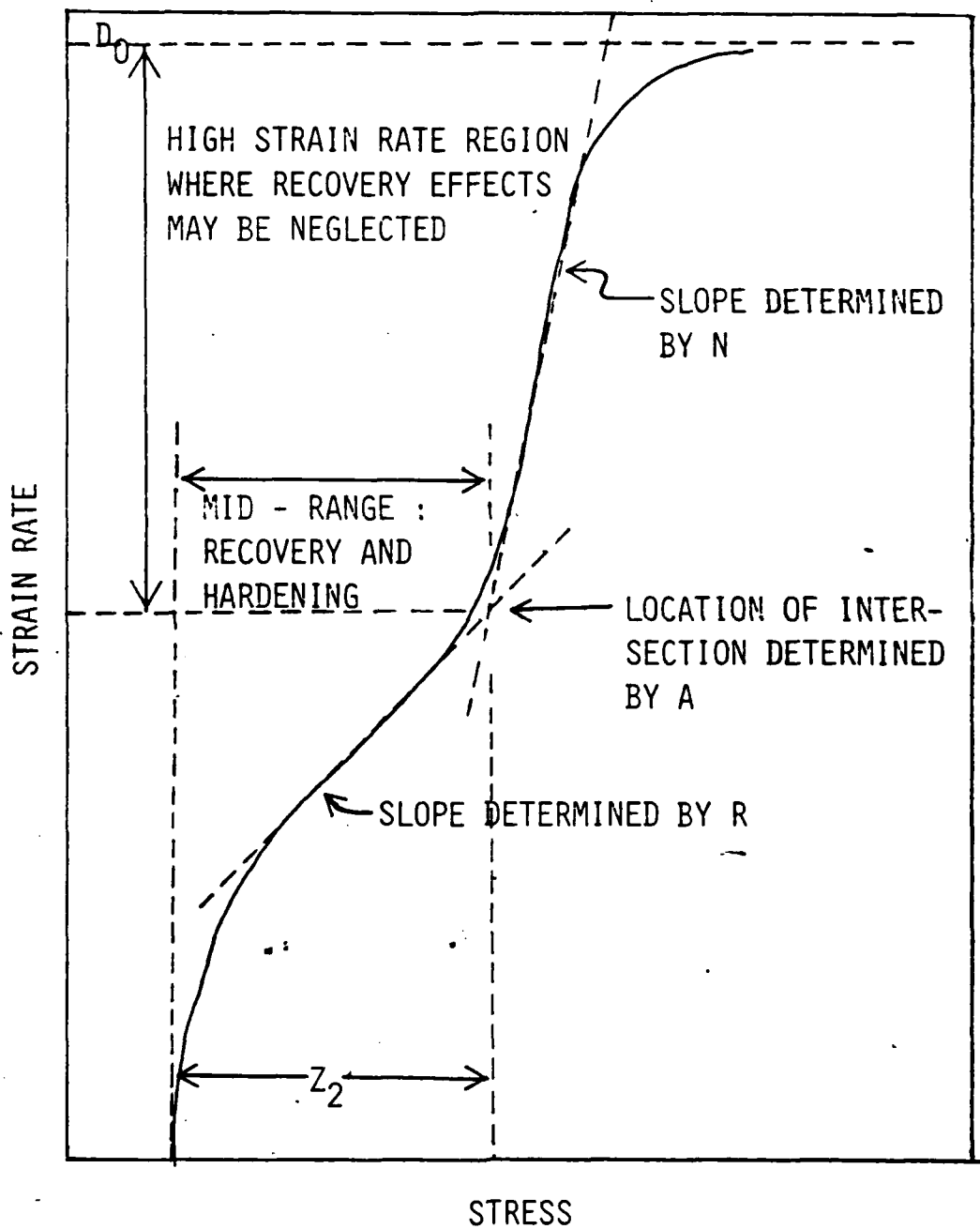


Figure 5. Strain Rate Versus Stress Curve:  
A Guide to the Information

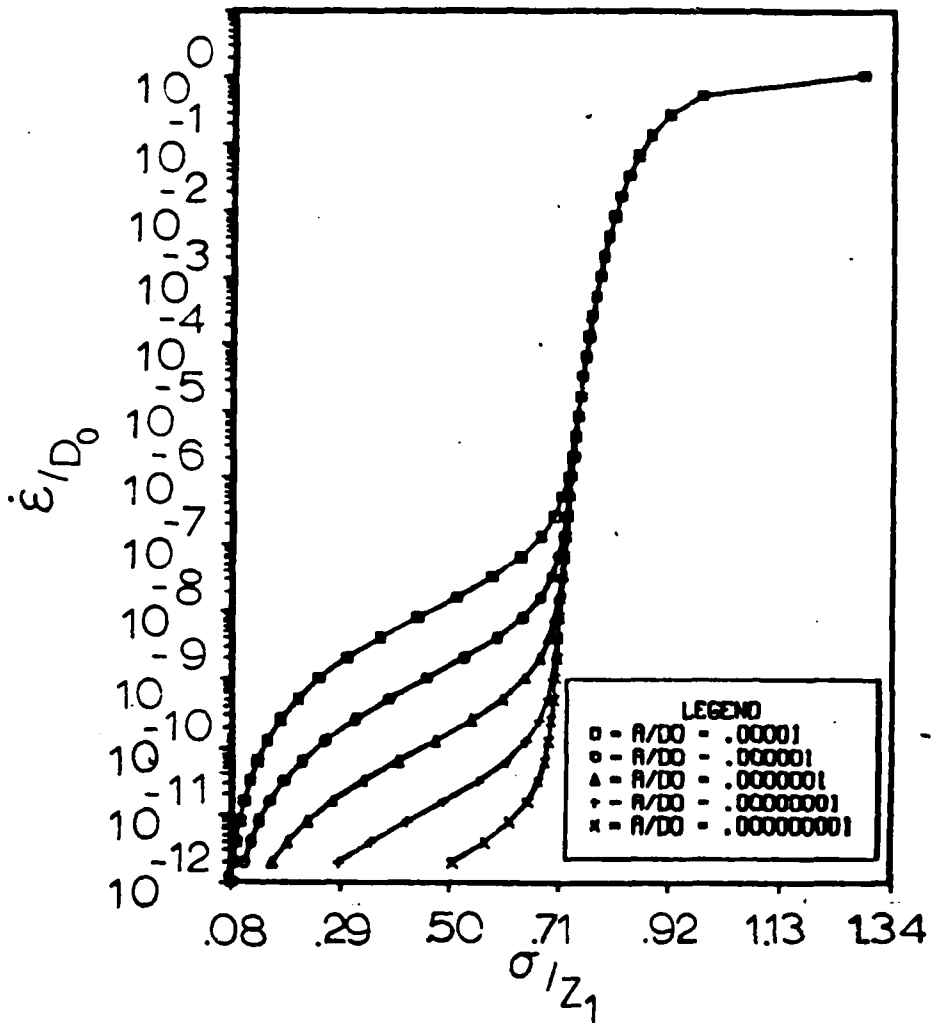


Figure 6. Variation of  $A/D_0$  -

were to be written as a function of the onset of recoverability,  $r$  would be the curvature of that function. Where the value of  $A/D_0$  determines at which strain rate recovery begins to be important,  $r$  determines how quickly recovery becomes a dominant characteristic (see Figure 7). As with  $A$ , the effect of changing  $r$  is not seen at strain rates too high to allow thermal recovery of plastic work to be significant.

$Z_2/Z_1$  is the dimensionless form of the coefficient  $Z_2$ . A value for

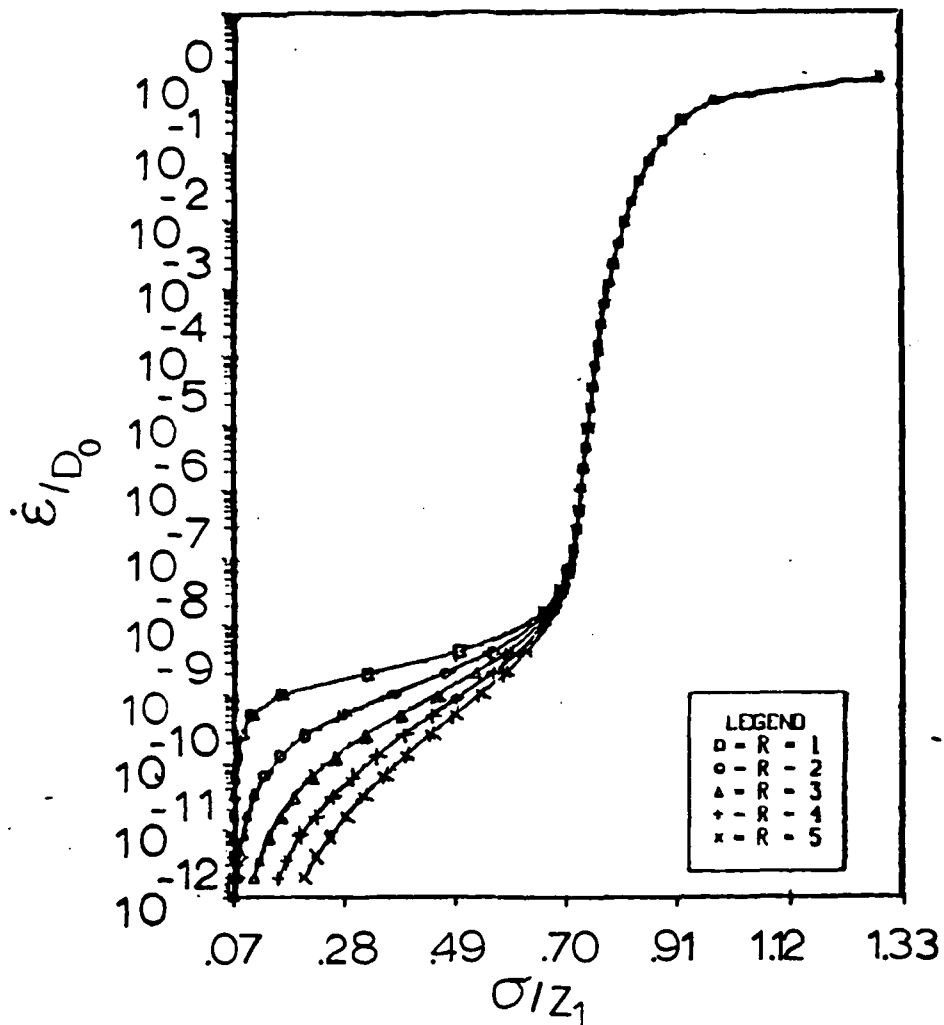


Figure 7. Variation of  $r$

$Z_1$  is determined mathematically when a value is selected for  $n$ ; thus the behavior illustrated in Figure 7 is that of  $Z_2$ . The value of  $Z_2$  controls where the curve becomes strain rate insensitive at very low strain rates. The value of  $Z_2$  represents the minimum recoverable value of hardness.

A more complete discussion of the material coefficients is to be found in Appendix A.

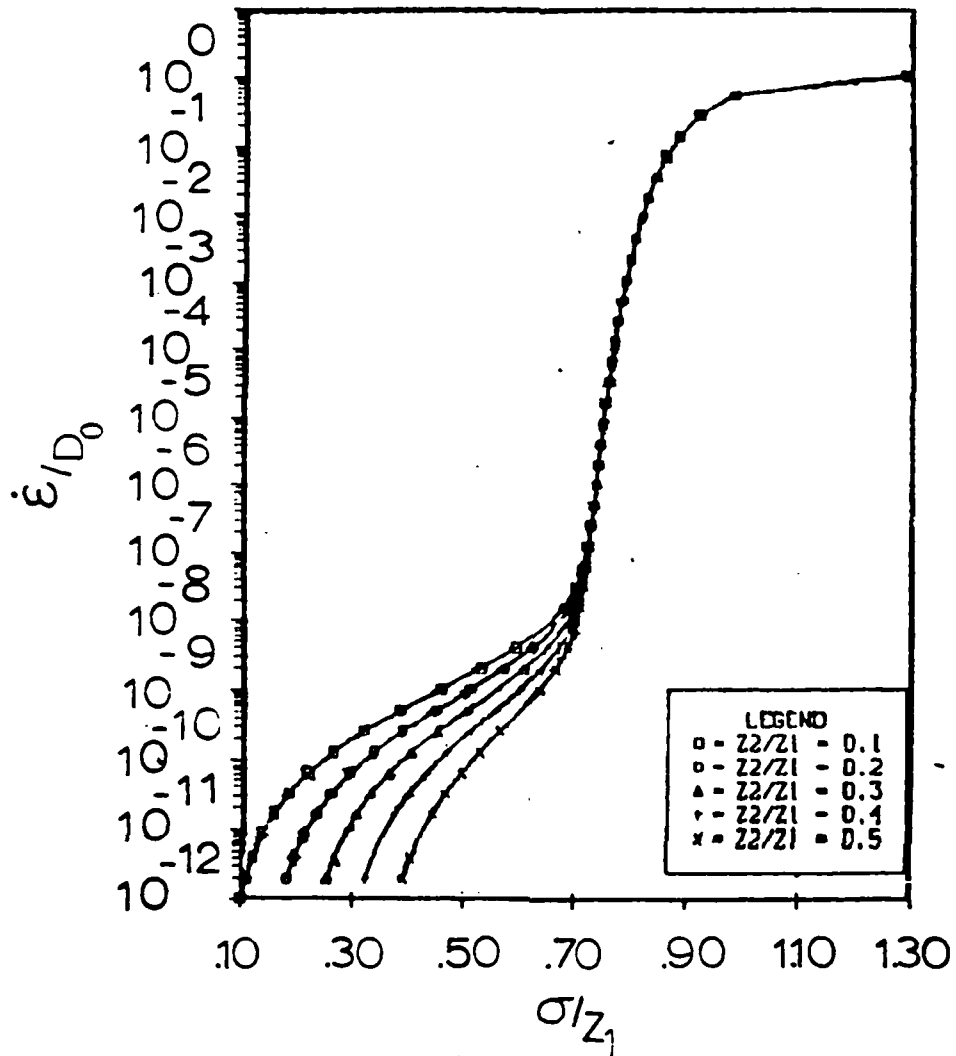


Figure 8. Variation of  $Z_2$

### III. Applications to IN 718

Use of the constitutive equations developed in the preceding section to model material behavior requires that appropriate values be determined for the coefficients. In this exercise, the material to be modeled was Inconel 718, at 1200<sup>o</sup>F. The data was provided by the Materials Laboratory, Air Force Wright Aeronautical Laboratories. Constant strain rate tensile test, creep test and cyclic loading test data were provided.

The linear relationship between  $\ln \left( -\ln \left( \frac{\sqrt{3} \dot{\epsilon}^P}{2D_o} \right) \right)$  and  $\ln \sigma$  for high strain rates (Equation (21)) provides a starting point for the determination of the material coefficients of the Bodner model. Equation (21) is repeated here for continuity:

$$\ln \left( -\ln \left( \frac{\sqrt{3} \dot{\epsilon}^P}{2D_o} \right) \right) = -2n \ln \sigma + (2n \ln Z_1 + \ln \frac{n+1}{2n}) \quad (21)$$

Considering the case of high strain rates, where recovery effects can be ignored, allows  $n$  and  $Z_1$  to be evaluated. If the appropriate experimental data is graphed as  $\ln \left( -\ln \left( \frac{\sqrt{3} \dot{\epsilon}^P}{2D_o} \right) \right)$  versus  $\ln \bar{\sigma}$ , and a straight line approximation made to the data, the slope of the line will be  $-2n$ . A value for  $Z_1$  can then be determined mathematically, using Equation (21) and the coordinates of a point on the line. Plotting the high strain rate experimental data will thus allow  $n$  and  $Z_1$  to be evaluated.

The full data base, tabulated in Table III, was graphed in Figure 9. This allowed an initial evaluation to be made regarding which data points are representative of situations with high strain rates and no recovery. Specifically, the three data points of Figure 9 which came

TABLE III

Experimental Data Base; IN 718, 1200°F

Stress (KSI)	Strain rate	Comments
80	$4.0 \times 10^{-9} \text{ sec}^{-1}$	Creep test
100	$1.6 \times 10^{-8} \text{ sec}^{-1}$	Creep test
105	$1.8 \times 10^{-8} \text{ sec}^{-1}$	Creep test
110	$3.0 \times 10^{-8} \text{ sec}^{-1}$	Creep test
110	$3.0 \times 10^{-8} \text{ sec}^{-1}$	Creep test
110	$3.0 \times 10^{-8} \text{ sec}^{-1}$	Creep test
110	$2.8 \times 10^{-8} \text{ sec}^{-1}$	Creep test
110	$3.6 \times 10^{-8} \text{ sec}^{-1}$	Creep test
120	$1.7 \times 10^{-7} \text{ sec}^{-1}$	Creep test
120	$1.4 \times 10^{-7} \text{ sec}^{-1}$	Creep test
120	$1.5 \times 10^{-7} \text{ sec}^{-1}$	Creep test
125	$4.0 \times 10^{-7} \text{ sec}^{-1}$	Creep test
125	$3.0 \times 10^{-7} \text{ sec}^{-1}$	Creep test
130	$8.3 \times 10^{-7} \text{ sec}^{-1}$	Creep test
134	$1.1 \times 10^{-6} \text{ sec}^{-1}$	Constant strain rate
135	$5.5 \times 10^{-6} \text{ sec}^{-1}$	Creep test
140	$7.0 \times 10^{-6} \text{ sec}^{-1}$	Creep test
142	$1.3 \times 10^{-5} \text{ sec}^{-1}$	Constant strain rate
147	$1.6 \times 10^{-3} \text{ sec}^{-1}$	Constant strain rate



from constant strain rate tensile tests were under consideration. They were based on strain rates of  $1.6 \times 10^{-3} \text{ sec}^{-1}$ ,  $1.3 \times 10^{-5} \text{ sec}^{-1}$ , and  $1.1 \times 10^{-6} \text{ sec}^{-1}$ . It was decided that the data point representative of the  $1.1 \times 10^{-6} \text{ sec}^{-1}$  strain rate was within the recovery regime (see Appendix B for a discussion of this determination).

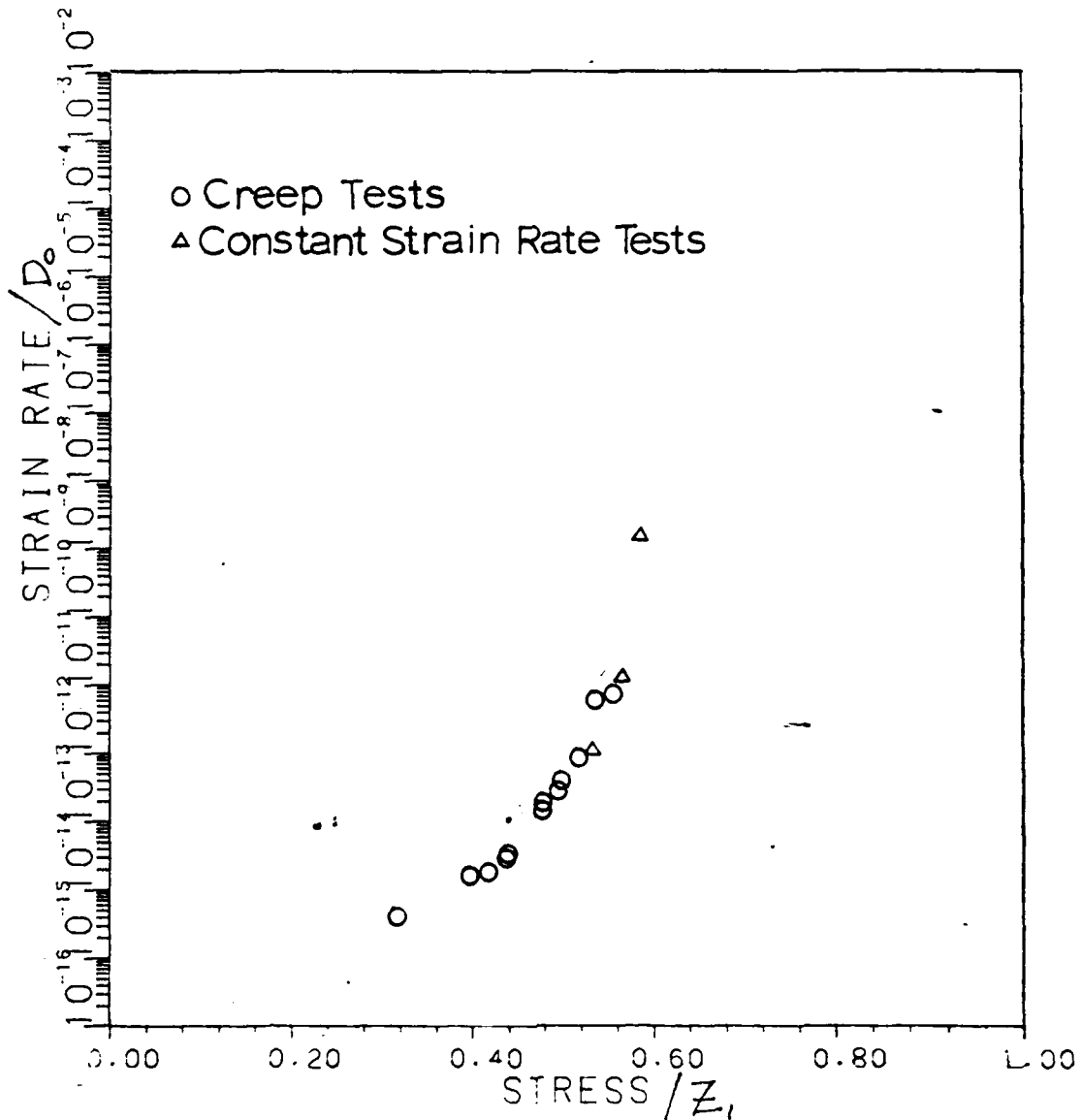


Figure 9. Experimental Data Base; IN 718, 1200°F

The two remaining data points were graphed on  $\ln(-\ln(\frac{\sqrt{3}\dot{\epsilon}^P}{2D_0}))$  versus  $\ln \sigma$  axes, where  $\dot{\epsilon}^P$  was considered to be equal to the total constant strain rate  $\dot{\epsilon}$  in each case. A straight line was drawn to characterize this data. The results are depicted in Figures 10 and 57.

According to Equation (21), the slope of this line was twice the negative value of the coefficient  $n$ . Three values for  $n$  were determined to be fairly characteristic of the data. The slope was first determined using the coordinates of the two data points, resulting in a value of

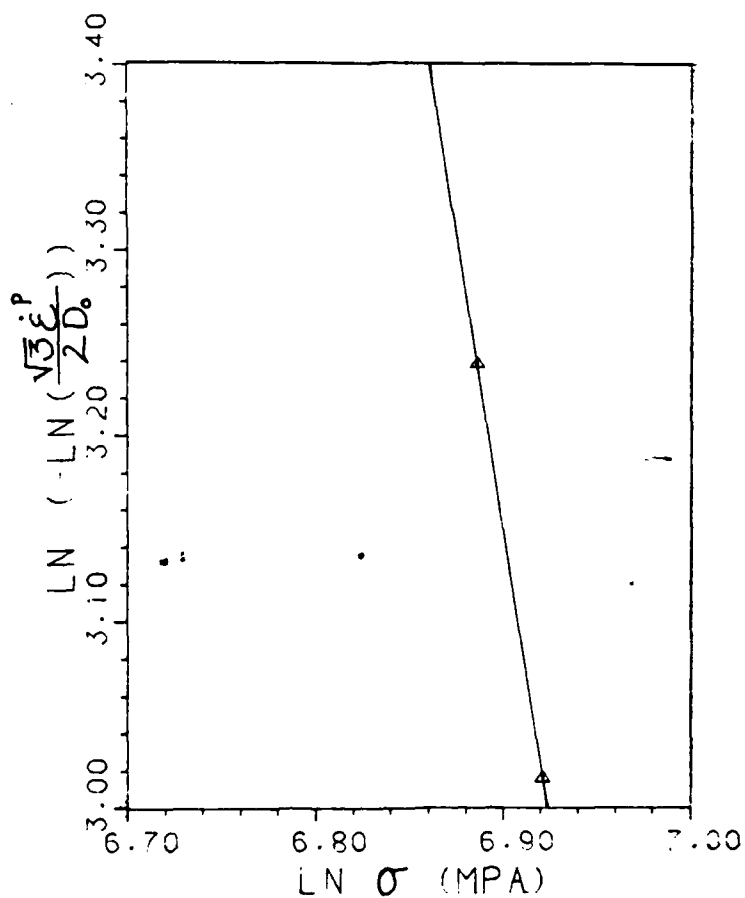


Figure 10. Determination of  $n$  and  $Z_1$

$n = 3.211$ . Working graphically, to evaluate the effect on accuracy of a graphical technique, a second slope was measured which yielded a value of  $n = 3.125$ . For comparison, the line representing a value of  $n = 3.0$  was drawn on the graph (see Figure 57); within the limits on accuracy imposed by the graphical methods, this line also seems fairly representative of the data. For a final point of comparison, the line representing  $n = 2.5$  was also drawn. This line is not so different from the lines representing the other values. It would appear that the proper discrimination of the best value for  $n$  is not possible from this representation of the data. The four values for  $n$  were carried forward -- two limiting values (2.5 and 3.211) and the two intermediate values (3.0 and 3.125) -- in the hope that further comparison with the data would provide a more solid basis for choosing a value for  $n$ .

For each value of  $n$ , a corresponding value for  $Z_1$  was computed using Equation (21). A more detailed description of the determination of values for  $n$  and  $Z_1$  is to be found in Appendix B.

The second study undertaken, to determine values for  $m$  and  $Z_0$ , was prompted by the linear relationship between  $\ln(Z_1 - Z)$  and the inelastic work  $W_p$  at high strain rates (Equation (23), repeated here for convenience):

$$\ln(Z_1 - Z) = \ln(Z_1 - Z_0) - mW_p \quad (23)$$

Again, data from high strain rate tensile tests was used, this time to evaluate  $m$  and  $Z_0$ . The data used in this step came from a single constant strain rate test at  $\dot{\epsilon} = 1.3 \times 10^{-5} \text{ sec}^{-1}$ . This data was chosen because the strain rate was fast enough to allow use of Equation (23) --

which neglects recovery effects -- and because the experimental stress-strain curve was well defined and well-behaved (see Figure 11).

Evaluation of the data began with the computation of the plastic strain rate indicated by the data. The line representing Young's Modulus ( $23.6 \times 10^3$  KSI) [10] was drawn on the experimental stress-strain curve and the origin translated to meet the initial condition of zero strain at zero stress. The values for total strain at selected stress levels were read off the graph; plastic strain was derived from these values by subtracting off the elastic strain as indicated by Hooke's Law.

Plastic work was then computed from a graphical presentation of this information. A trapezoidal integration was done on the graph of stress versus plastic strain (see Figure 12). The value of plastic work at the data points provided the abscissa for the graph representing the relationship of Equation (23).

To find the values for  $Z = \sigma \left[ \frac{2n}{n+1} \ln \frac{2D_o}{\sqrt{3}\epsilon^p} \right]^{1/2n}$ , the value of plastic strain rate had to be computed for each data point. This was derived from the total strain rate by subtracting off the elastic strain rate indicated by the time derivative of Hooke's Law. Then, using Equation (24), a value of  $Z$  was computed at each point. The data was presented graphically as in Figures 13 through 16.

One problem revealed in this procedure is that there is not a clear best straight line approximation to the data. Perhaps this is due to scatter of the experimental data; perhaps the model simply does not adequately represent the material behavior. Whatever the cause, the data used in this study seemed to follow a bi-linear distribution, and

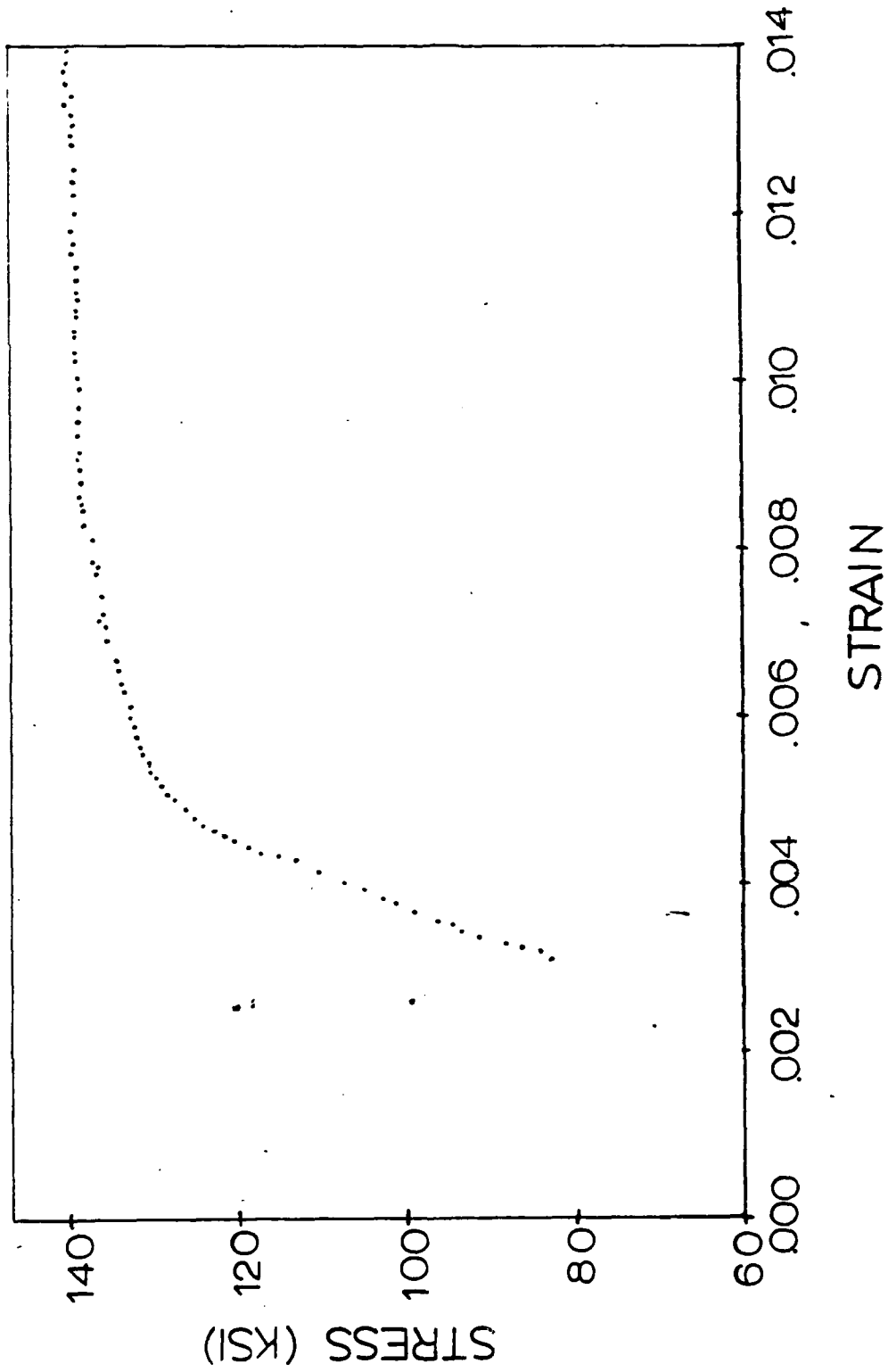


Figure 11. Experimental Stress-Strain Curve

three lines were taken from each graph (Figures 13 - 16) as representative of the data. At this point, for each of the four values of  $n$  (and  $Z_1$ ) there were three values of  $m$  (and  $Z_0$ ), making a total of 12 data sets to be evaluated. It was hoped that further comparison with the data would indicate which set best models the experimental results.

The determination of values for  $m$  and  $Z_0$  is presented in greater detail in Appendix C.

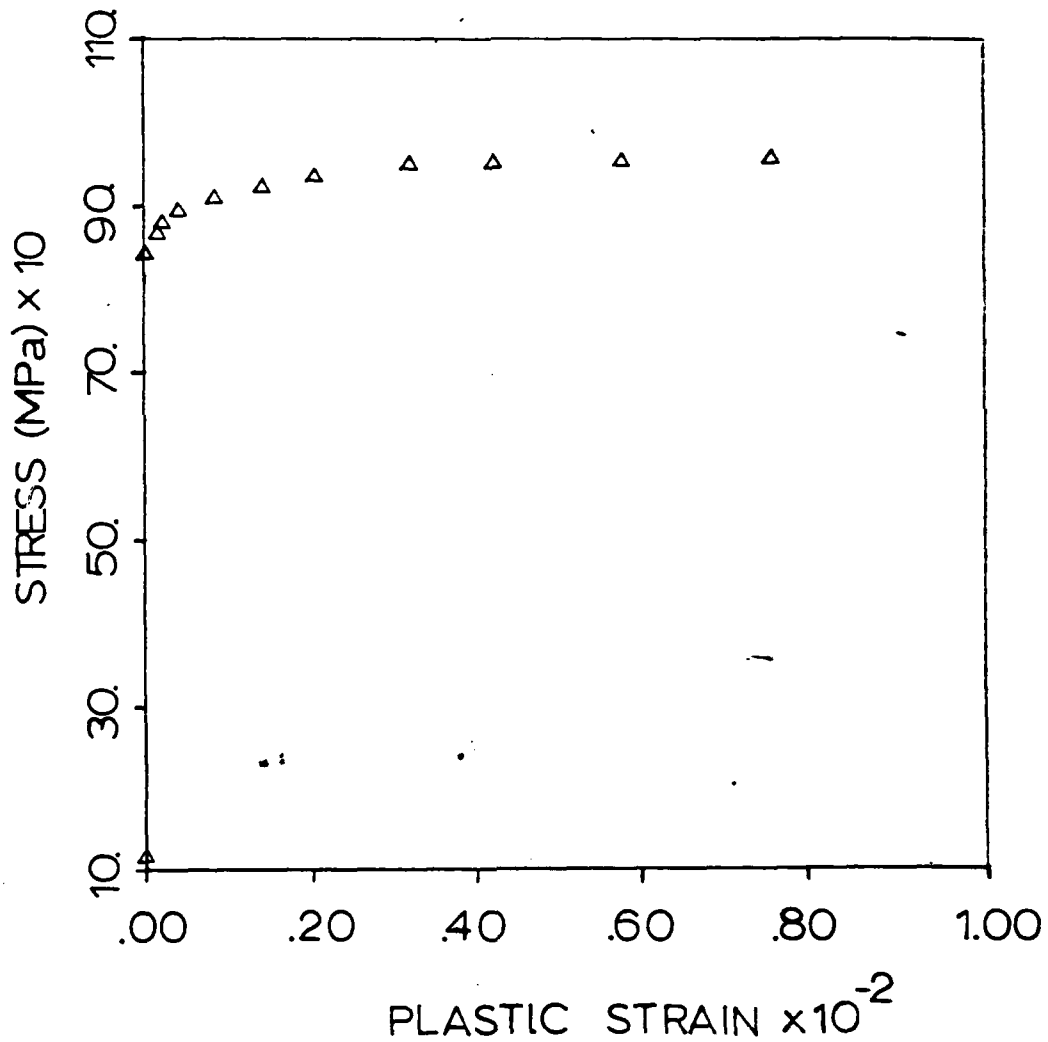


Figure 12. Stress vs Plastic Strain,  
IN 718, 1200°F,  $\dot{\epsilon} = 1.3 \times 10^{-5} \text{ sec}^{-1}$

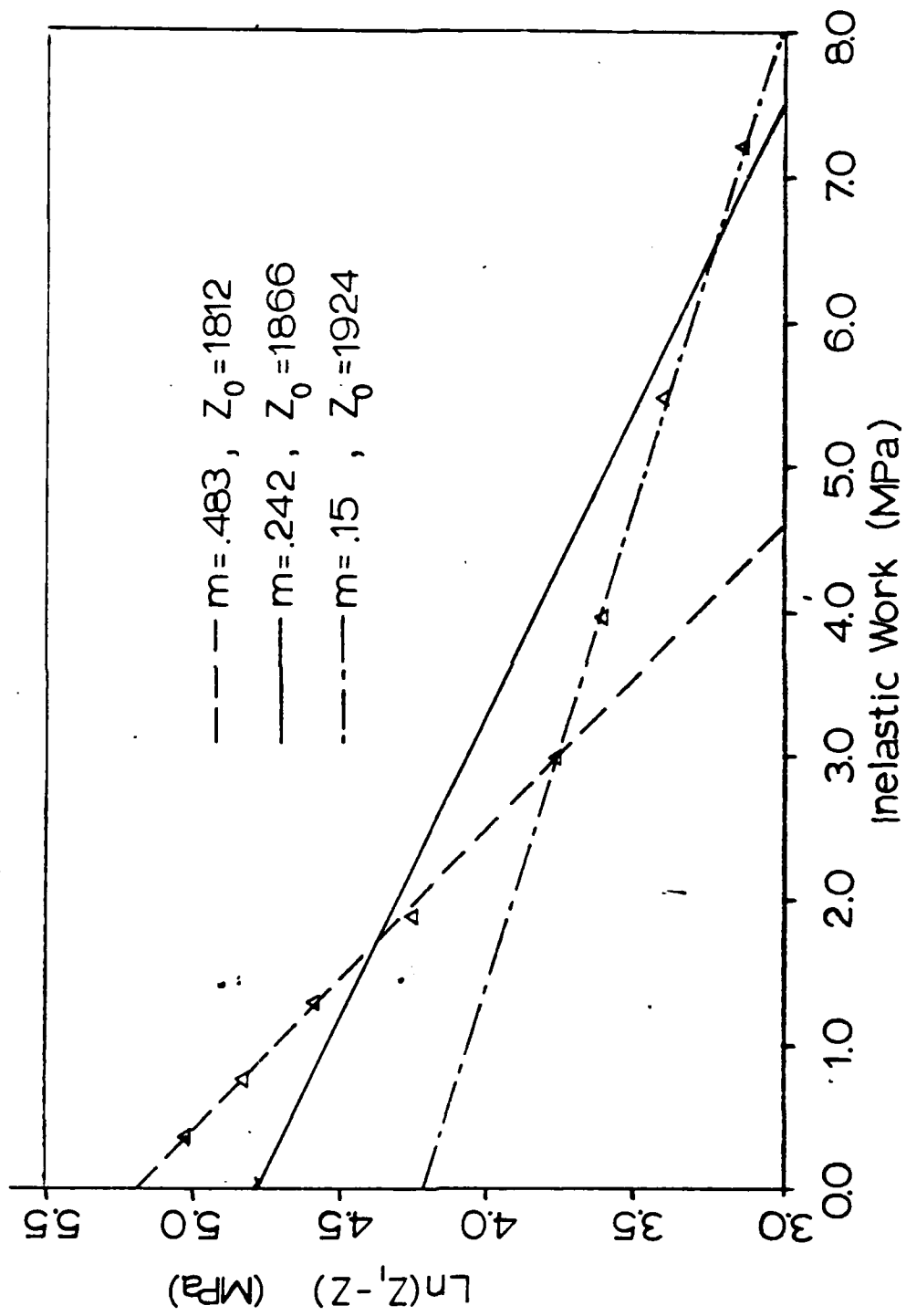


Figure 13. Determination of  $m$  and  $Z_0$ ,  $n = 2.5$

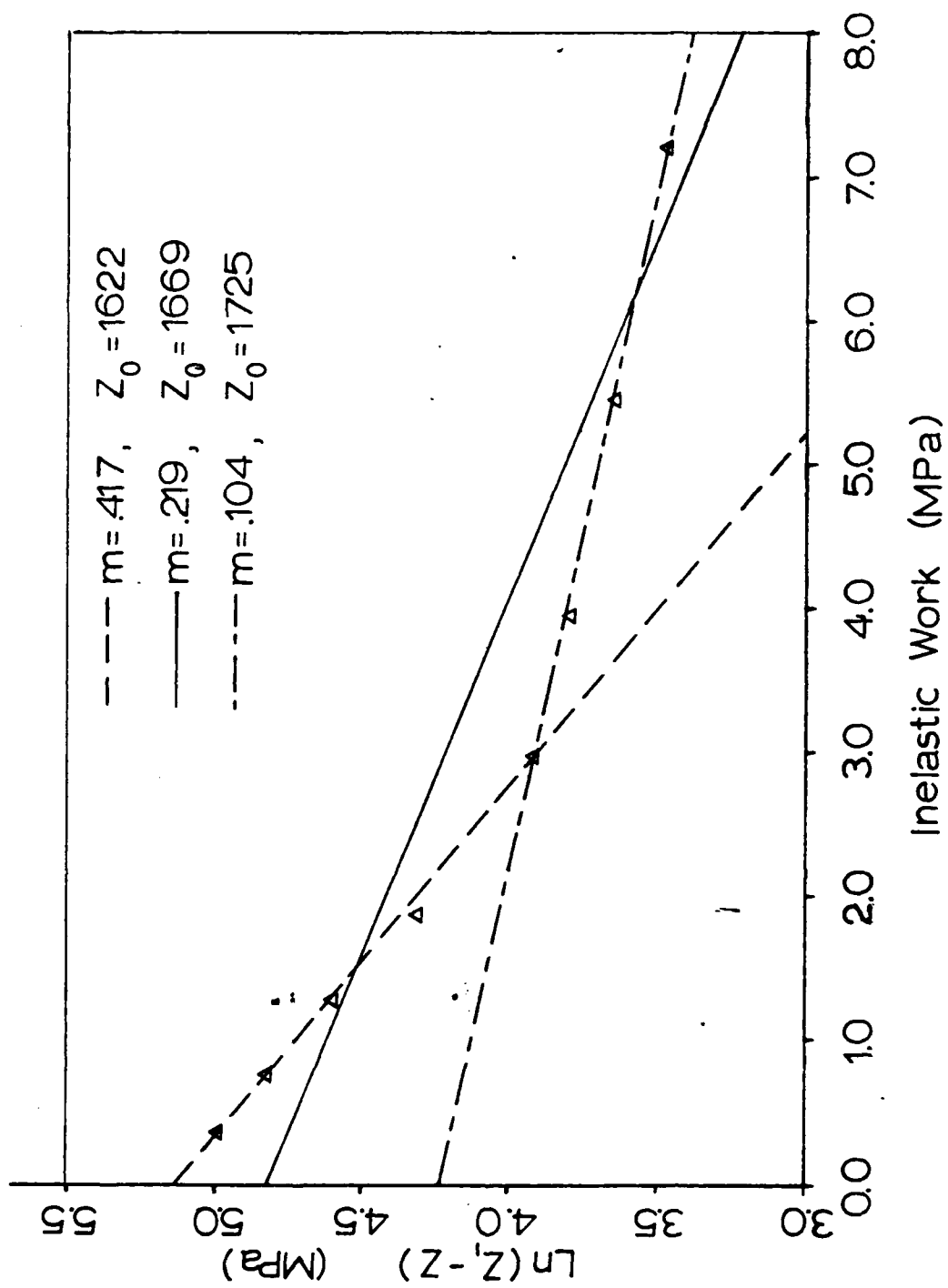


Figure 14. Determination of  $m$  and  $Z_0$ ,  $n = 3.0$



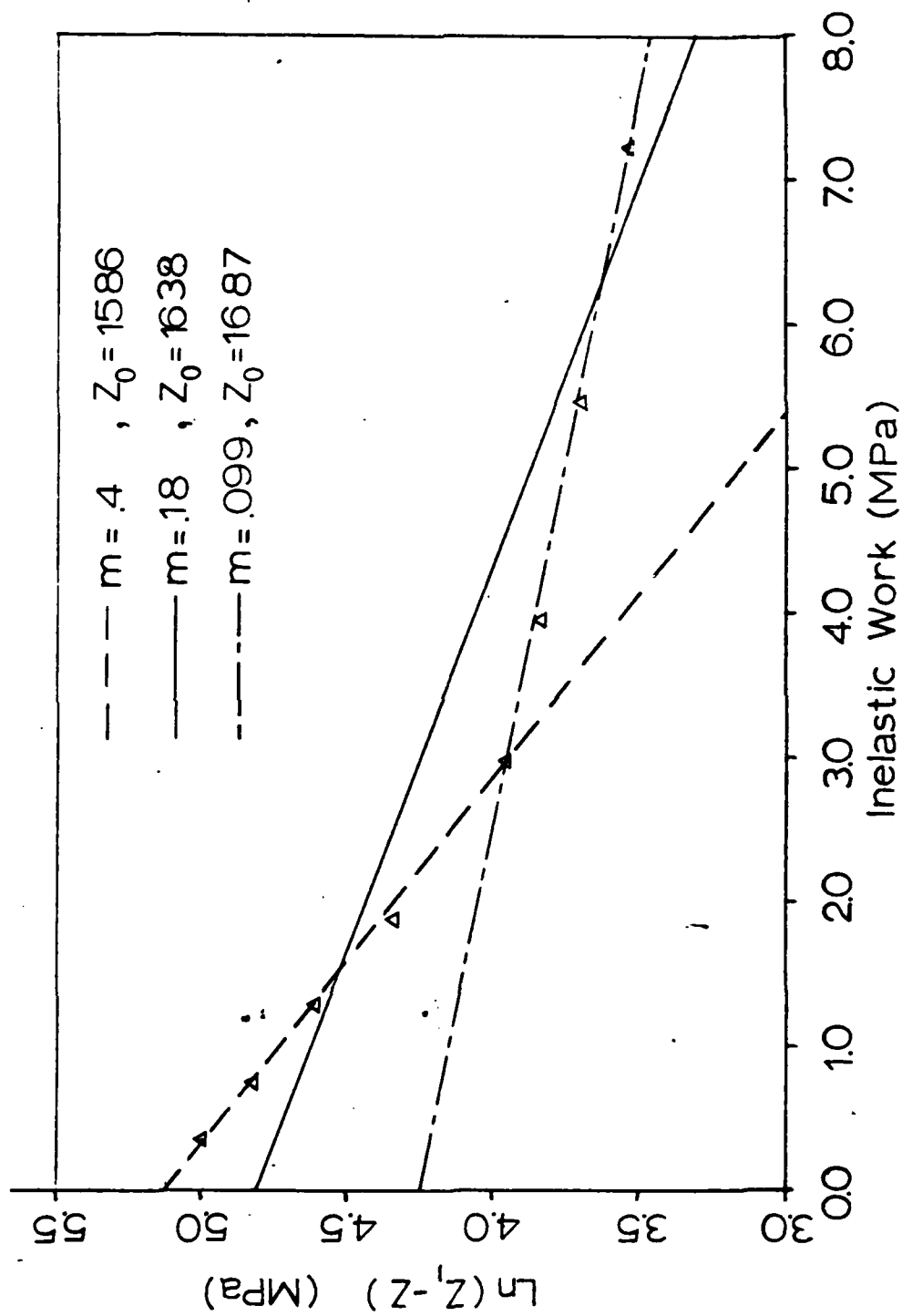


Figure 15. Determination of  $m$  and  $Z_0$ ,  $n = 3.125$

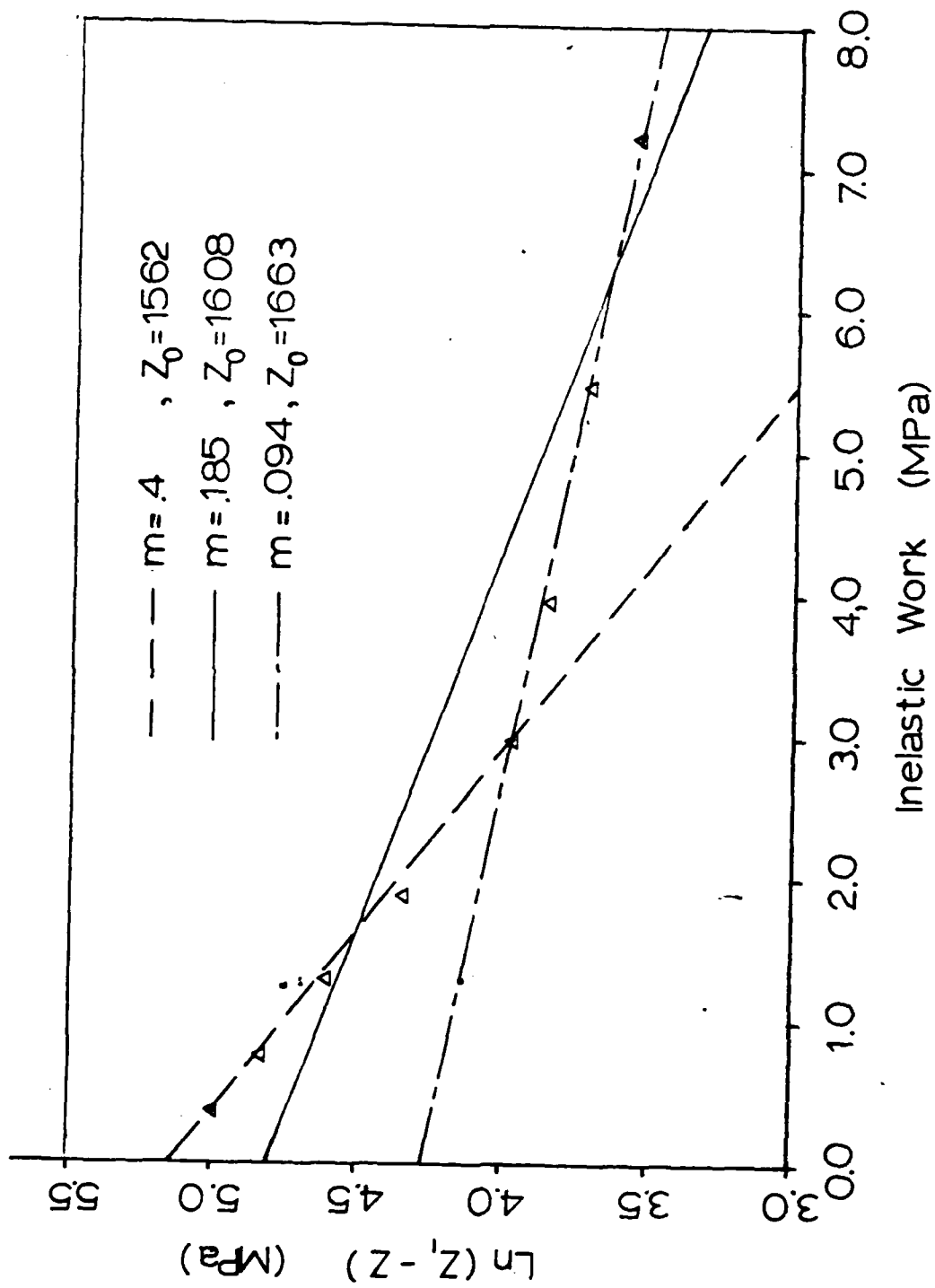


Figure 16. Determination of  $m$  and  $Z_0$ ,  $n = 3.211$

Some parametric studies were next undertaken, in an attempt to refine the selection of values for the coefficients  $n$  and  $Z_1$ . A set of dimensionless strain rate versus stress curves were prepared; the experimental data and the Bodner model predictions were plotted for each value of  $n$  and  $Z_1$ . The results are contained in Figures 17 through 20. The fit of model to data in each case is measured by how nearly the curve of the model passes through the two (high strain rate, no recovery) data points indicated by arrows. In each case, the fit is quite good. Within the limits on accuracy imposed by the graphical techniques employed, all values are arguably adequate.

Stress-strain curves were used next to compare the model predictions with the data in another fashion. Values for  $A$ ,  $r$ , and  $Z_2$  were selected without too much concern for their accuracy; because these coefficients appear only in the recovery term of Equation (15), they do not impact material behavior at strain rates too fast for recovery to be significant. This is illustrated in the studies of Figures 48, 49, 51, 52, 54, and 55. Using the different values of  $n$ , stress-strain curves were then drawn to investigate whether varying  $n$  had any effect on the stress-strain curve of the model. The results, contained in Figure 1, show that the four curves are barely distinguishable from one another.

Because there was apparently no basis in the data for discriminating between the four values of  $n$  and  $Z_1$ , the value of  $n = 3.0$  was selected simply for the convenience provided by an integer value. This choice is rather arbitrary; comparison with available data show only that the model predictions based on  $n = 3.0$  fit the data as well as the predictions based on any other  $n$  value under consideration.

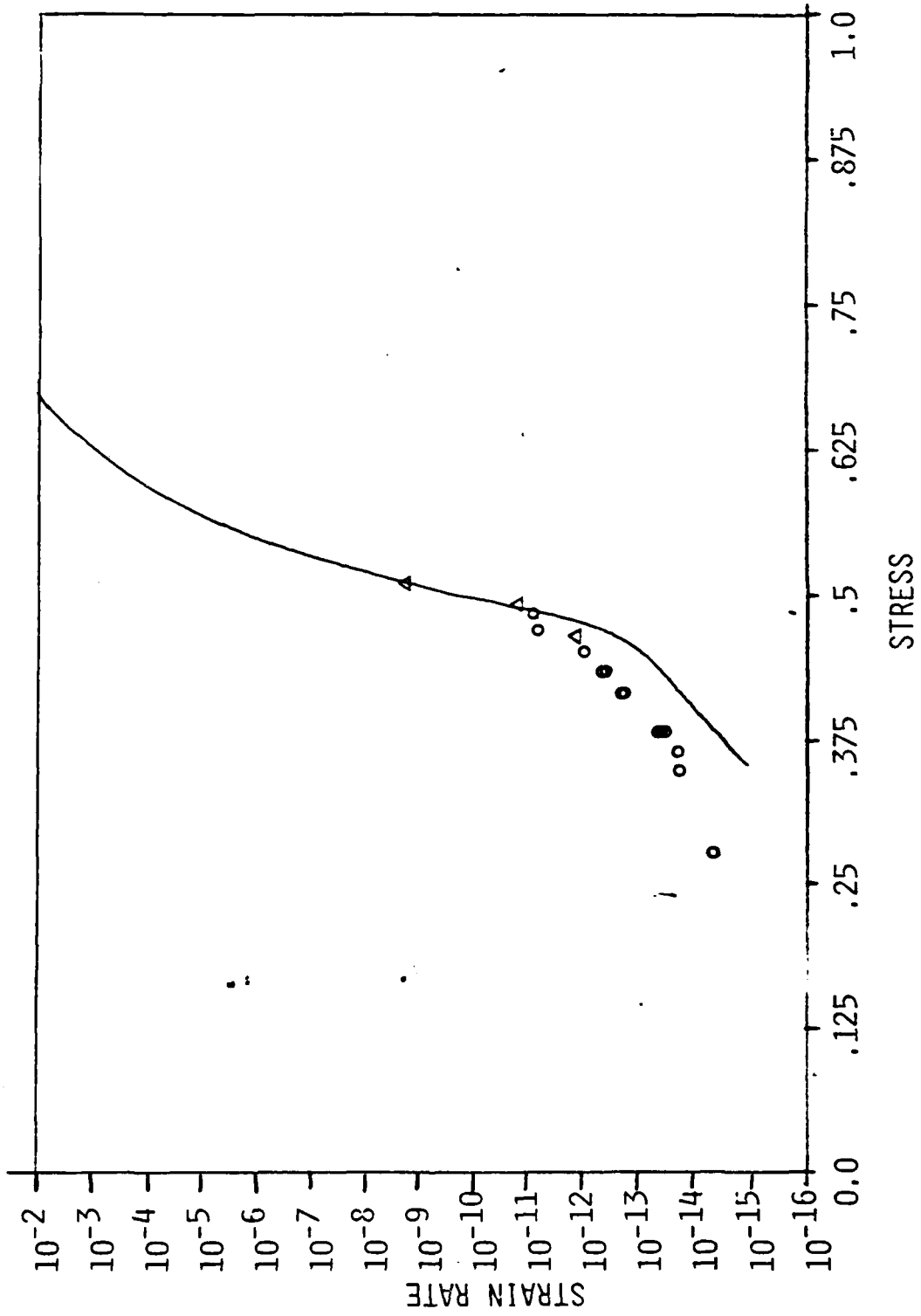


Figure 17. Fit of Bodner Model to High Strain Rate Data,  $n = 2.5$

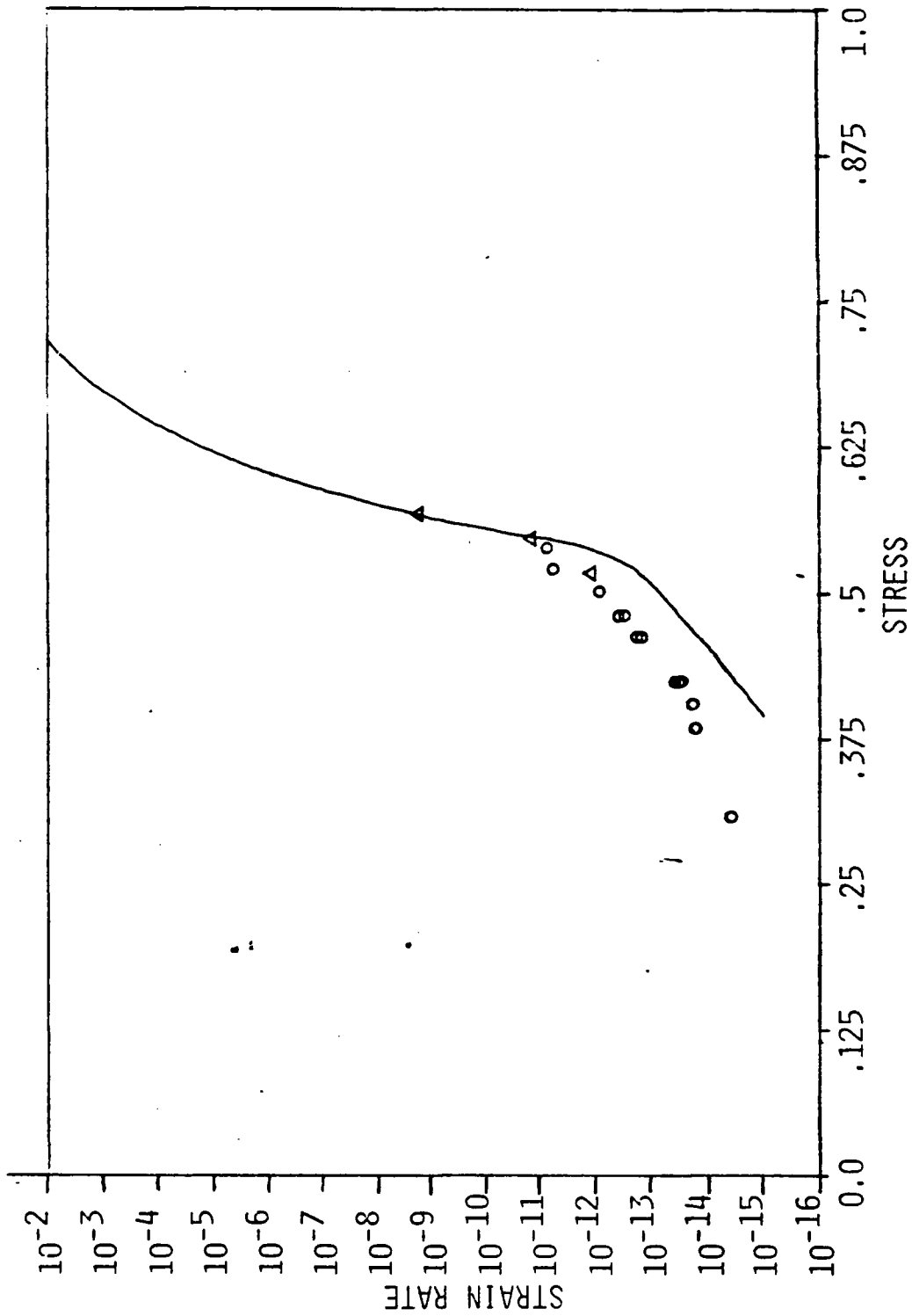


Figure 18. Fit of Bodner Model to High Strain Rate Data,  $n = 3.0$

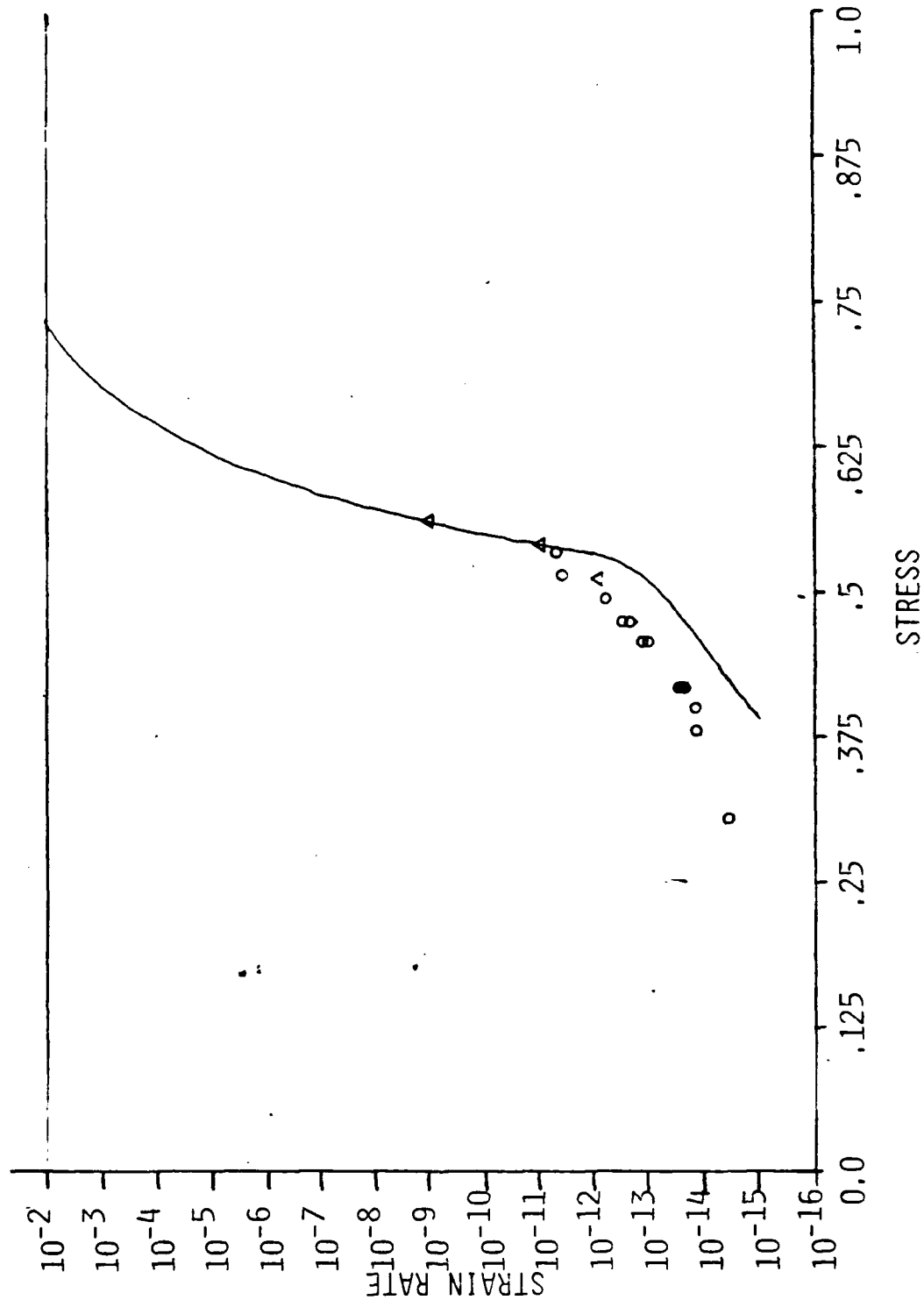


Figure 19. Fit of Bodner Model to High Strain Rate Data,  $n = 3.125$

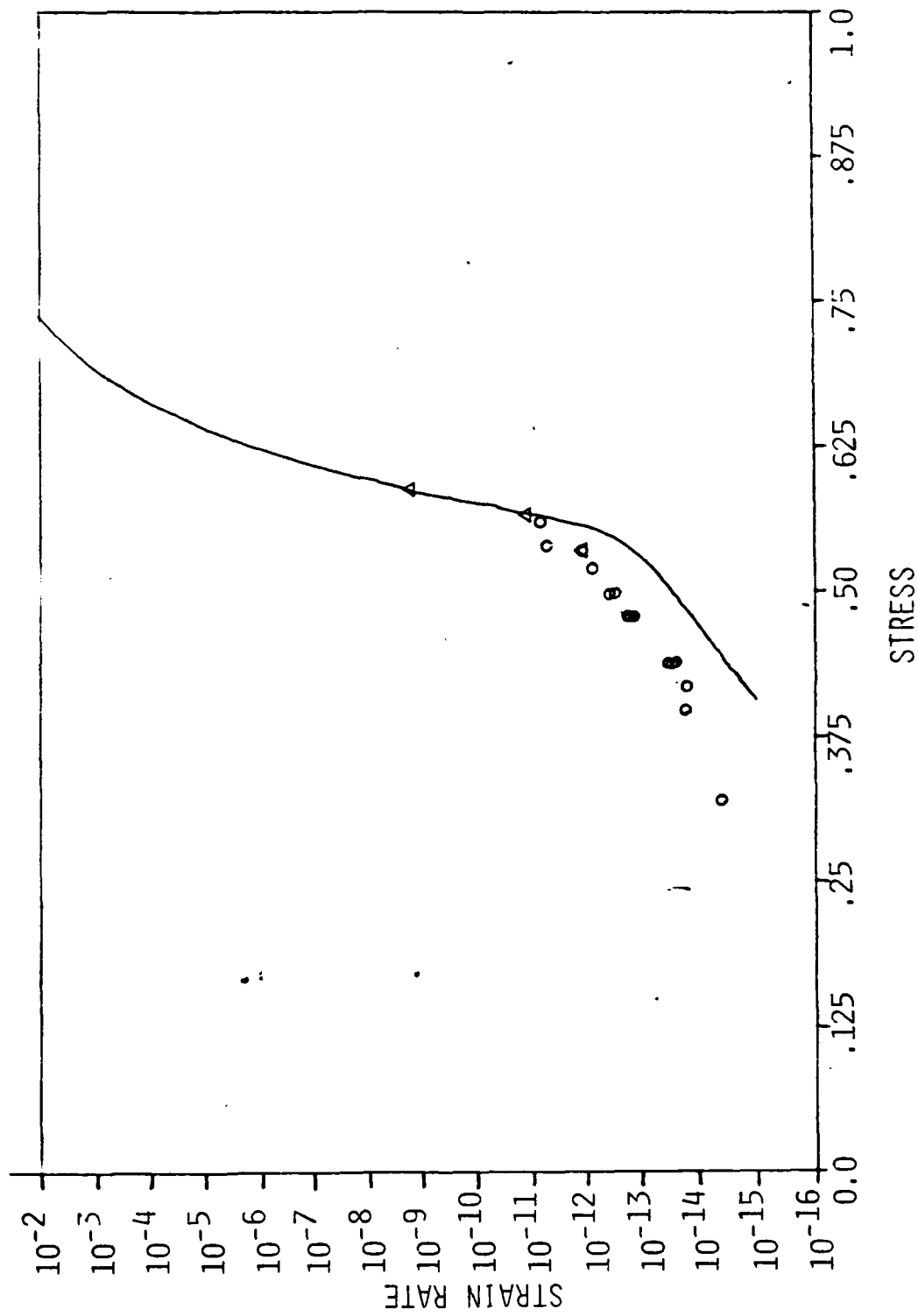


Figure 20. Fit of Bodner Model to High Strain Rate Data,  $n = 3.211$

The data base used in this work provided only two points ( $\dot{\epsilon} = 1.3 \times 10^{-5} \text{ sec}^{-1}$  and  $\dot{\epsilon} = 1.6 \times 10^{-3} \text{ sec}^{-1}$ ) with which to evaluate  $n$  and  $Z_1$ . Having a third data point -- at, say,  $\dot{\epsilon} = 1.0 \times 10^{-4} \text{ sec}^{-1}$  -- would have allowed significantly more confidence in the values thus established for  $n$  and  $Z_1$ . The relatively strain rate insensitive behavior of IN 718 under the conditions of these tests allowed appropriate coefficient values to be determined from only two data points. For a more strain rate sensitive material, however, the exact determination of coefficient values would likely require at least three appropriate data points.

With a value of  $n = 3.0$  and the corresponding  $Z_1$  value selected, the material behavior predicted by the Bodner model for the three values of  $m$  (and  $Z_0$ ) were compared with the data. It is apparent from these results, presented in Figure 21, that the choice of values for  $m$  and  $Z_0$  significantly impact the shape of the model's predicted stress-strain curve. If the  $m$ - $Z_0$  values suggested by the steepest line fit of Figure 14 (which corresponds to  $m = .417 \text{ MPa}^{-1}$  and  $Z_0 = 1622 \text{ MPa}$ ) are used, the front of the model's stress-strain curve in Figure 21 fits the experimental data more closely. If the shallowest line fit of Figure 14 is used (corresponding to  $m = .105 \text{ MPa}^{-1}$  and  $Z_0 = 1725 \text{ MPa}$ ), then the back of the stress-strain curve fits the data more closely. And if the "mean" line of Figure 14 is used ( $m = .219 \text{ MPa}^{-1}$  and  $Z_0 = 1669 \text{ MPa}$ ) the resulting stress-strain curve doesn't quite fit the data either at the front or the back, but it isn't too far off in either place.

The values of  $m$  and  $Z_0$  which enabled the model to closely fit the front of the stress-strain curve were selected as the best fit. The material behavior in the smaller strain range is of greater engineering



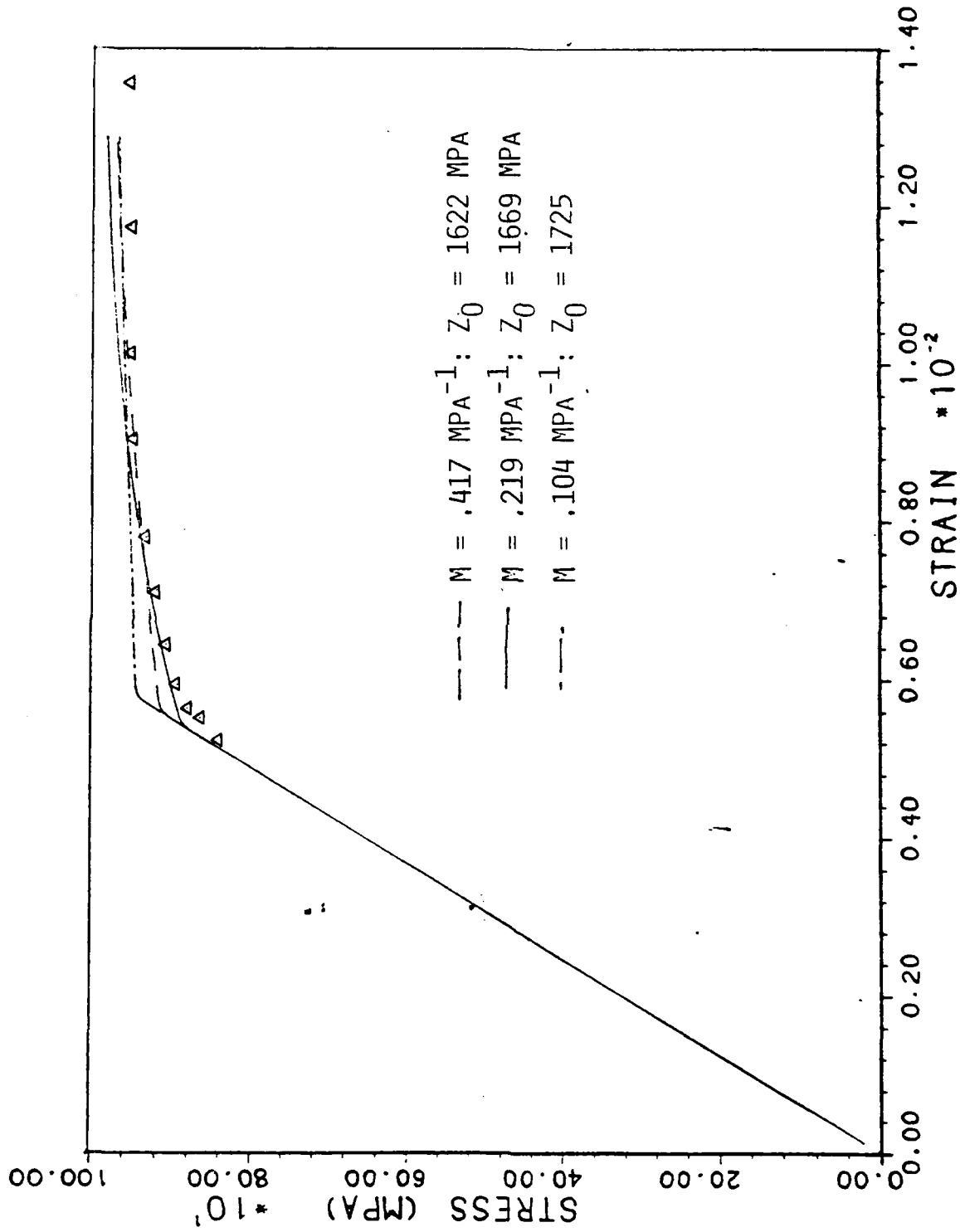


Figure 21. Determination of  $m$  and  $Z_0$ : Fit of Model to Stress-Strain Data

interest; in cases of cyclic loading this is the range of strains that is most likely to be studied. Recognizing that material behavior predicted by the model for large strains will not likely fit experimental data very well, values of  $m = .417 \text{ MPa}^{-1}$  and  $Z_0 = 1622 \text{ MPa}$  were selected as representative of the material.

After values were determined for  $A$ ,  $r$ , and  $Z_2$ , the matter of appropriate values for  $m$  and  $Z_0$  was again examined. Analytical predictions according to the Bodner model of material behavior in creep tests were compared with experimental data. Coefficient values depending on the "front" fit of Figure 14 ( $m = .417 \text{ MPa}^{-1}$  and  $Z_0 = 1622 \text{ MPa}$ ) and values depending on the "mean" fit ( $m = .219 \text{ MPa}^{-1}$  and  $Z_0 = 1669 \text{ MPa}$ ) were both used. The results of this study are depicted in Figures 22 and 23.

Figure 22 shows the Bodner model predictions under a 135 KSI load using both the "front" fit values of  $m$  and  $Z_0$  and the "mean" fit values. Under this load, the "mean" fit values provide a very good model of the secondary creep strain rate -- better than that provided by the "front" fit values of  $m$  and  $Z_0$ . Yet Figure 23 -- which depicts the same information as in Figure 22 except the load is 140 KSI -- shows that neither pair of values gives a very accurate model of the measured material behavior. The inaccuracies caused by the curve fitting techniques on semi-log axes are revealed here; an error in predicted strain rate of the same order as the strain rate is as good as can be expected. It would appear that creep behavior does not lend itself to use in evaluating  $m$  and  $Z_0$  values.

With values selected for  $n$ ,  $m$ ,  $Z_0$  and  $Z_1$ , parametric studies were again used to determine appropriate values for the recovery coefficients,

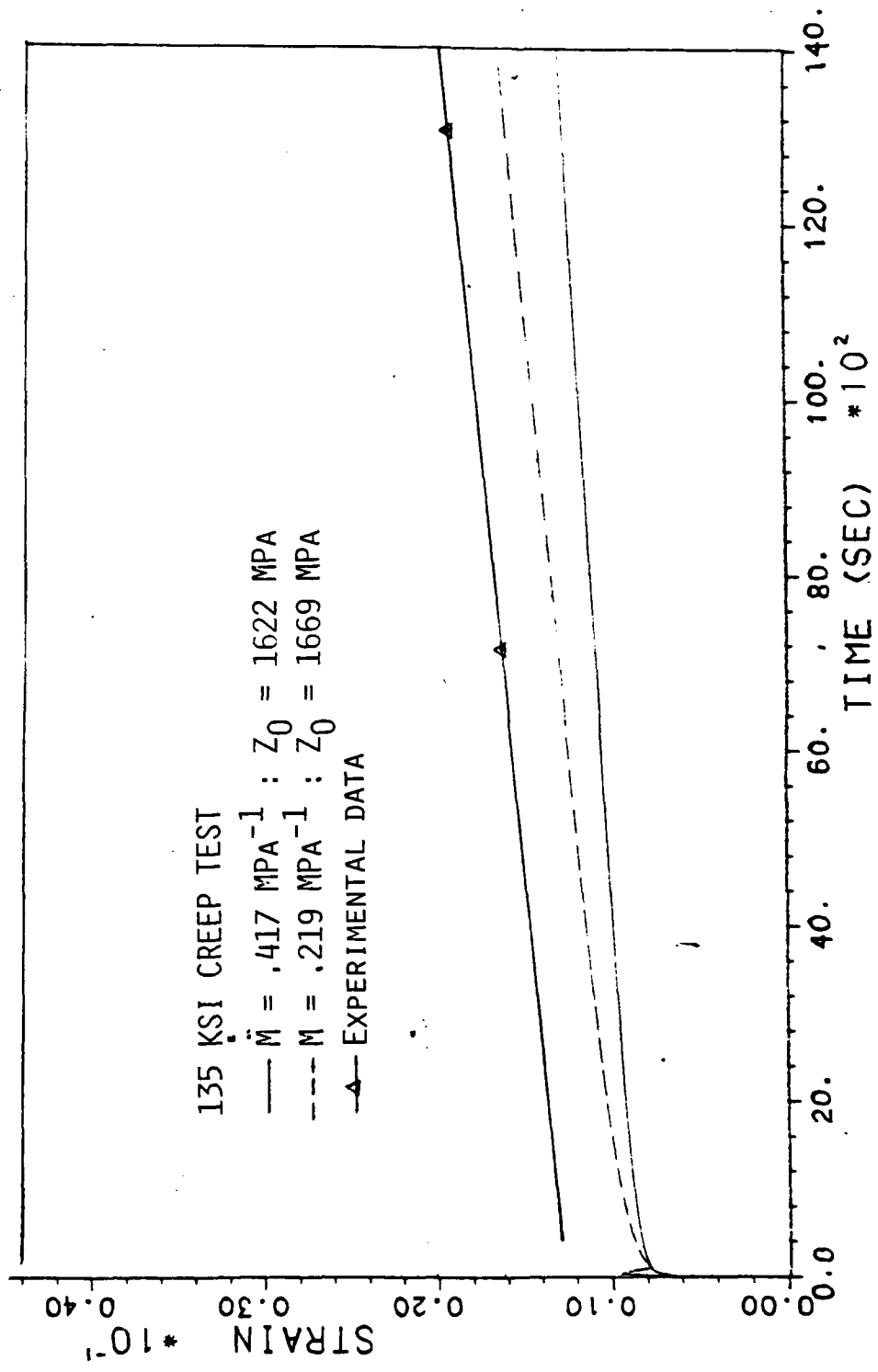


Figure 22. Creep Curves: Comparison of Bodner Model With Data

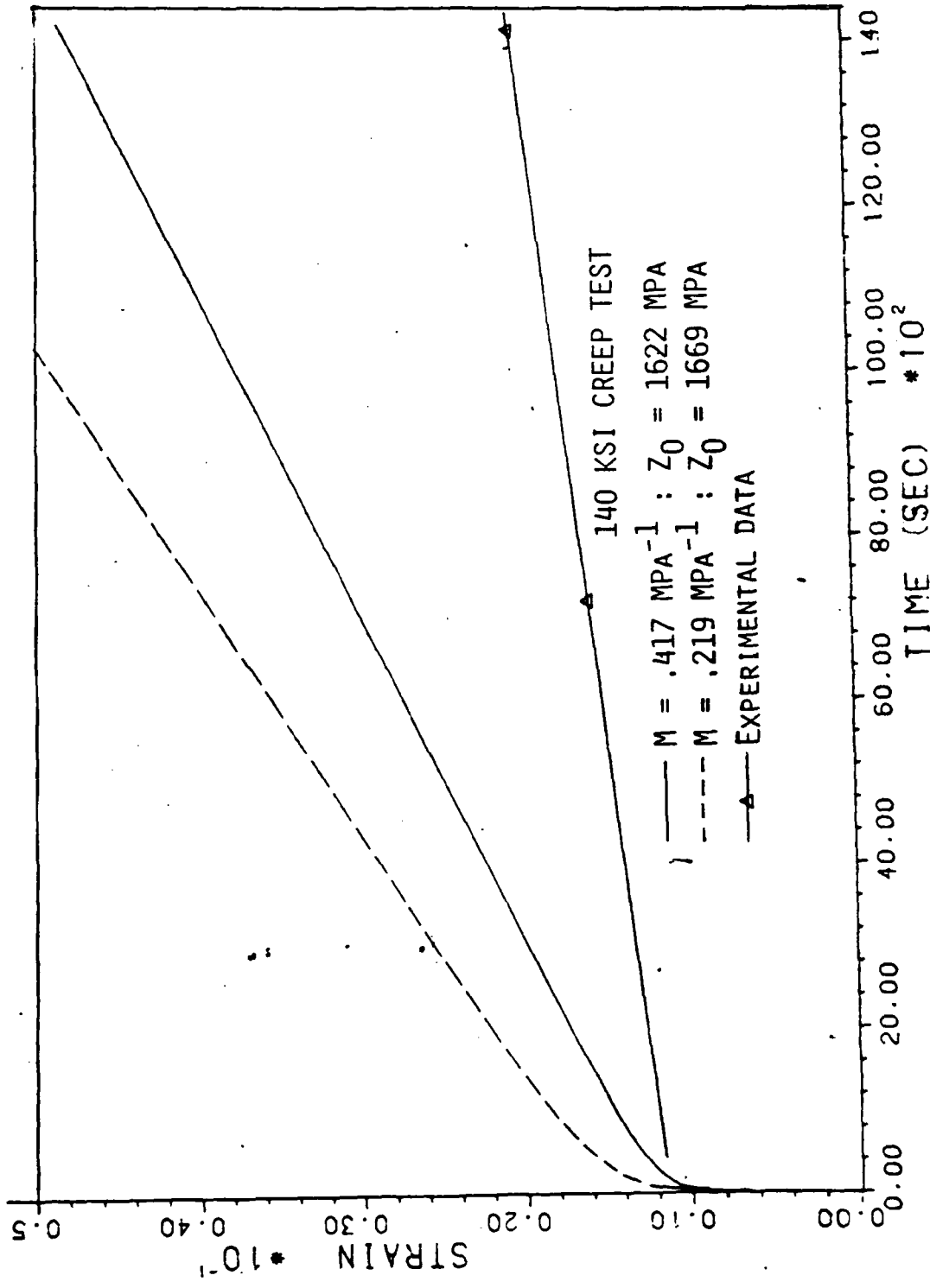


Figure 23. Creep Curves: Comparison of Bodner Model With Data

A,  $r$ , and  $Z_2$ . The general behavior of A,  $r$ , and  $Z_2$  are illustrated in Figures 6, 7, and 8. It was decided to fit A to the data first, then  $Z_2$ , and lastly  $r$ , using the strain rate versus stress presentation to establish the appropriate coefficient values.

The coefficient A controls the onset of significant recovery effects. Figure 24 presents the parametric study used to select a value of  $A = .0015 \text{ sec}^{-1}$ .

The coefficient  $Z_2$  controls where the very low strain rate material behavior becomes strain rate insensitive once more. This region of the strain rate versus stress curve is of little interest in practical engineering applications, and without a significantly more extensive data base an accurate value of  $Z_2$  cannot be established. For the purpose of these applications it is sufficient that the return to strain rate insensitive behavior occur below the strain rate range of the data. Figure 25 contains the parametric study done on  $Z_2$  at this point; a value of  $Z_2 = 718 \text{ MPa}$  was chosen. If a smaller value had been selected, the curve would have indicated a return to strain rate insensitive behavior at an even lower strain rate. This would not have affected the ability of the Bodner model to predict material behavior. The only effect would have been to change the value selected for  $r$  -- since  $Z_2$  also affects the slope of the center portion of the curve.

The coefficient  $r$  controls the slope of the mid-section of the strain rate versus stress curve. Figure 26 contains the parametric study used to arrive at the value  $r = 7.0$ .

At this point a complete data set has been determined. It is tabulated in Table IV. The fit of the Bodner model to the experimental

TABLE IV

Coefficient Values for the Bodner Model, IN 718, 1200°F

Coefficient	Description	Value
$D_0$	Limiting value shear strain rate	$10^6 \text{ sec}^{-1}$
$n$	Strain rate sensitivity parameter	3.0
$m$	Rate of work hardening	$.417 \text{ MPa}^{-1}$
$Z_0$	Initial value of hardness	1622 MPa
$Z_1$	Saturation hardness	1795 MPa
$Z_2$	Minimum recoverable hardness	718 MPa
$r$	Exponent on recovery term	7.0
$A$	Coefficient in recovery term	$.0015 \text{ sec}^{-1}$
$E$	Young's modulus	$162.5 \times 10^3 \text{ MPa}$

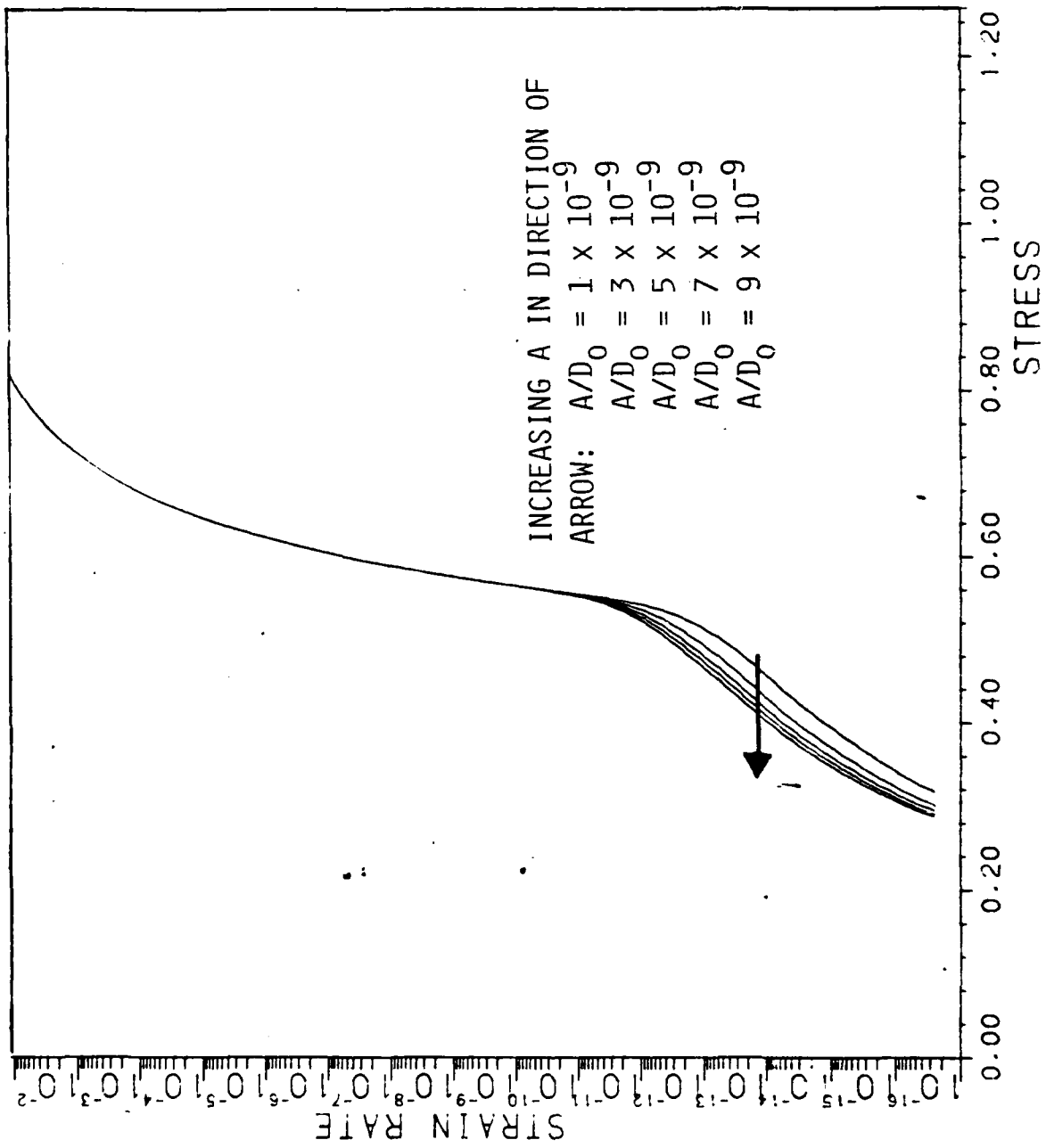


Figure 24. Parametric Study Used To Evaluate A

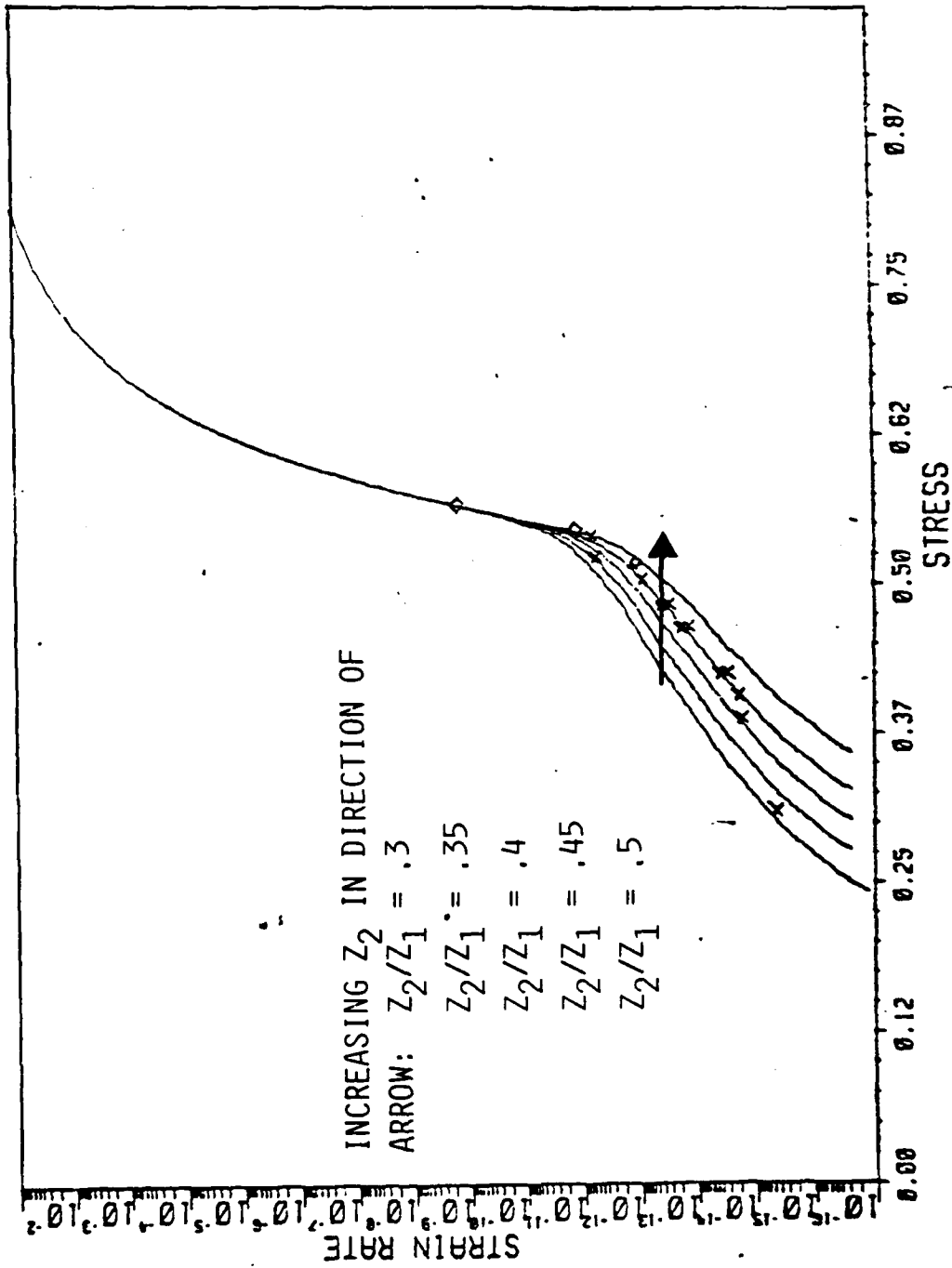


Figure 25. Parametric Study Used To Evaluate  $Z_2$



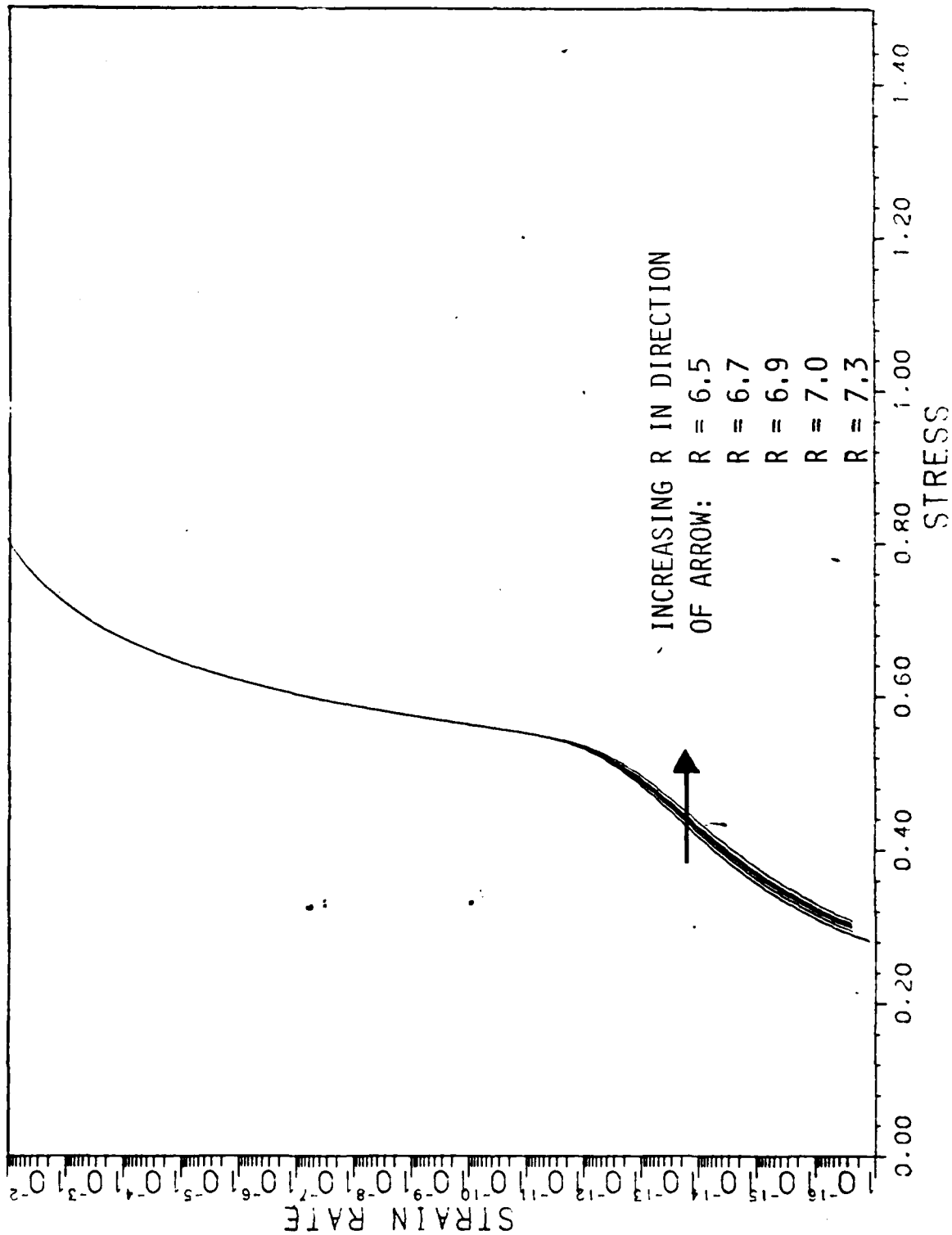


Figure 26. Parametric Study Used To Evaluate r

data using these values is presented in Figure 27.

It is apparent from this figure that no attempt was made to bring the curve predicted by the Bodner model through the two lowest data points ( $\dot{\epsilon} = 4.0 \times 10^{-9} \text{ sec}^{-1}$  and  $\dot{\epsilon} = 1.6 \times 10^{-8} \text{ sec}^{-1}$ ). The model lacks the flexibility required to bring the curve back up through those two points before it turns downward sharply in the very slow strain rate portion of the curve. The very slow strain rates associated with these points render that portion of the data less important to engineering applications; matching the rest of the data was considered adequate at this time.

Thus values were established for the coefficients of the Bodner model for Inconel 718. Figure 28 serves as a brief descriptive guide to the steps followed during the evaluation process.

Studies of material behavior under cyclic loading conditions were performed using the coefficient values determined in this work. Various strain rate and stress control situations were explored. The results of this study are discussed in the following sections.

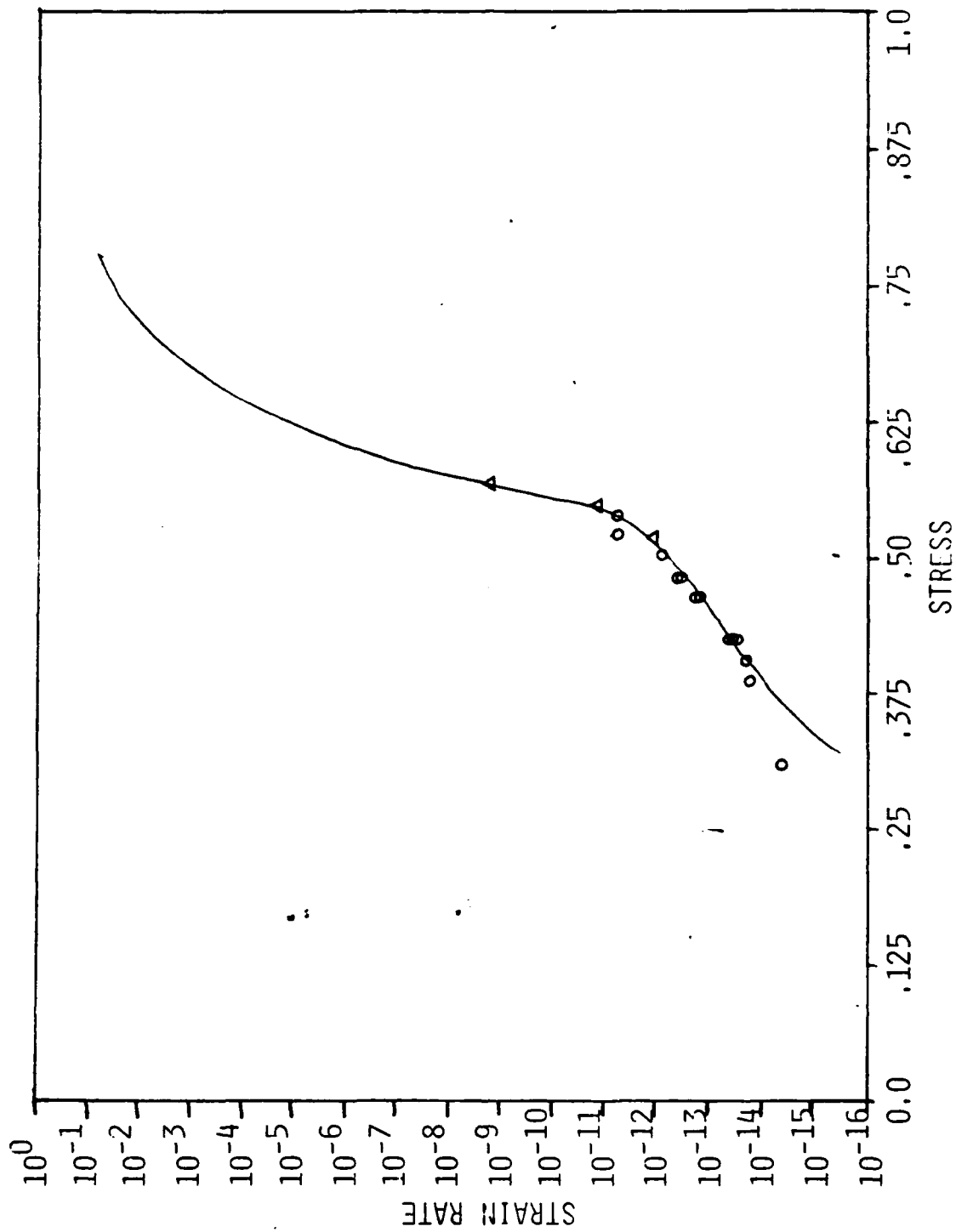


Figure 27. Fit of the Bodner Model to Data, All Coefficients Evaluated

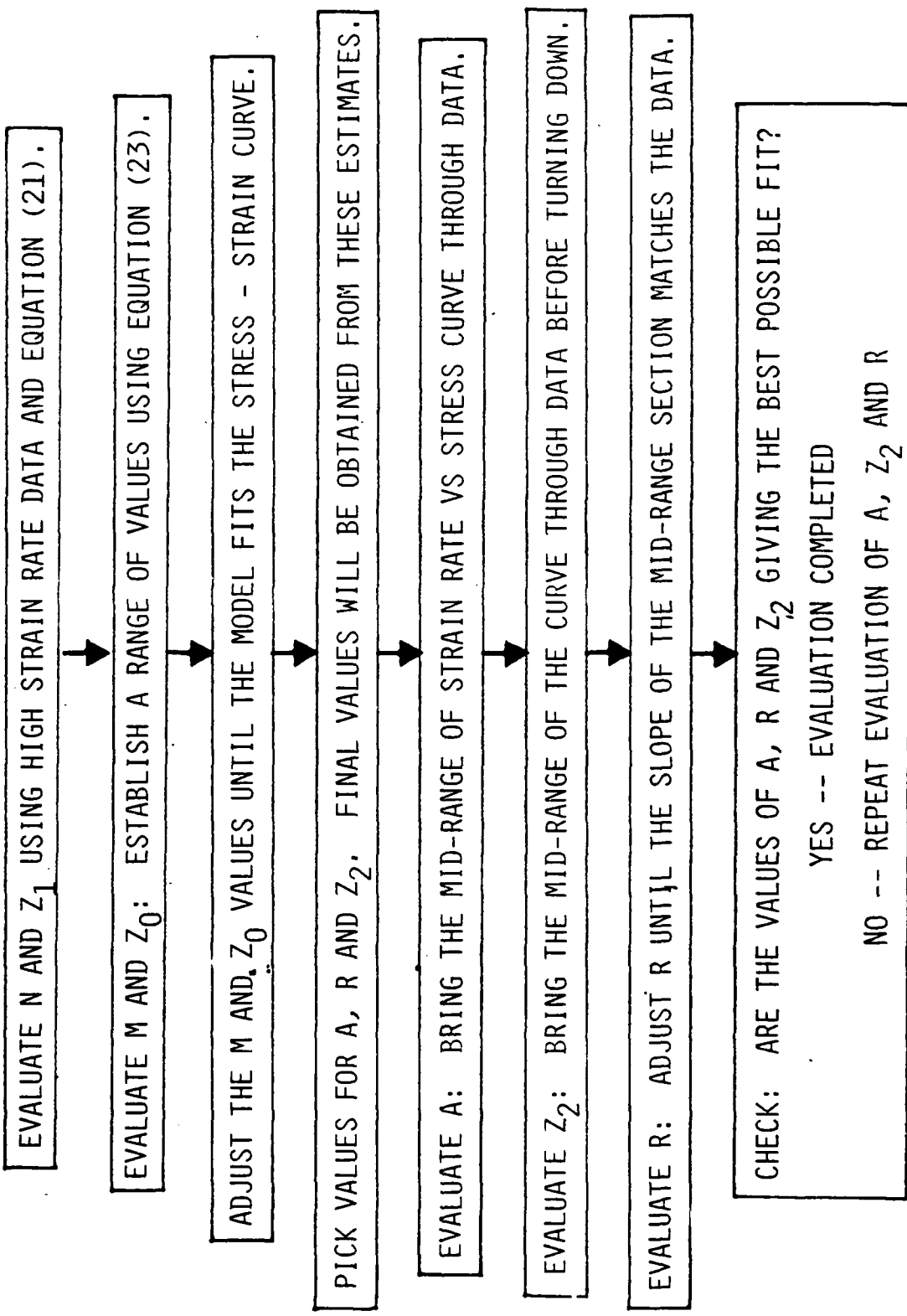


Figure 28. Procedure for Evaluating Coefficients

#### IV. Load Cycling Effects Using The Bodner Constants As Evaluated

Analytical studies were conducted of the material behavior under cyclic loading as predicted by the Bodner material model developed in previous sections. The formulation of the equations incorporated into this study is contained in Equations (16) through (20). Fully isotropic ( $q = 1$ ) and fully directional ( $q = 0$ ) strain hardening conditions were modeled. Additionally, Bodner has indicated [7] that it is possible to represent strain softening by incorporating a negative value of  $q$  into the model. This last case is interesting, for if it compares well with data then the Bodner material model is very comprehensive. It would show the model can consider the range of material characteristics from strain hardening to softening, including anisotropic plastic hardening. The results of the uniaxial analyses were compared with experimental fatigue data. This section describes in detail the cyclic loading study carried out.

Figures 29 and 30 contain experimental data obtained from the Air Force Wright Aeronautical Laboratories for IN 718 at  $1200^{\circ}\text{F}$  gathered under cyclic loading conditions. Figure 29 depicts the material behavior measured for a strain-controlled test ( $\pm .8\%$  strain) while Figure 30 depicts the material behavior measured during a stress-controlled test ( $\pm 120$  KSI). From these two figures it is clear that IN 718 exhibits some strain softening behavior. Later cycles require lower stress levels to achieve comparable strains than do earlier cycles. This phenomenon is especially prominent in Figure 29, where the stress level for maximum strain is getting smaller in absolute value for each

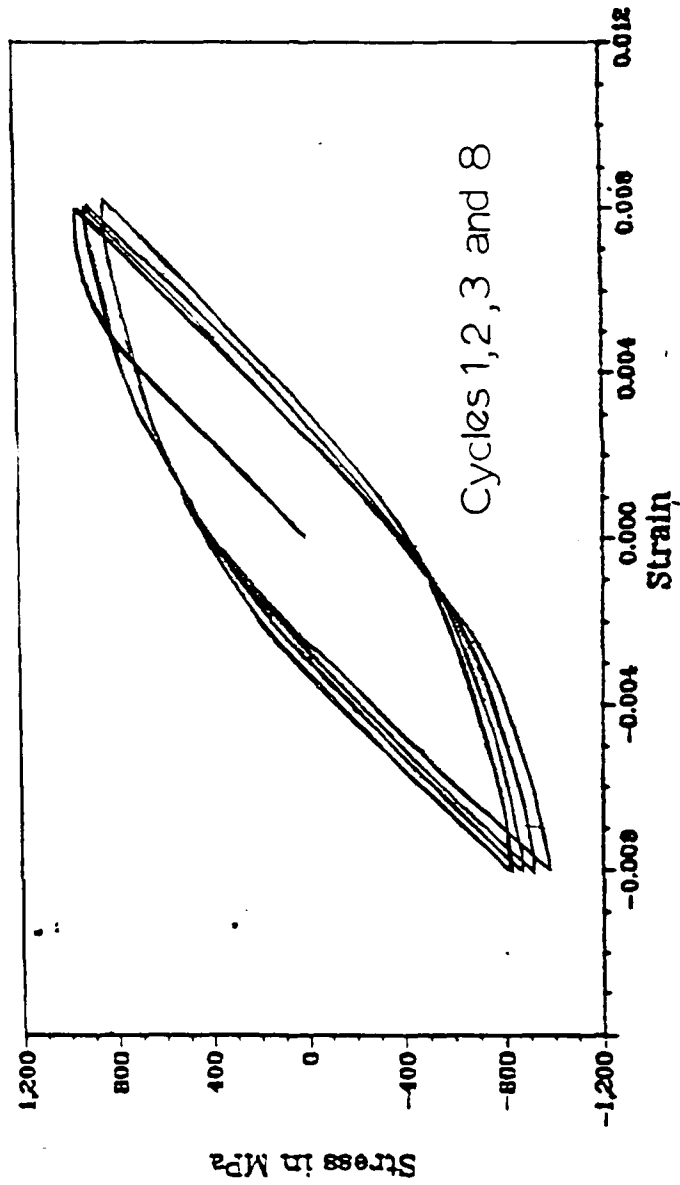


Figure 29. Experimental Cyclic Loading Data, IN 718, 1200°F (Strain Control,  $\pm .8\%$ )

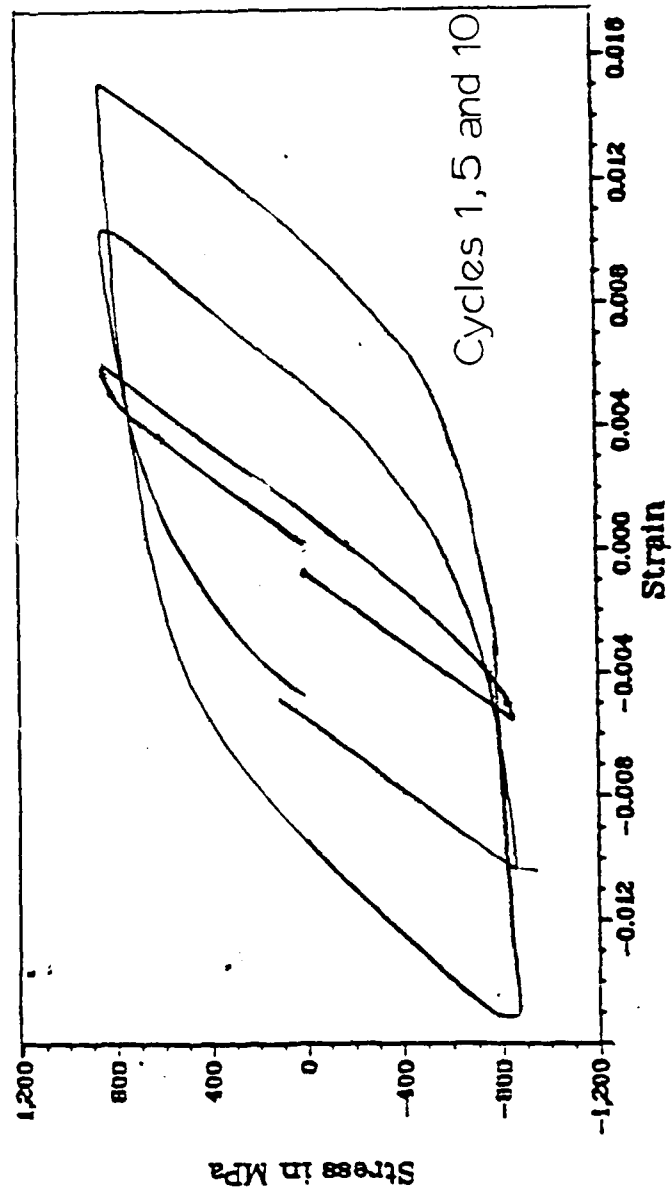


Figure 30. Experimental Cyclic Loading Data, IN 718, 1200°F (Stress Control,  $\pm 120$  KSI)

successive cycle. Figure 30 indicates that the plastic work is continuously increasing over the cycles shown. Both of these phenomena in each figure are observed over a limited number of cycles and therefore judgments that are construed are based entirely on this limited cyclic number. Further cyclic loading in particular may reduce the amount of strain softening evidenced each cycle. Figures 31 and 32 illustrate the behavior predicted by the Bodner model for IN 718 using values of  $q = 1$  (Figure 31) and  $q = 0$  (Figure 32). In both cases, the cycles repeat without change as early as the third cycle. The behavior depicted in these figures is that of strain hardening. Figure 31 shows isotropic hardening ( $q = 1$ ) while Figure 32 shows directional strain hardening ( $q = 0$ ). Comparison of these two figures with the experimental data of Figure 29 indicates that these Bodner model predictions represent the first cycle fairly well but do not indicate the softening behavior evidenced by the material. This was to be expected; values of  $q$  between zero and one imply isotropic/kinematic strain hardening, not softening.

It was suggested [7] that  $q < 0$  be used to model cases of strain softening. It is enlightening to examine what effect a negative value -- say,  $q = -.1$  -- has on the cyclic equations governing changes in hardness in this formulation (Equations (16) through (20)).

Initially, as Equation (16) indicates,

$$z^t = z^c = z_0 \quad (16)$$

Given that the initial loading is tensile, observe that

$$U_\alpha = 1 \quad (28)$$



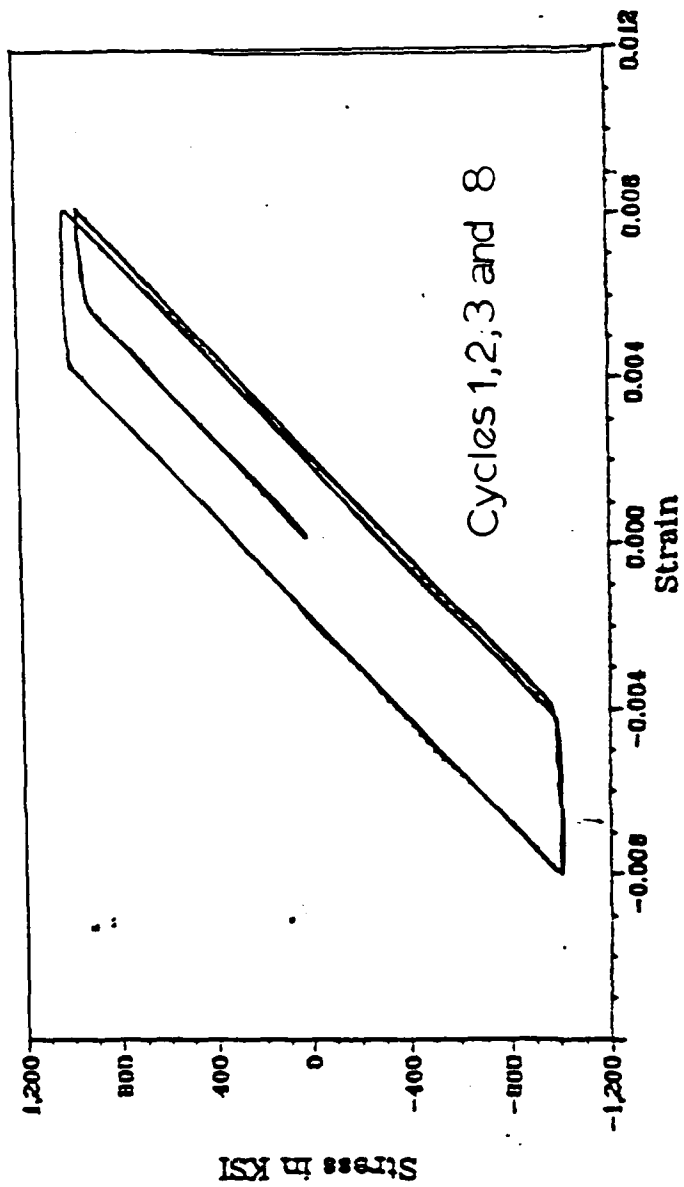


Figure 31. Bodner Model Prediction of Cyclic Loading Behavior: Strain Control,  $q = 1$

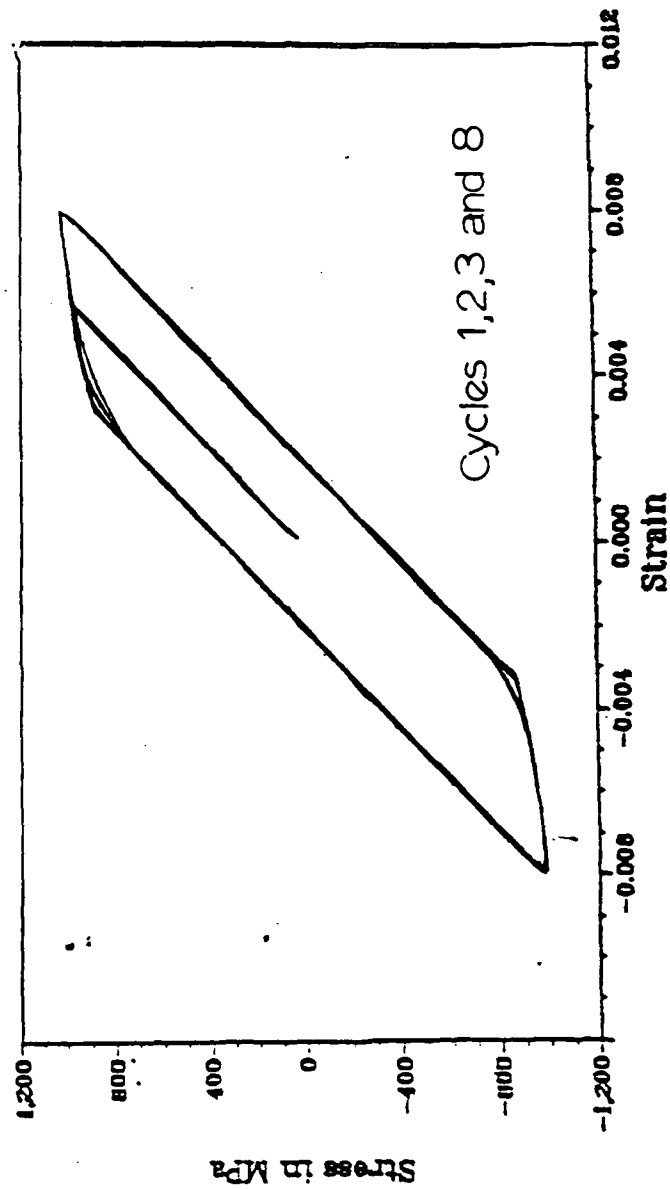


Figure 32. Bodner Model Prediction of Cyclic Loading Behavior: Strain Control,  $q = 0$

Thus the two time rates of change of hardness are

$$\dot{Z}^t = -.1 \dot{Z} + (1.1) \dot{Z} = \dot{Z}_{(1)} \quad (29a)$$

$$\dot{Z}^c = -.1 \dot{Z} - (1.1) \dot{Z} = -1.2 \dot{Z}_{(1)} \quad (29b)$$

where

$$\dot{Z}_{(1)} = m (Z_1 - Z^t) \sigma \dot{\epsilon}^p - A Z_1 \left[ \frac{Z^t - Z_2}{Z_1} \right]^r \quad (30)$$

At the end of the first loading time increment  $\Delta t$ , the two values of hardness are

$$Z_{(1)}^t = Z_0 + \dot{Z}_{(1)} \Delta t_1 \quad (31a)$$

$$Z_{(1)}^c = Z_0 - 1.2 \dot{Z}_{(1)} \Delta t_1 \quad (31b)$$

It can be seen from this that while the hardness of the specimen in tension is increasing, the hardness in compression is decreasing at a faster rate. As soon as the load becomes compressive, it is the value of  $Z^c$  that is used to express material hardness. Since this value is less than the value for  $Z^t$  at this time -- indeed, less than the original value  $Z_0$  -- it is clear that the material will be softer in compression loading subsequent to the application of the tensile load.

Figure 33 illustrates this behavior through a graph of the computer output of  $Z^t$  and  $Z^c$  over eight cycles using a value of  $q = -.1$ . The values of  $Z^t$  and  $Z^c$  were plotted every quarter cycle to show the general behavior of the hardness values without going into much detail. As the value of  $Z^t$  increases during the application of a tensile load, the value of  $Z^c$  decreases; as the value of  $Z^c$  increases during the application

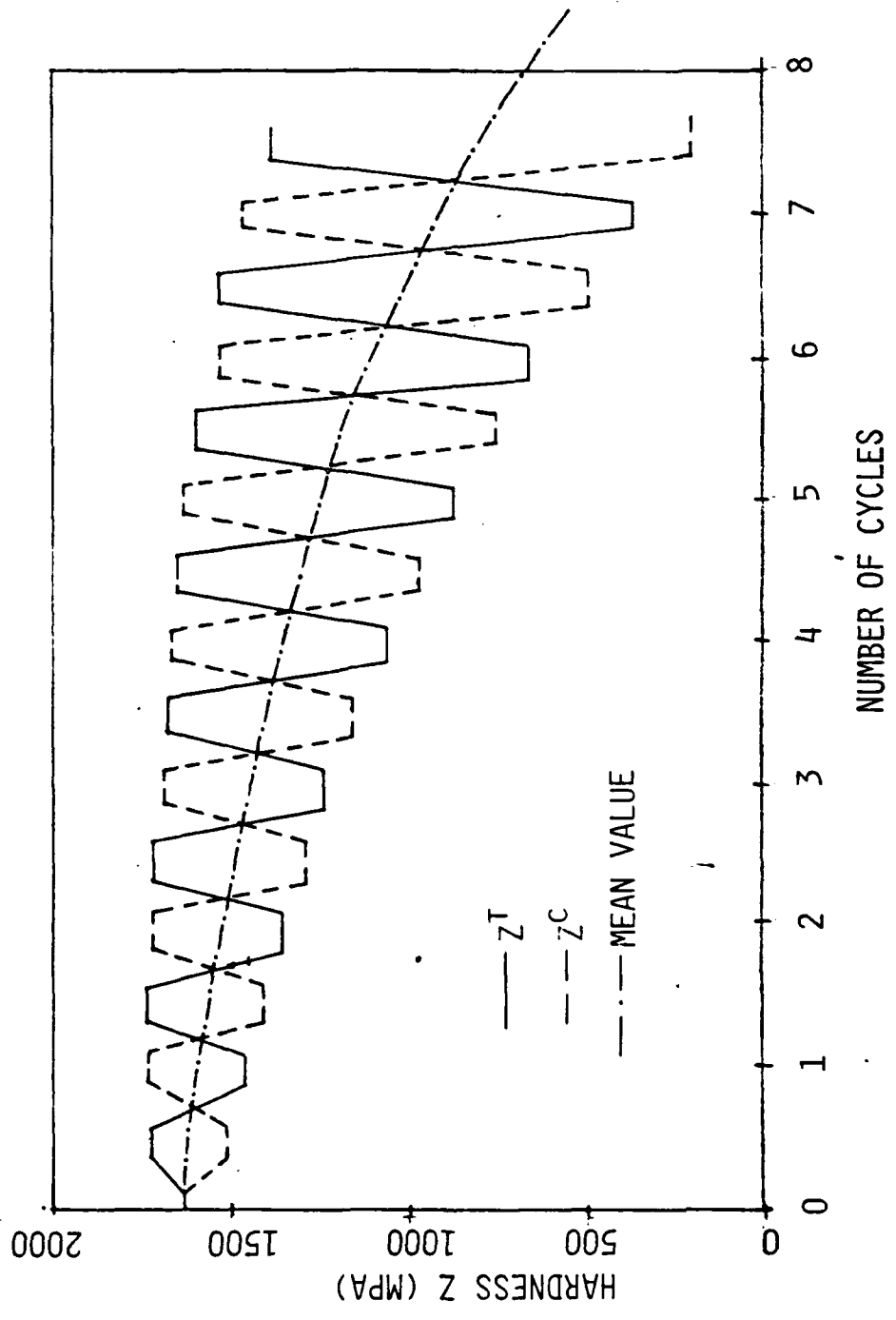


Figure 33. Behavior of  $Z^T$  and  $Z^C$  During Application of a Cyclic Load

of a compressive load, the value of  $Z^t$  decreases. And with each cycle, the average value of  $Z$  is lower. Each time  $Z^t$  and  $Z^c$  reach a minimum value, it is less than the cycle before; each time they reach a maximum value, it is less than the cycle before. This decrease in  $Z$  is what is called strain softening and it can be directly related to the character of the stress-strain curve.

Figures 34 and 35 depict the Bodner model predictions for  $q = -.05$  and  $q = -.1$ , respectively. As in the cases of  $q = 0$  and  $q = 1$ , the model's loop is quite similar to that of the data, both in size and shape. These two figures, however, possess an additional characteristic; they show clearly the strain softening trend illustrated by the experimental data. The loops do not stabilize in these early cycles; the material softening is still evidenced by both model and data in the tenth cycle. The similarity between Figure 29 and Figures 34 and 35 is striking. Small negative values of  $q$  do indeed enable the modeling of the behavior of IN 718 under a cyclic load.

Consider now the case of stress-controlled test situations. Figure 30 illustrates the experimentally measured behavior of IN 718 under a cyclic load of  $\pm 120$  KSI. The evidence of strain softening is dramatic. Figures 36 and 37 contain the Bodner model predictions for  $q = 1$  and  $q = 0$ ; not surprisingly, the model predictions do not match the data very well, overall. The early cycles are matched fairly well, but again the model's loop stabilizes where the experimental one continues to grow.

Figures 38 and 39, however, model the material behavior quite well, using values of  $q = -.05$  and  $q = -.1$ . The shape of the initial loading cycle matches the data in both size and shape. The model then goes on

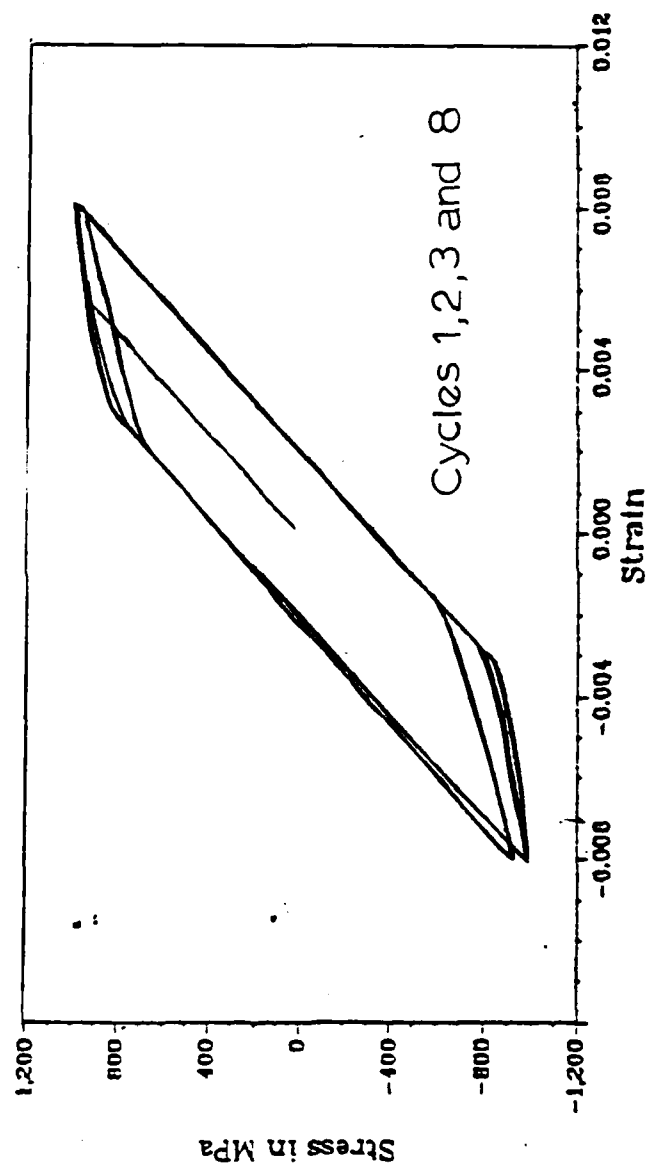


Figure 34. Bodner Model Prediction of Cyclic Loading Behavior: Strain Control,  $q = -.05$

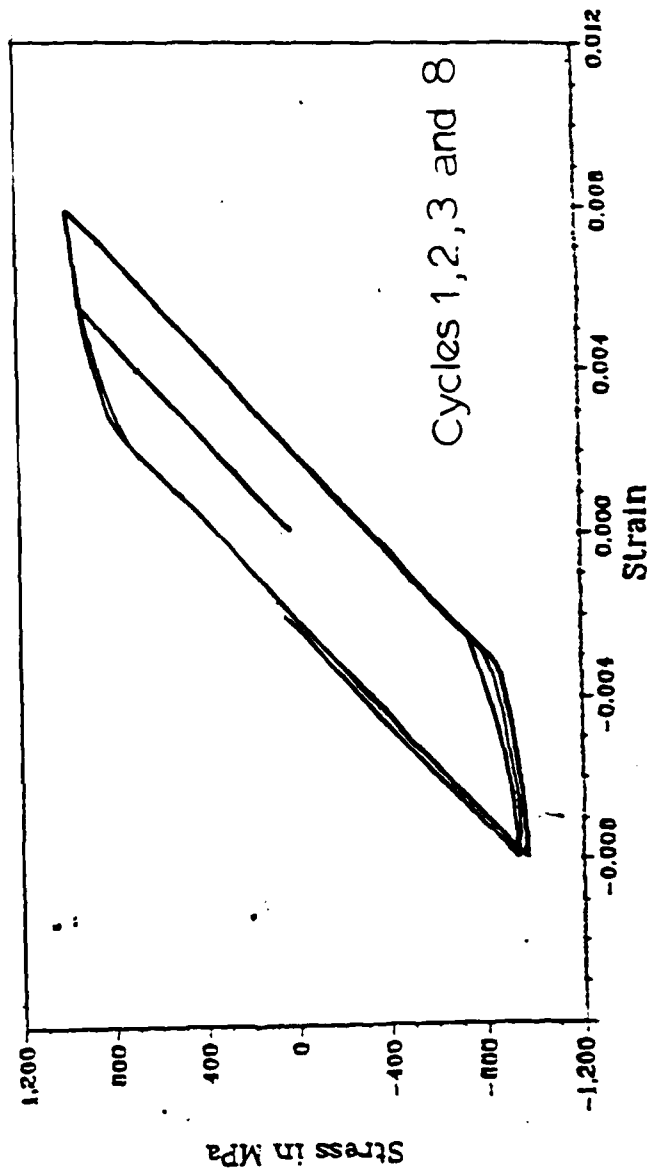


Figure 35. Bodner Model Prediction of Cyclic Loading Behavior: Strain Control,  $q = -0.1$

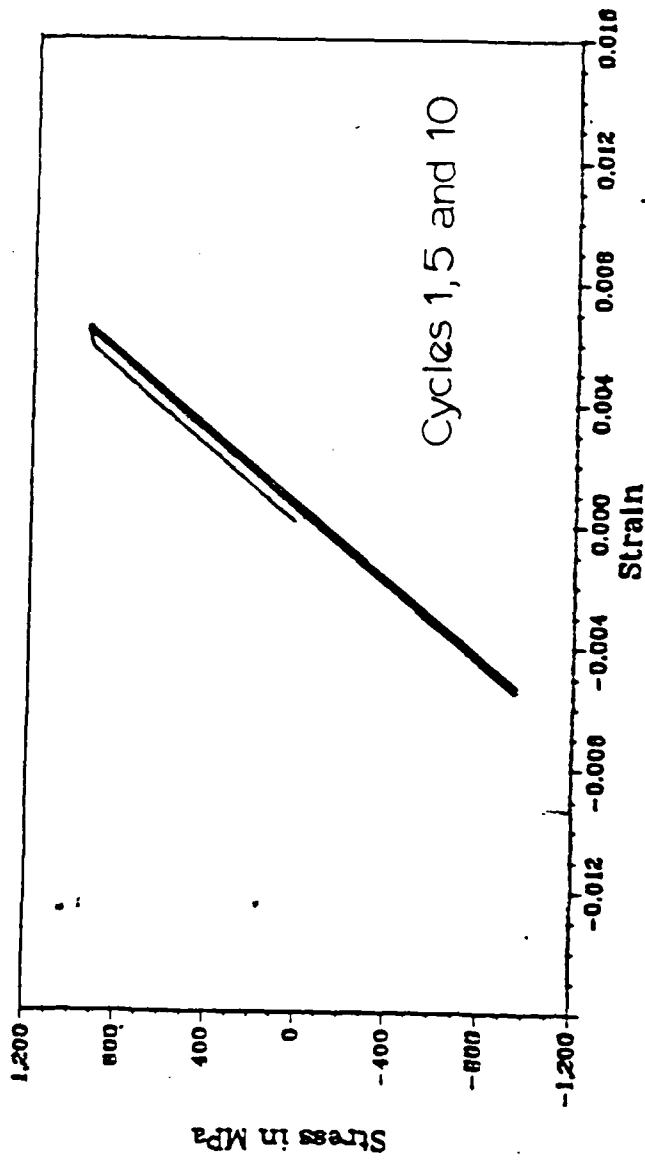


Figure 36. Bodner Model Prediction of Cyclic Loading Behavior: Stress Control,  $q = 1$



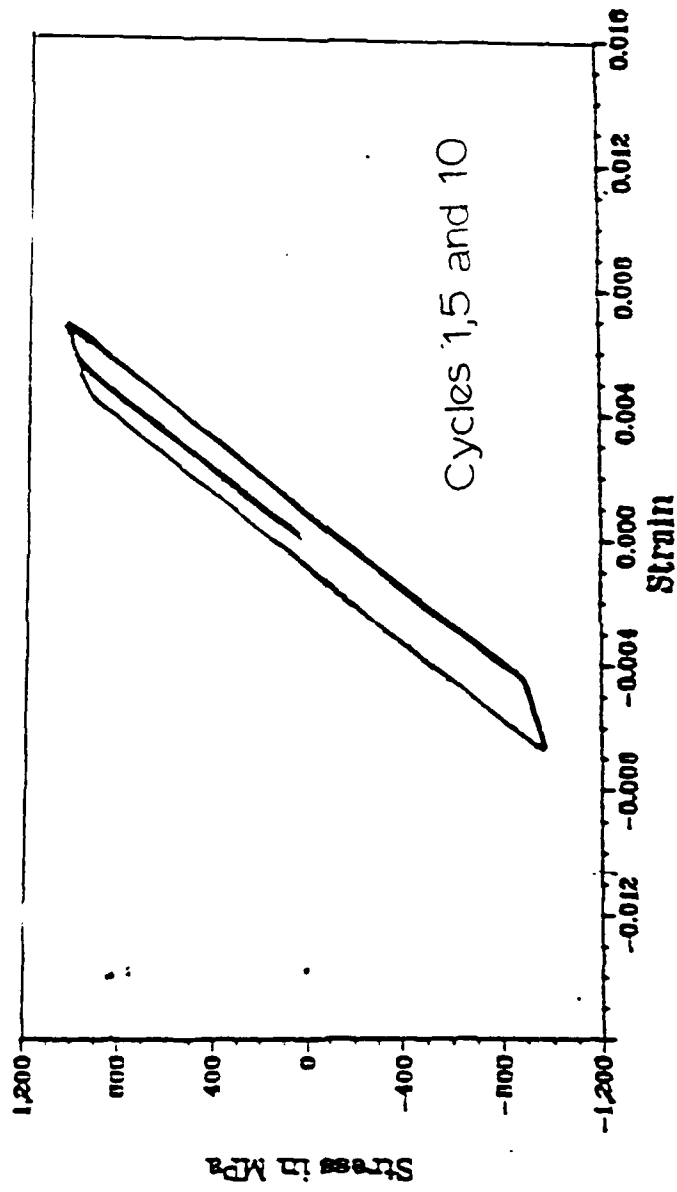


Figure 37. Bodner Model Prediction of Cyclic Loading Behavior: Stress Control,  $q = 0$

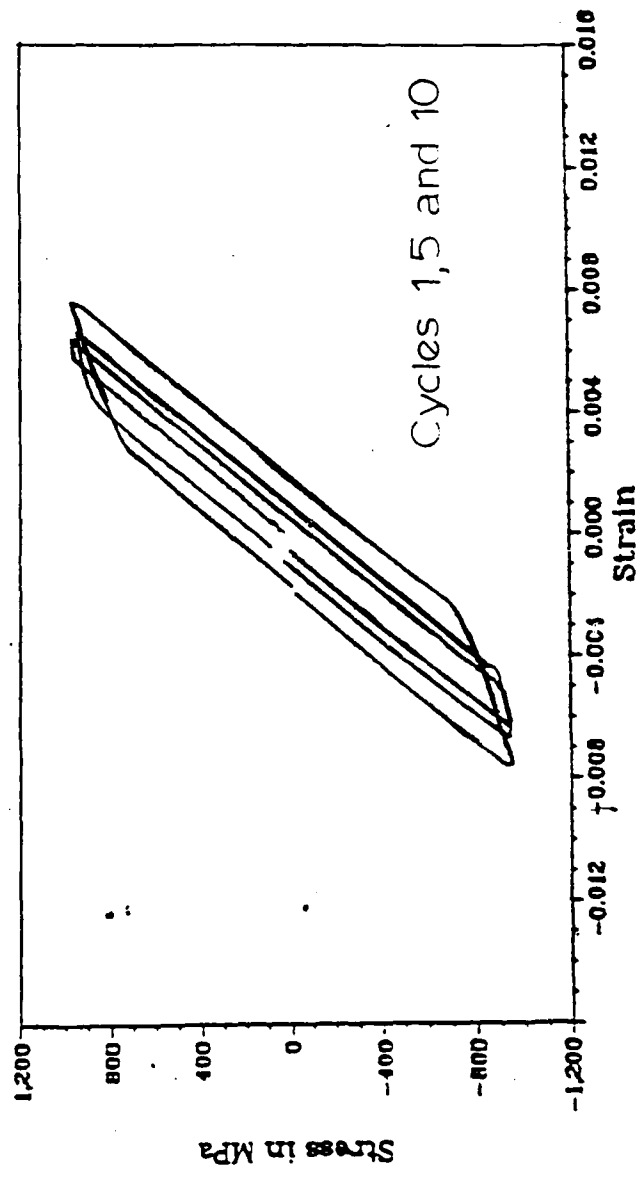


Figure 38. Bodner Model Prediction of Cyclic Loading Behavior: Stress Control,  $q = -.05$

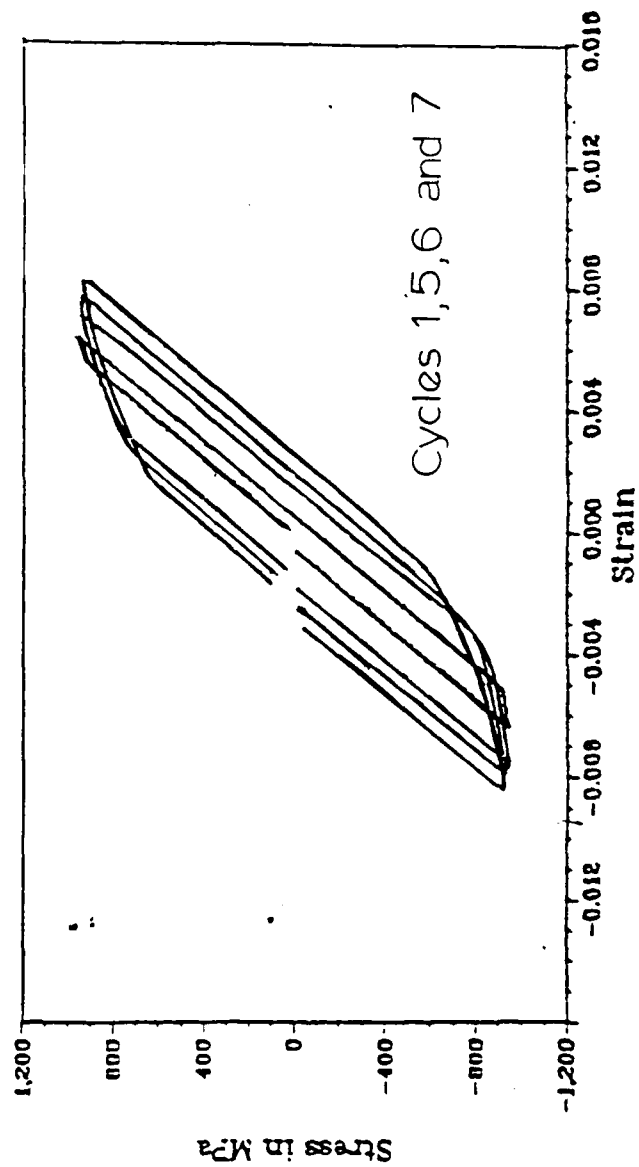


Figure 39. Bodner Model Prediction of Cyclic Loading Behavior: Stress Control,  $q = -.1$

to predict a growing and spreading of the loops just as the experimental data shows. The loops of the data are growing faster than the model's, but the trend is the same.

It is thus seen that the Bodner material model possesses a remarkable flexibility in the realm of plasticity. It can represent both isotropic and directional strain hardening as well as strain softening. With the addition of only a single parameter,  $q$ , the formulation of Equations (16) through (20) allowed the extension of the model from monotonic loading to cyclic load application, with remarkable results.

There is a problem, however, that limits the uses of this model for strain softening situations with negative values for  $q$ . There is no mechanism in this formulation to impose a minimum value of hardness. There is no constraint in how small  $Z$  may get; eventually a negative value is reached and the equations make no sense. Figure 33, which is based in Bodner's model for the case of  $q = -.1$ , shows how the values of  $Z^t$  and  $Z^c$  approach zero when the mean curve is considered. This basic short-coming may be overcome by the addition of a parameter limiting the strain softening representation. For a small number of cycles, though, and a  $q$  whose absolute value is less than or equal to .1, the model can be used to illustrate strain softening material behavior.

The limitations imposed by this aspect of Bodner's model are not great, considering the remarkable flexibility it still has. It is clear that the potential is here for a tool that will handle a wider range of strain softening behavior; all that is required is the incorporation of a mechanism for imposing a limiting value of softness.

## V. Conclusions

The following conclusions are made regarding the nature and evaluation of the Bodner material coefficients and the use of this formulation to model cyclic loading conditions. These results are generalizations based on work done with IN 718 at 1200<sup>o</sup>F and on a review of the literature concerning modeling of rate-dependent material behavior:

1. Evaluation of the Bodner model material coefficients requires the following minimum experimental data base:

a. Two, preferably three, data points for the strain-rate versus stress curve where test conditions are high strain rate with no recovery.

b. At least one stress-strain curve done under high strain rate/no recovery conditions; the curve should extend out at least to where the plastic strain equals the elastic strain.

c. Several data points spread across the lower strain rate portion of the curve, spanning the strain rates of interest to the researcher.

2. Each coefficient of the Bodner model has characteristic effects on material behavior that can be discerned individually.

3. A systematic procedure can be established for determining appropriate values for the Bodner model coefficients; it is contained in this thesis.

4. Evaluation of coefficient values is in some significant amount subjective in nature. Some judgement must be made regarding which strain rates comprise the region of interest; some evaluation of what constitutes a "best fit" to the stress-strain curve (e.g. in the evaluation of

m and  $Z_0$ ) must be made.

5. Because of the subjective nature of coefficient evaluation, no two researchers are likely to arrive at the same exact coefficients from a given data base. Differences in material behavior, if any, will be traceable to the fundamental assumptions of the individual researcher (e.g. which strain rates are important, which data points are "bad data", etc.).

7. Cyclic behavior predicted under this formulation of the constitutive equations models experimental results quite well. Both strain hardening and strain softening (for sufficiently small values of  $q$  and relatively few cycles) can be modeled.

8. Further development of the cyclic formulation of the equations must incorporate a mechanism for imposing a minimum hardness that may be reached under softening conditions.

## APPENDIX A

### Discussion of the Coefficients

This appendix contains a detailed discussion of each material coefficient of the Bodner-Partom plastic flow law. The parametric studies serve to illustrate the impact of the various coefficients on material behavior predicted by the Bodner model. The figures are ordered so that the variables are presented in the order in which they were studied in the applications section. Figure 5 provides some general guidance regarding the information contained in the figures. Each figure is accompanied by a discussion of the properties revealed by the graphical presentation.

#### The Coefficient $D_0$

$D_0$  is the limiting value of the plastic strain rate in shear. For this entire exercise, it has been assumed to have a constant value of  $10^6$   $\text{sec}^{-1}$ . Earlier work has used a value of  $10^4$  [1,2]; however, recent work [19] indicates that a value of  $10^6$  is more appropriate.  $D_0$  effects at what point the ultra high strain rate portion of the strain rate versus stress curve bends off to asymptotically approach  $D_0$ ; for as strain rates approach  $D_0$ , the stress necessary to sustain these strain rates becomes infinite. Changing the value of  $D_0$  biases the entire curve up or down, but does not effect the relationships between the other coefficients.

#### The Coefficients $n$ and $Z_1$

The coefficient  $n$  describes the material's strain rate sensitivity. The high strain rate version of Equation (10) (Equation (21)) contains

only  $D_0$  -- assumed to be constant at  $10^6 \text{ sec}^{-1}$  --  $n$ , and  $Z_1$ . Thus  $n$  and  $Z_1$  control a significant portion of the material's high strain rate behavior. The constant  $n$  has been determined [18] to be inversely related to temperature; the form of the relationship is

$$n = \frac{a}{T} + b \quad (32)$$

The coefficient  $n$  is also inversely related to the "intrinsic velocity of dislocation motion" [1] in the atomic lattice -- meaning that lower values of  $n$  correspond to higher dislocation velocities and freer movement of dislocations. The coefficient  $n$  is not dependent on loading history [1]. It is thus descriptive of the way the material itself responds to the introduction, propagation, and elimination of dislocations, not to the effect those dislocations have on material behavior.

Values for  $n$  and  $Z_1$  are tied together mathematically; at high strain rates the relationship is that of Equation (21):

$$\ln \left( -\ln \left( \frac{\sqrt{3}\epsilon^{\cdot} P}{2D_0} \right) \right) = -2n \ln \sigma + (2n \ln Z_1 + \ln \left( \frac{n+1}{2n} \right)) \quad (21)$$

$Z_1$  represents the saturation (maximum) value of  $Z$ . In a high strain rate situation, where there is no recovery,  $Z = Z_1$ .

#### Figure 40

This figure depicts the combined effects of variations in  $n$  and  $Z_1$ . Strain rate sensitivity, dependent on  $n$ , is observed in that high (but not ultra high) strain rate section of the curve where recovery effects are negligible. Decreasing  $n$  has the effect of increasing strain rate sensitivity; this is seen in the shallower slope of the curve at lower



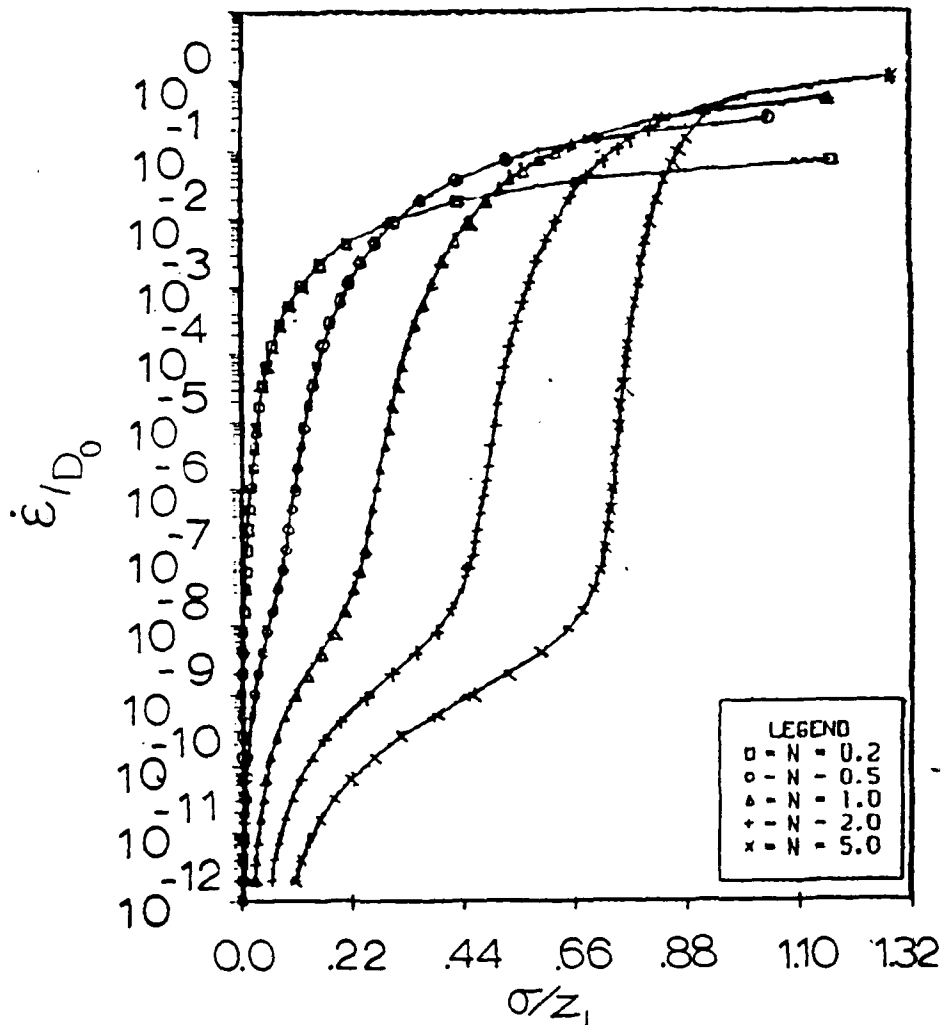


Figure 40. Variation of  $n$ , All Other Coefficients Constant

values of  $n$ . As the strain rates go down, recovery effects are no longer negligible, and the significance of a given value of  $n$  as a strain rate sensitivity parameter becomes obscured. At high strain rates, where  $Z = Z_1$ , the equations reduce to the closed form of Equation (24):

$$\frac{Z_1}{\sigma} = \left( \frac{2n}{n+1} \ln \left[ \frac{2D_0}{\sqrt{3}\epsilon^{\cdot} P} \right] \right)^{\frac{1}{2}n} \quad (24)$$

Again,  $D_0$  (a constant),  $n$  and  $Z_1$  are the only coefficients present; hence

$n$  and  $Z_1$  are the only coefficients capable of modifying the high strain rate portion of the strain rate versus stress curves of this parametric study.

The translation of the curve along the x-axis is due to the choice of  $Z_1$  as the non-dimensionalizing agent.

#### Figures 41 and 42

The range of values of  $n$  and  $Z_1$  which emerge from the interpretation of the data (Figures 9 and 56) is presented in Figures 41 and 42. In Figure 41 there is clearly more than one saturation stress represented. This is due to the fact that the point B of Figure 56 (through which the four lines representing the values for  $n$  all pass) corresponds to a strain rate of  $1.185 \times 10^{-3} \text{ sec}^{-1}$ . Only at that strain rate do all four  $n$  values correspond to the same saturation stress. Yet the variation in  $n$  from 3.0 to 3.211 is not significant in Figure 41. From Figure 42 it is clear that the change in the curve slope caused by changing  $n$  such a small amount is not significant. An arbitrary choice of  $n = 3.0$  was made, based on a graphical comparison with experimental data (Figures 16 through 19).

#### The Coefficients $m$ and $Z_0$

The coefficient  $m$  describes the rate of work hardening exhibited by the material. Its value also determines how long work hardening effects will be dominant and recovery effects negligible as strain rate is decreased. Mathematically, it is the value of  $m$  coupled to the value of  $A$  that determines above what strain rates hardening effects dominate so completely.

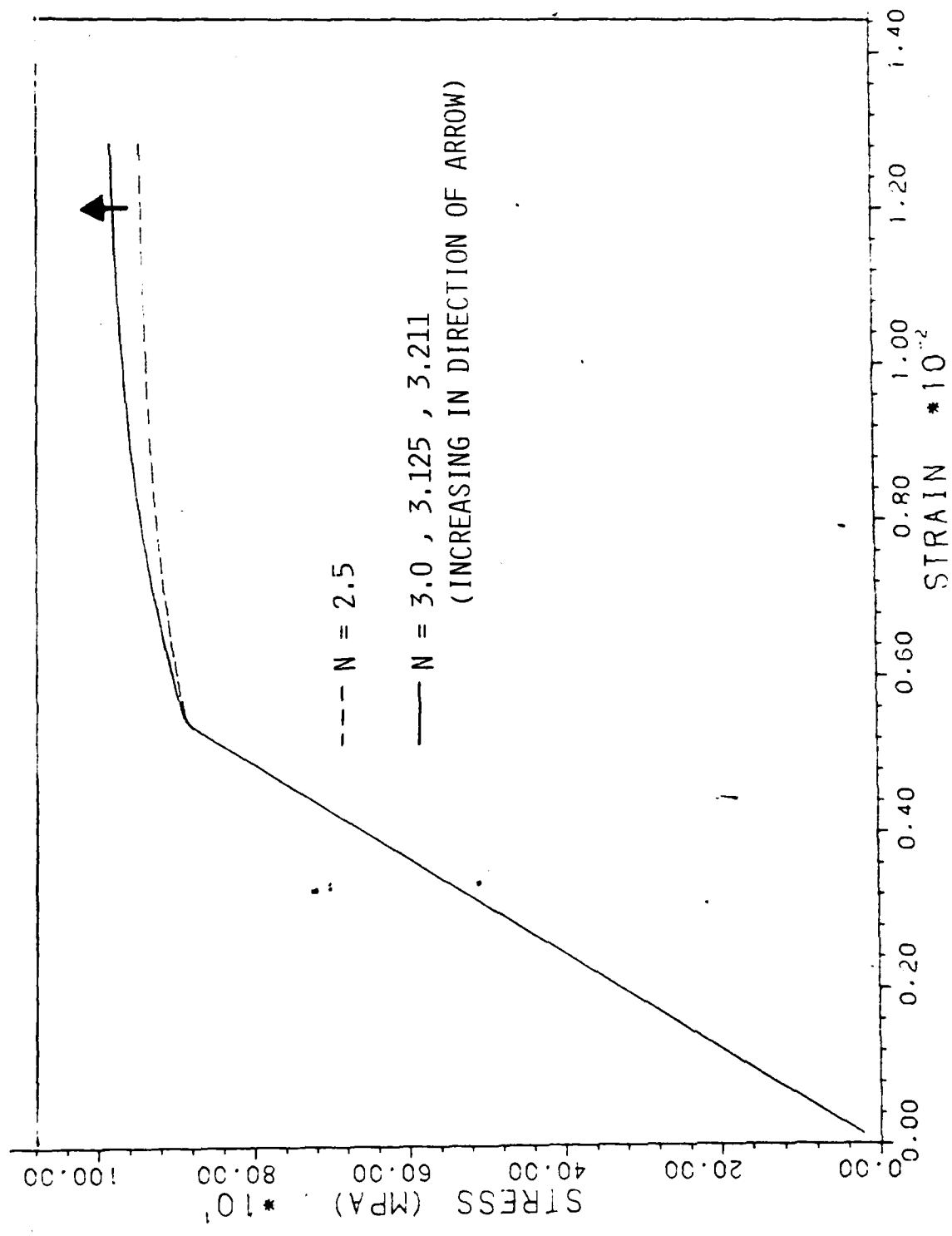


Figure 41. Variation of n

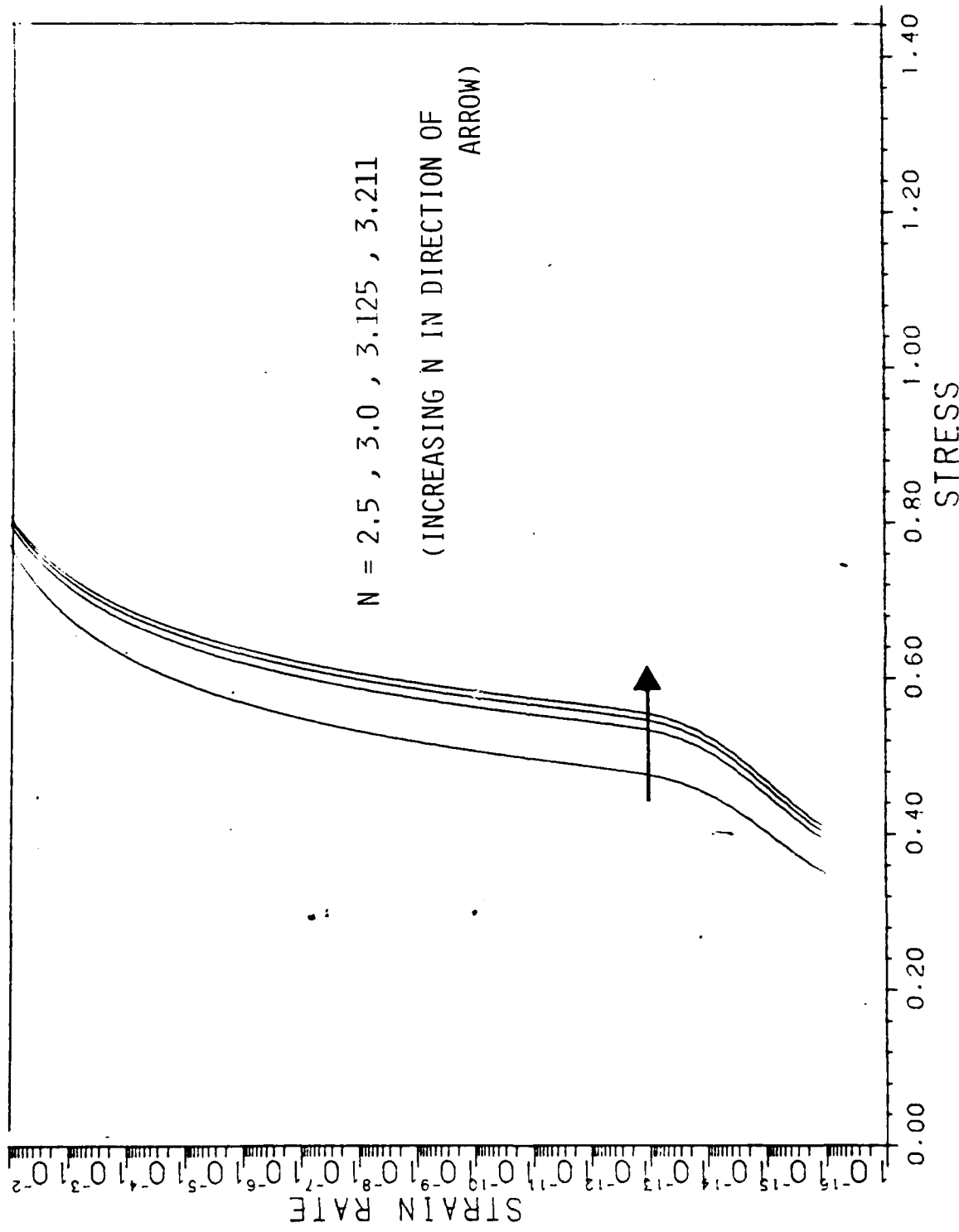


Figure 42. Variation of  $n$

$Z_0$  is linked mathematically to  $m$  much as  $Z_1$  is linked to  $n$ . This relationship is expressed in Equation (23):

$$\ln (Z_1 - Z) = \ln (Z_1 - Z_0) - mW_p \quad (23)$$

$Z_0$  represents the initial state of hardness in the present loading; the lower the value of  $Z_0$ , the more hardening must be accomplished before saturation is reached and  $Z = Z_1$ .  $Z_0$  is dependent on temperature.

Figure 43

The coefficient  $m$  times  $Z_1$  is the non-dimensional form of the coefficient describing the rate of work hardening,  $m$ . Once a value is established for  $Z_1$ , the behavior depicted by Figure 43 represents variations in  $m$ . If one compares Figure 43 with Figure 49, considering Equation (15):

$$\dot{Z} = m(Z_1 - Z)\sigma\dot{\epsilon}^p - AZ_1 \left[ \frac{Z - Z_2}{Z_1} \right]^r \quad (15)$$

it is observed that  $A$  and  $m$  hold analogous positions as multiplicative coefficients in the two terms of Equation (15). Increasing  $A$  has much the same effect as decreasing  $m$ , which is to evidence the effects of recovery phenomena at higher strain rates. The interface between the high strain rate regime (where there are no significant recovery effects) and the strain rate region where both recovery and hardening are important is controlled by this balance between  $A$  and  $m$ .

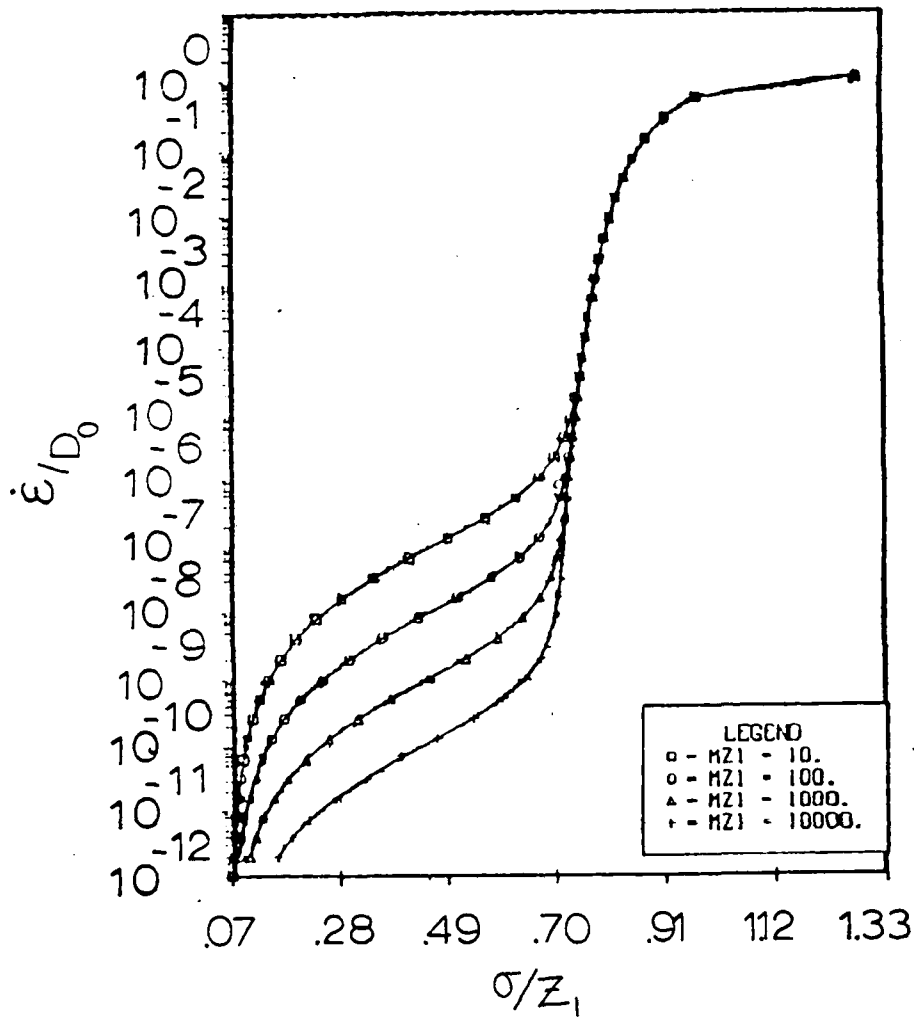


Figure 43. Variation of  $m$  Times  $Z_1$ , All Other Coefficients Constant

Figure 44

At high strain rates, where recovery effects are negligible, the effect of varying  $m$  is illustrated in Figure 44. As  $m$  is increased, the shape of the stress-strain curve is slightly more rounded. The effects of varying  $m$  by 10% are shown in Figure 44; the trend is consistent, if not significant.

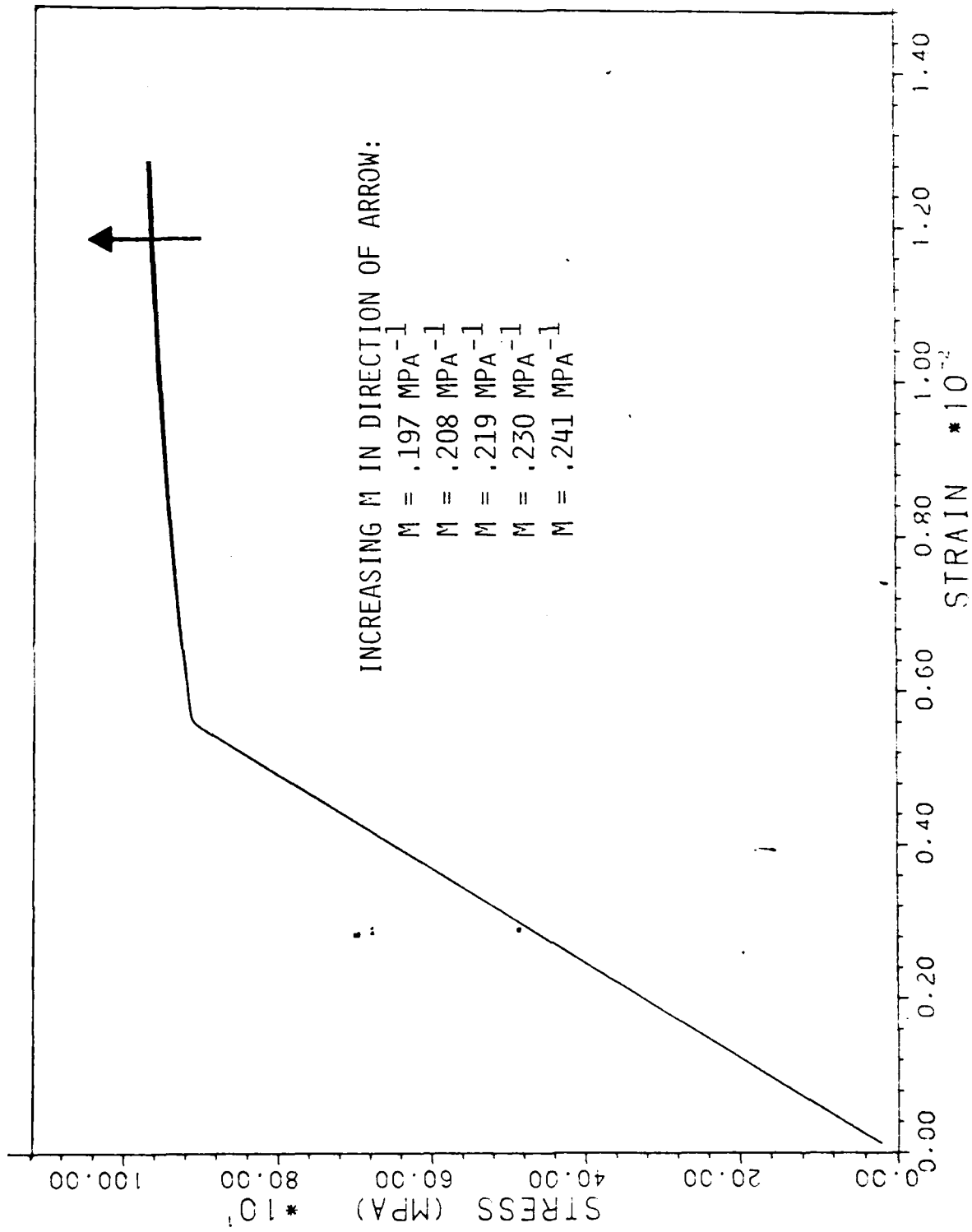


Figure 44. Variation of  $m$ , All Other Coefficients Constant

#### Figure 45

The coefficients  $m$  and  $Z_0$  are linked mathematically. Lower values of  $m$  are paired with higher values of  $Z_0$ . Figure 45 depicts the effect of choosing various interpretations of the data graphed in Figure 13. Using the  $m$  and  $Z_0$  values from the first linear portion of the data of Figure 13 (the "front" values of  $Z_0$  and  $m$ ) results in a better fit of the front of the stress-strain curve of the data. Using the  $m$  and  $Z_0$  values from the second linear portion of the data of Figure 13 (the "back" values) results in a flatter stress-strain curve that matches the saturation stress level of the data more precisely. The choice of  $m$  and  $Z_0$  significantly effects the ability of the model to accurately predict material behavior as depicted on the stress-strain curve.

#### Figure 46

The effect of varying  $Z_0$  is illustrated in Figure 46. Since  $Z_0$  represents the state of hardness at the beginning of the present loading, the difference between the hardness at the start and the maximum hardness  $Z_1$  describes the hardening that may go on during the loading.

#### The Coefficient A

A is the coefficient in the expression for the thermal recovery of work hardening. The magnitude of A (relative to the magnitude of  $m$ ) determines at which strain rates recovery becomes significant. For lower values of A, thermal recovery remains a less significant phenomenon until relatively slower strain rates are reached. Changes in A do not significantly impact material behavior at strain rates too fast for recovery effects to be significant, since A is tied strictly to the recovery mechanism.



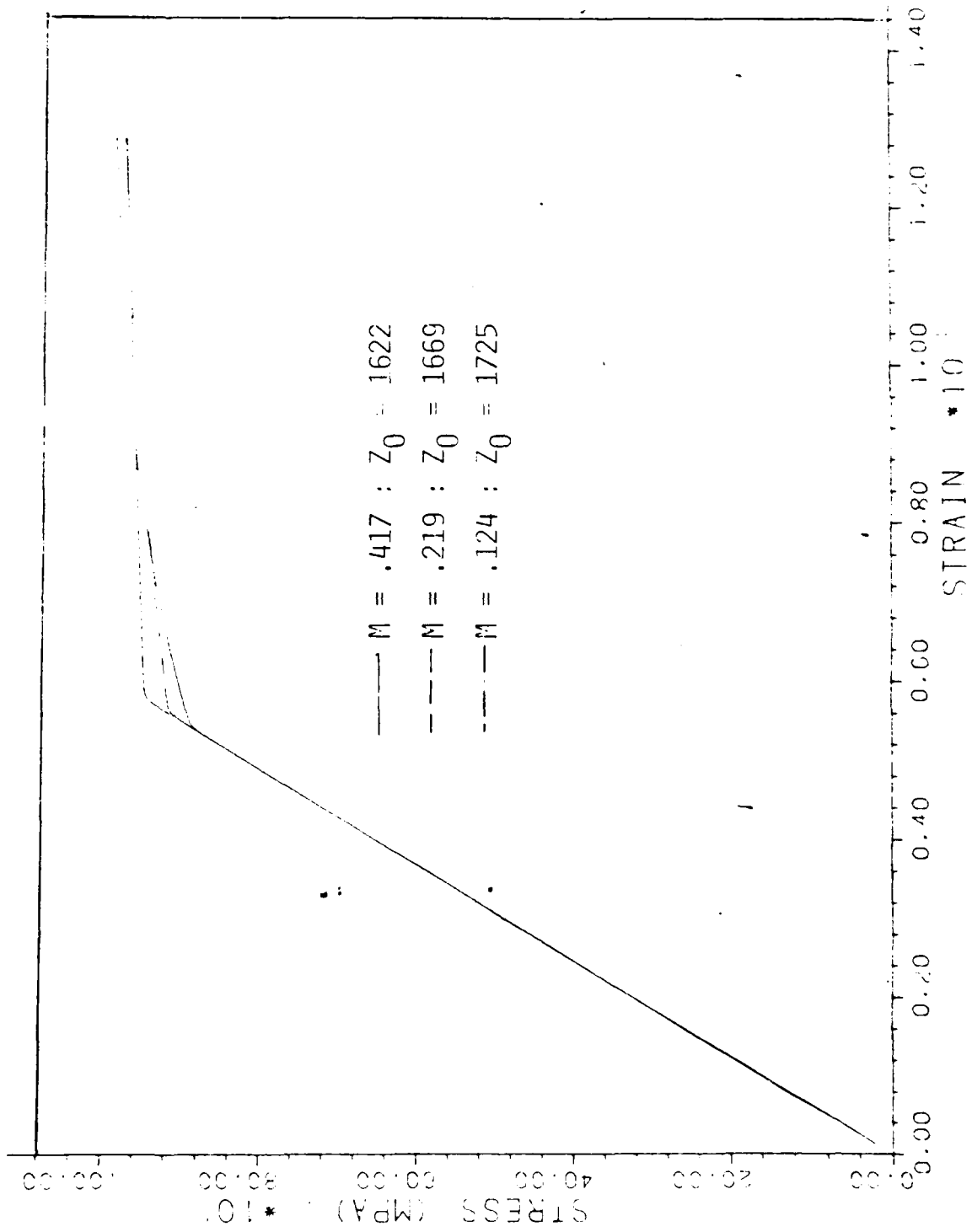


Figure 45. Variation of  $m - Z_0$  Pairs, As Indicated By Figure 14

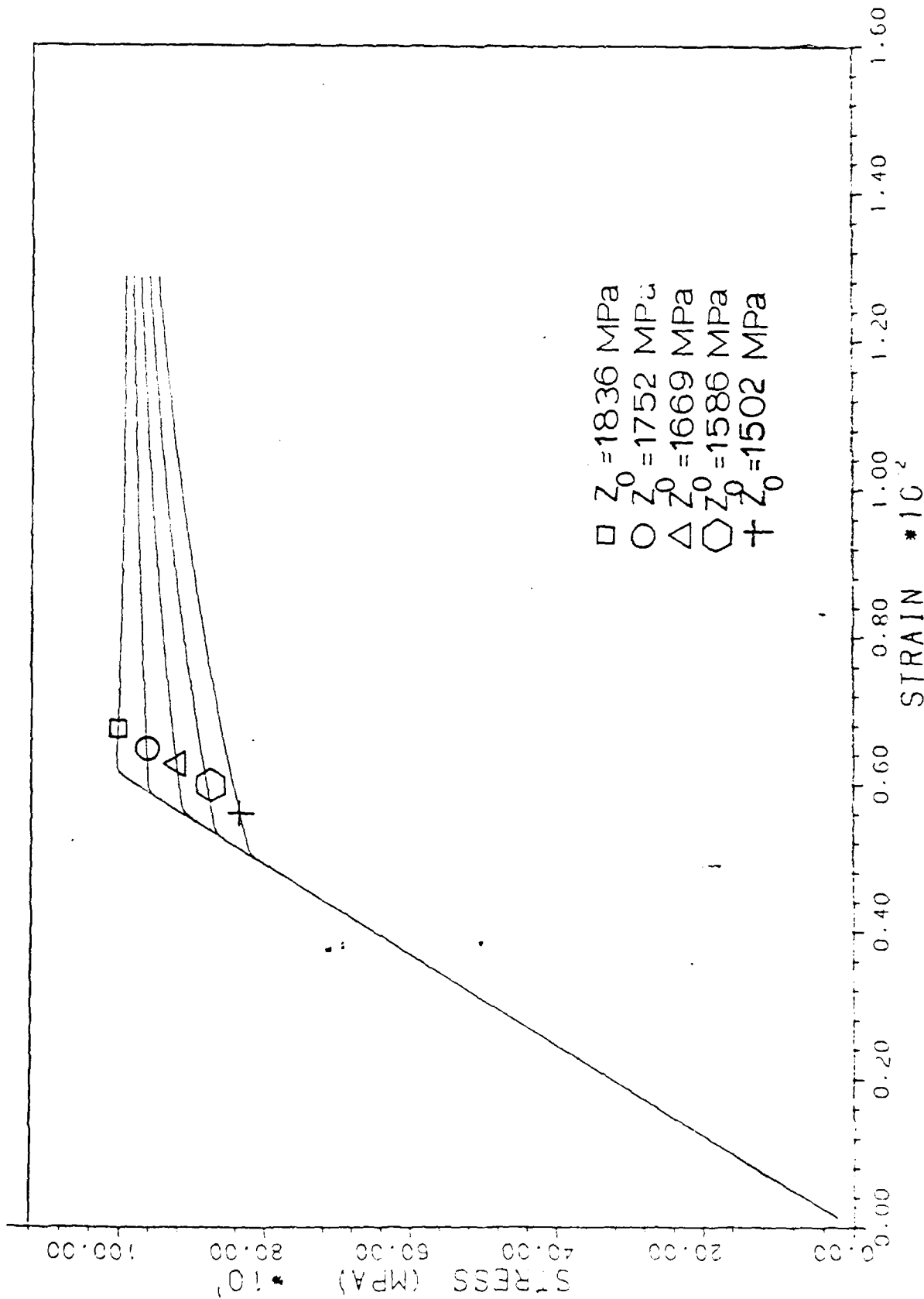
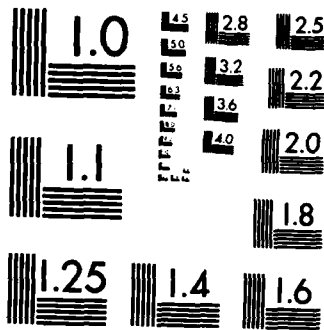


Figure 46. Variation of  $Z_0$ , All Other Coefficients Constant





MICROCOPY RESOLUTION TEST CHART  
NATIONAL BUREAU OF STANDARDS-1963-A

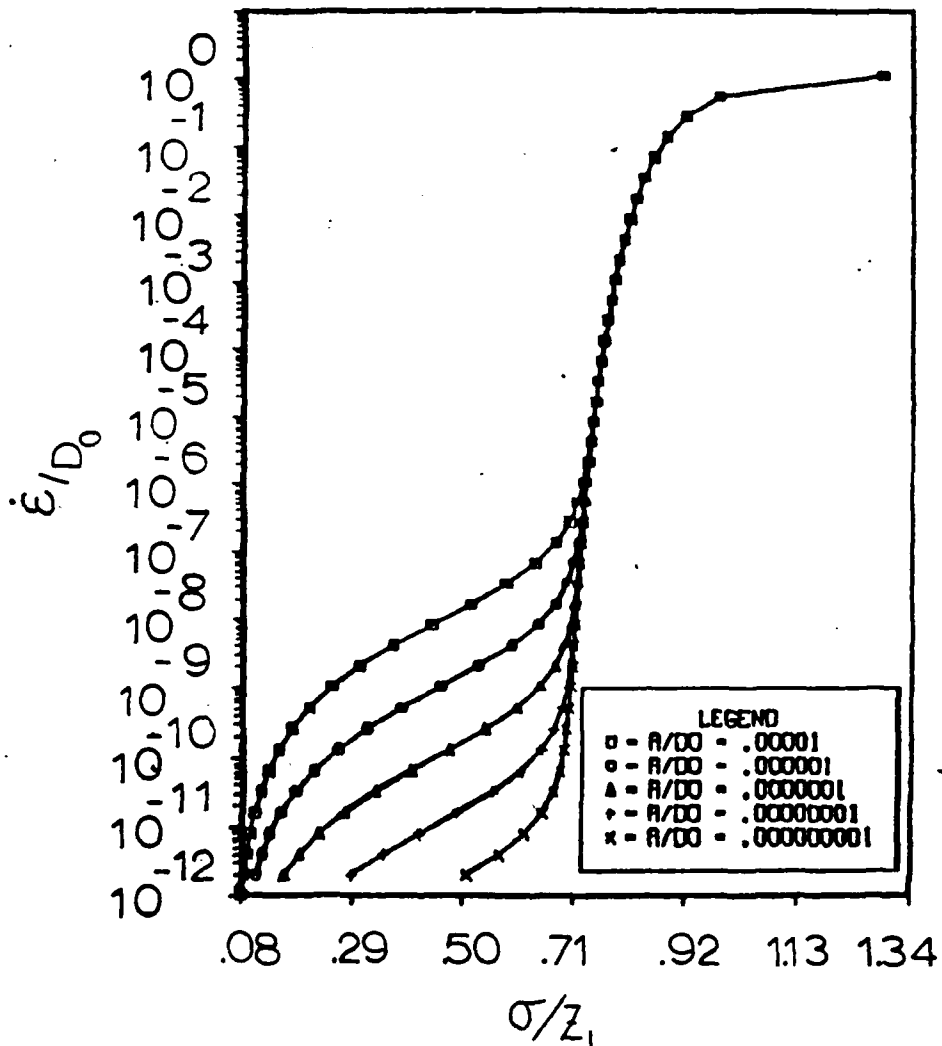


Figure 47. Variation of  $A/D_0$ , All Other Coefficients Constant

Figure 47

The coefficient A (or  $A/D_0$  in the non-dimensionalized form) is the coefficient in the expression for thermal recovery of work hardening. The "branching" effect in the lower left of this figure shows how the primary effect of changing A is to extend the region where recovery is a significant feature of material behavior. The onset of thermal recovery is determined by this variable (once a value for m is established through study of the high strain rate material behavior); for larger values of A,

thermal recovery dominates at higher strain rates.

#### Figures 48 and 49

Changes in A are not significant for strain rates faster than that at which recovery becomes evident. Figure 48 is an analytically generated stress-strain curve for  $\dot{\epsilon} = 1.3 \times 10^{-5} \text{ sec}^{-1}$ ; it shows clearly that changes in A for A at least as small as 0.001 are not significant for this strain rate. Figure 49 is an analytically generated stress-strain curve for  $\dot{\epsilon} = 1.1 \times 10^{-6} \text{ sec}^{-1}$ ; here, changes in A are significant until A is at least as small as 0.00001. These figures show that it is a balance between the strain rate in question and the magnitude of A that determines whether smaller values of A will impact material behavior at the strain rate in question. Larger values of A, whose effect is to extend the region where recovery effects are significant, will cause visible changes in the curve as soon as the implied change in A makes the strain rate relatively slow enough to allow recovery effects to surface.

#### The Coefficient $Z_2$

The coefficient  $Z_2$  represents the material hardness at the completely non-work hardened -- or fully recovered -- condition. It is the minimum recoverable hardness of the material, and it is dependent on the temperature conditions.

#### Figure 50

Once a value is established for  $Z_1$  through study of the material's high strain rate behavior, the material behavior depicted in Figure 50 becomes that of  $Z_2$ . A higher value of  $Z_2$  represents a harder condition

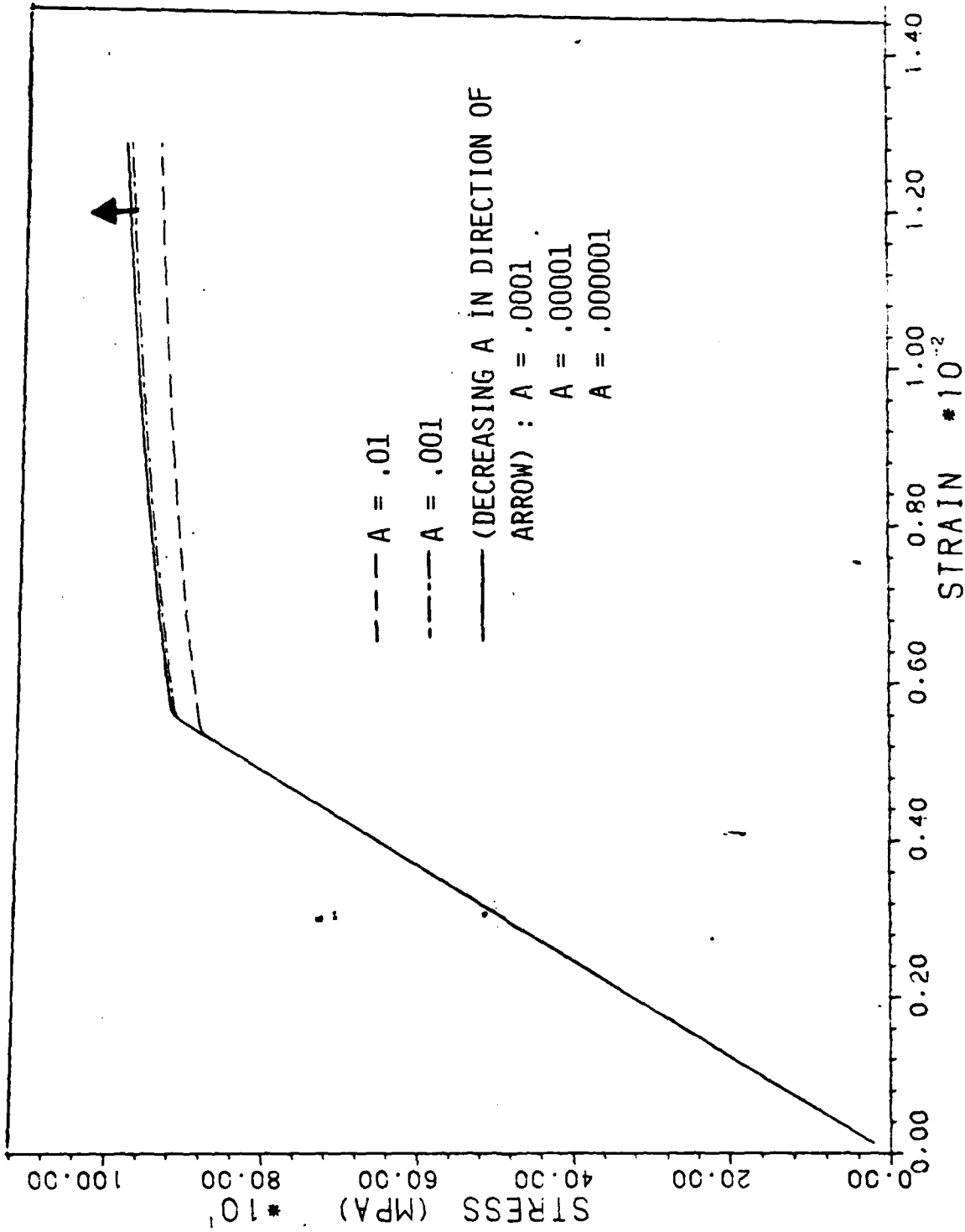


Figure 48. Variation of A at a High Strain Rate

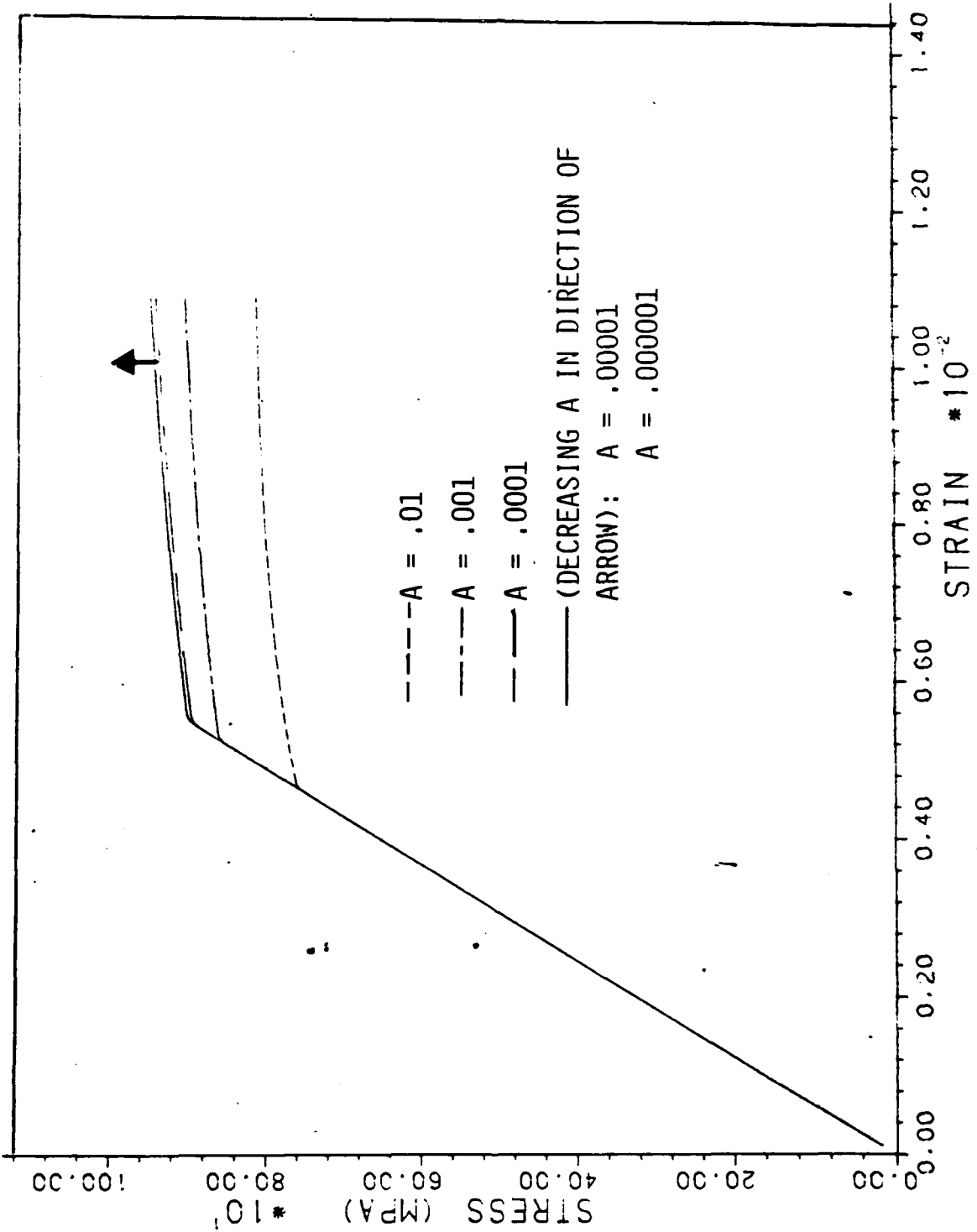


Figure 49. Variation of A at a Low Strain Rate



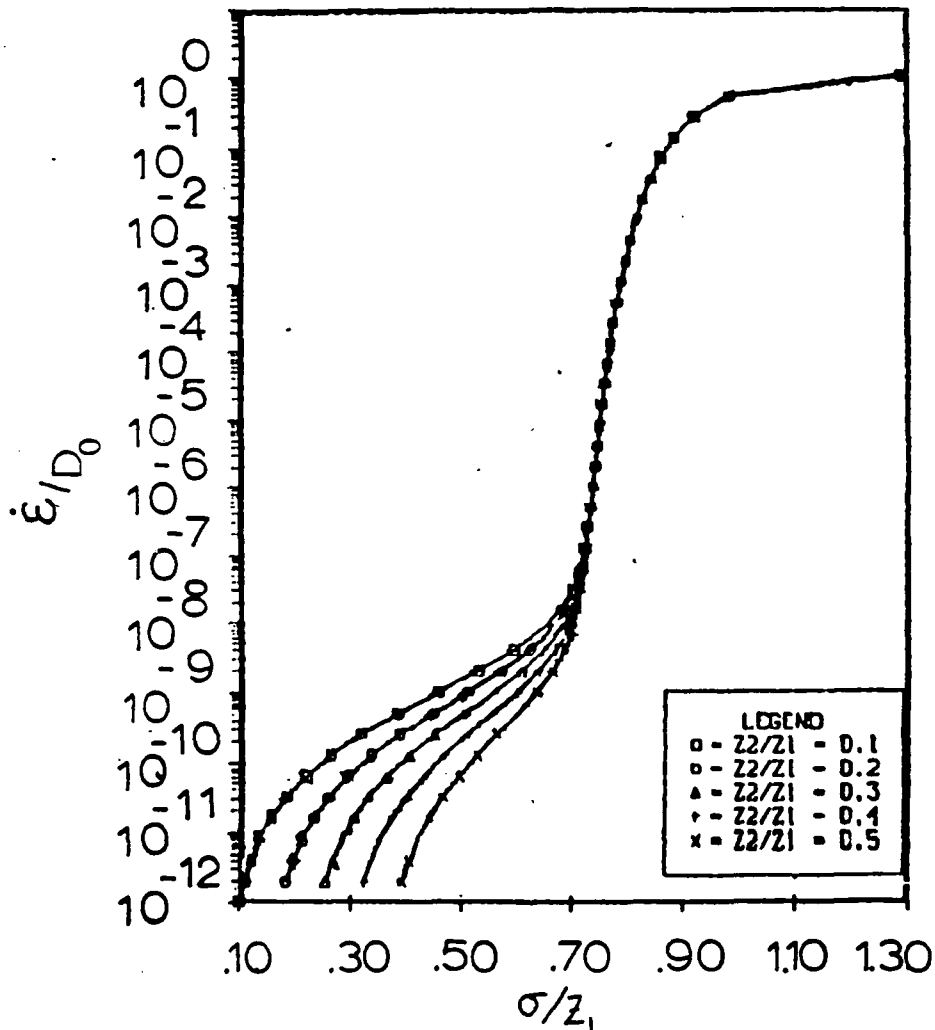


Figure 50. Variation of  $Z_2/Z_1$

when minimum hardness is achieved under recovery. On Figure 50,  $Z_2$  controls where the curve turns downward again at very low strain rates.

Figures 51 and 52

Like A,  $Z_2$  is part of the equation descriptive of recovery phenomena. Figure 51 shows that changing  $Z_2$  values at a high strain rate, where recovery is negligible, has no significant effect on the material behavior depicted by the stress-strain curve. A stress-strain curve set drawn for a slower strain rate, where recovery effects become significant,

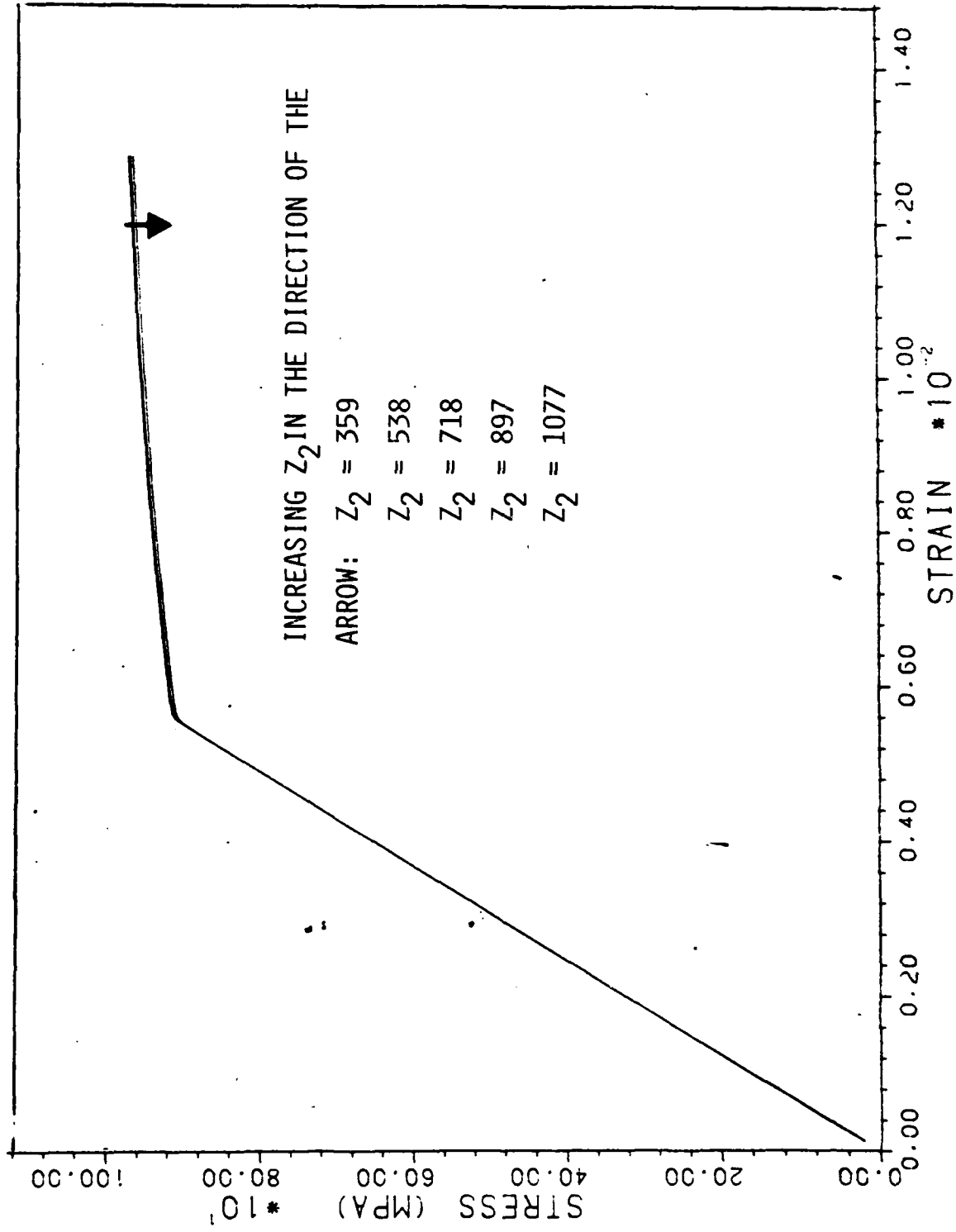


Figure 51. Variation of  $Z_2$  at a High Strain Rate

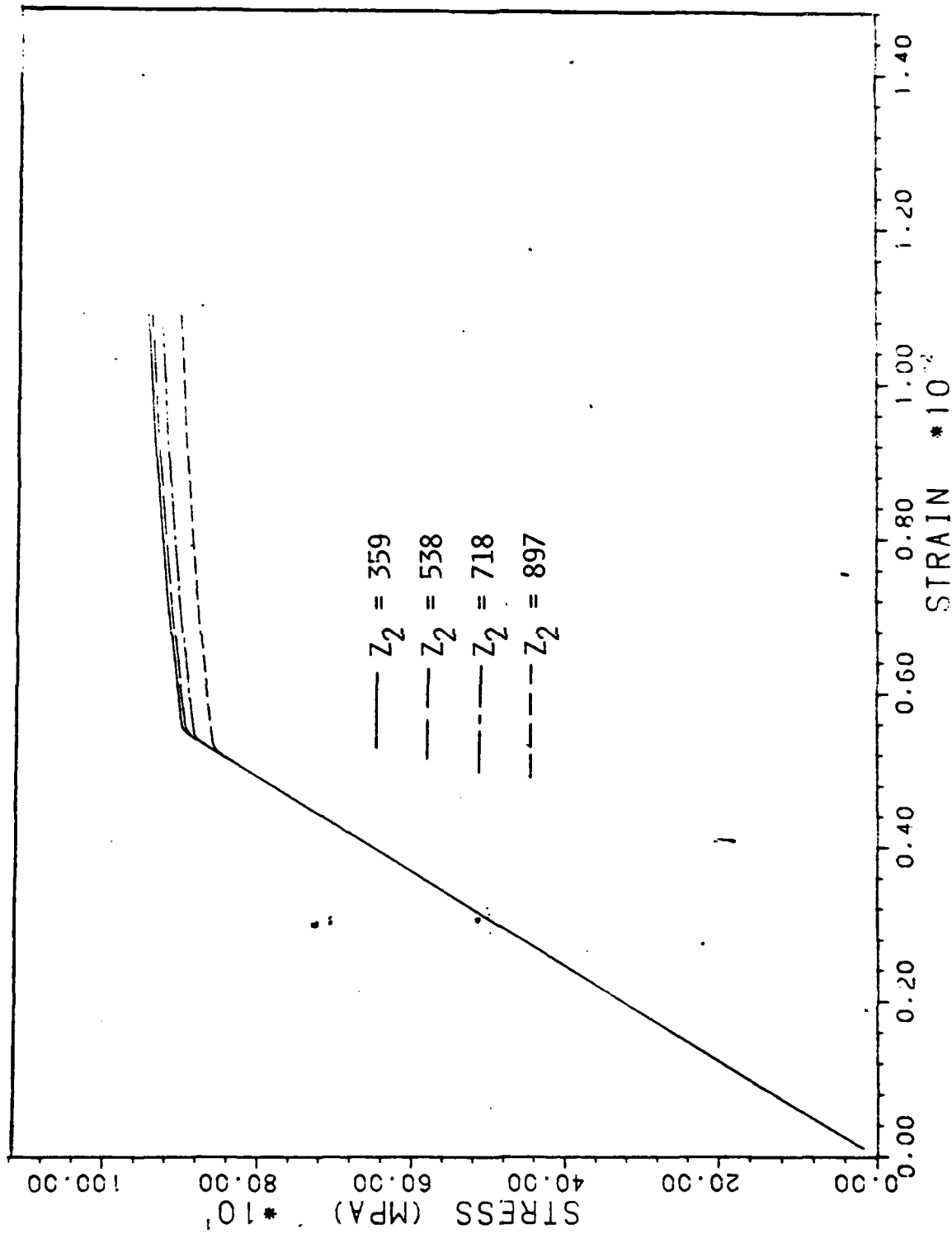


Figure 52. Variation of Z<sub>2</sub> at a Low Strain Rate

is shown in Figure 52. Here changes in  $Z_2$  are clearly visible.

#### The Coefficient r

The coefficient r appears as an exponent in the expression for thermal recovery of work hardening. If A (or  $A/D_0$ ) were to be written as a function of the onset of recovery, r would be the curvature of that function. Where the value of A determines at which strain rate recovery begins to be important, r describes how quickly recovery rises to dominance. As with A and  $Z_2$ , the effect of changing r is not seen at strain rates too fast to allow thermal recovery of plastic work to be significant.

#### Figures 53, 54, and 55

Figure 53 shows that the effect of changing r is to change the sensitivity of the recovery mechanism to strain rate. Figures 54 and 55 show quite clearly that changes in r do not effect material behavior at strain rates where thermal recovery is negligible. At a strain rate fast enough for recovery to be negligible (Figure 54), changes in r are not distinguishable on a stress-strain curve. At a slower strain rate where recovery effects become significant (Figure 55), increases in r are reflected in a higher stress level of the stress-strain curve over the domain shown.

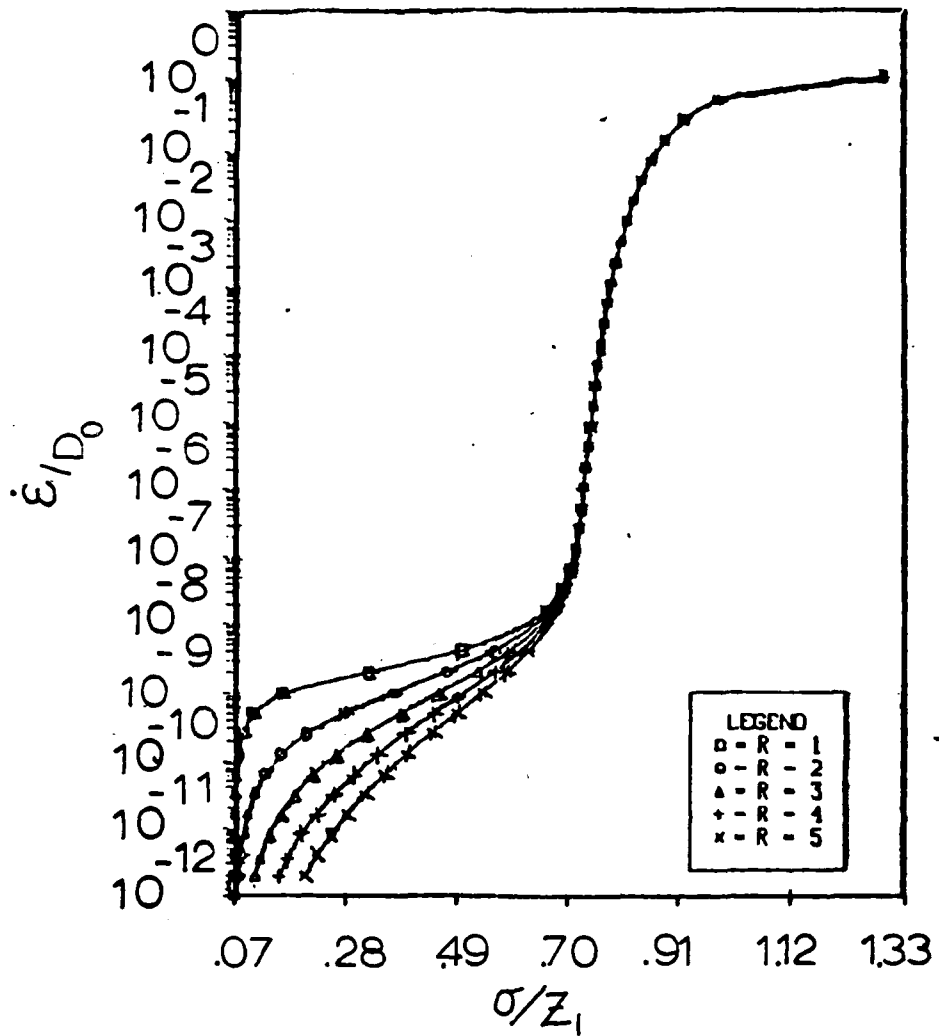


Figure 53. Variation of r —

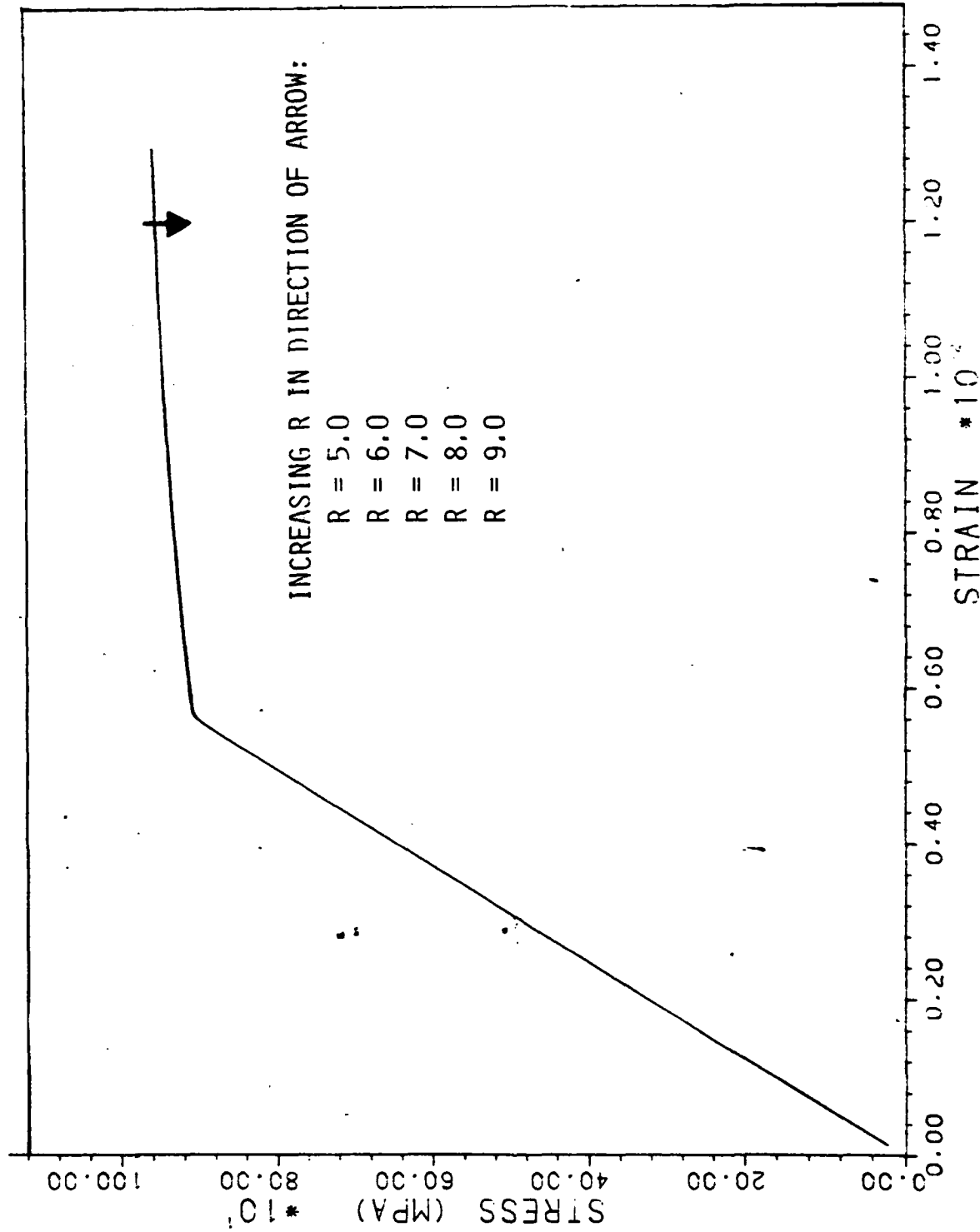


Figure 54. Variation of  $r$  at a High Strain Rate

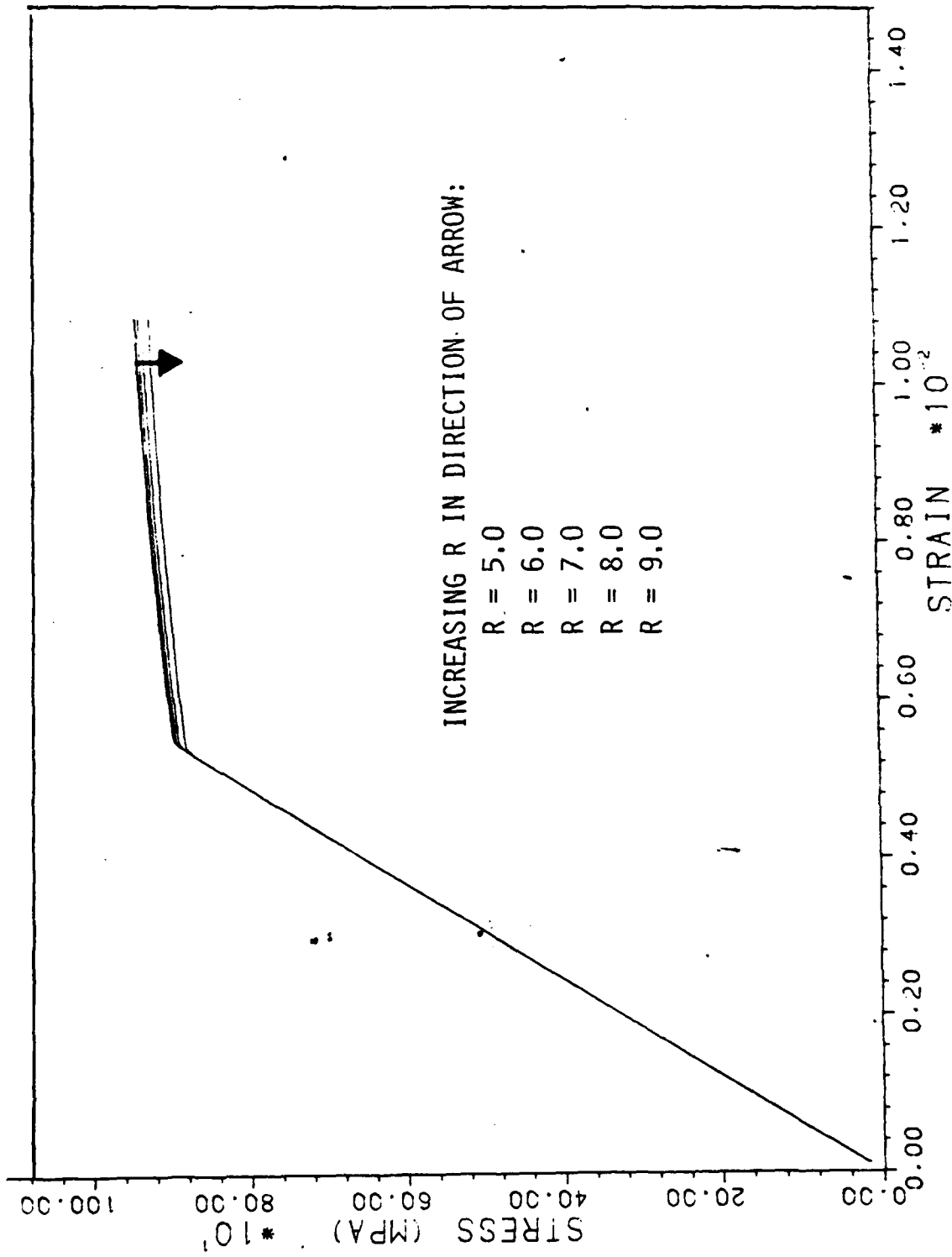


Figure 55. Variation of  $\tau$  at a Low Strain Rate

APPENDIX B

Determination of n and Z<sub>1</sub>

When both stress and strain rate are constant, the governing equation

$$\dot{\epsilon}^P = \frac{2}{\sqrt{3}} D_0 \frac{\sigma}{|\sigma|} \text{EXP} \left[ - \frac{n+1}{2n} \left( \frac{Z}{\sigma} \right)^{2n} \right] \quad (10)$$

says that Z must also be constant. Further, for high strain rate tests with no recovery the material must be in a fully work hardened state, "to obtain the maximum value of stress" [9], so that Z = Z<sub>1</sub>. For these steady flow conditions, Equation (21) follows:

$$\ln \left( -\ln \frac{\sqrt{3}\dot{\epsilon}^P}{2D_0} \right) = -2n \ln \sigma + \left( 2n \ln Z_1 + \ln \frac{n+1}{2n} \right) \quad (21)$$

Thus, it is seen that a linear relationship exists between  $\ln \left( -\ln \frac{\sqrt{3}\dot{\epsilon}^P}{2D_0} \right)$  and  $\ln \sigma$ . If high strain rate experimental data is graphed on appropriate axes ( $\ln \left( -\ln \frac{\sqrt{3}\dot{\epsilon}^P}{2D_0} \right)$  versus  $\ln \sigma$ ) the slope of a linear approximation to the data will determine a value for n. A value for Z<sub>1</sub> can then be computed mathematically.

The test data used for this procedure consisted of three constant strain rate tensile tests presented in Table V:

TABLE V  
Experimental Data, Constant Strain Rate Tensile Tests

Data Point	Strain Rate	Stress (KSI)	Stress (MPa)
1	1.1x10 <sup>-6</sup> sec <sup>-1</sup>	134	923.906
2	1.3x10 <sup>-5</sup> sec <sup>-1</sup>	142	979.065
3	1.6x10 <sup>-3</sup> sec <sup>-1</sup>	147	1013.539



Data point 1, with a strain rate of  $1.1 \times 10^{-6} \text{ sec}^{-1}$ , was considered at this stage even though the strain rate is suspected of being slow enough to allow non-negligible recovery effects to influence the data. Figure 56 shows the location of this data point on strain rate versus stress axes. If straight lines are drawn to characterize the two upper portions of the data (as in Figure 5), data point 1 is found to lie in the strain rate region where recovery effects are significant.

Using Equation (21) to compute the values for graphing leads to the following:

TABLE VI

Experimental Data, Formatted to Allow Determination of  $n$  and  $Z_1$

Data Point	$y = \ln(-\ln(\frac{\sqrt{3}\epsilon^p}{2D_0}))$	$x = \ln \sigma$
1	3.3207	6.8286
2	3.2376	6.8866
3	3.0154	6.9212

This data was graphed in Figure 57. It was clear that all three points were not part of a single linear trend. The validity of point 1 was suspect from the beginning; that point was simply discarded. The strain rate of  $1.1 \times 10^{-6} \text{ sec}^{-1}$  was apparently too slow to allow recovery effects to be neglected. This was verified by parametric studies contained in Appendix A, after a complete set of coefficients was obtained (Figures 48, 49, 51, 52, 54, and 55). At a strain rate of  $1.1 \times 10^{-6} \text{ sec}^{-1}$ , effects of varying  $A$ ,  $r$ , and  $Z_2$  are clearly seen; at a strain

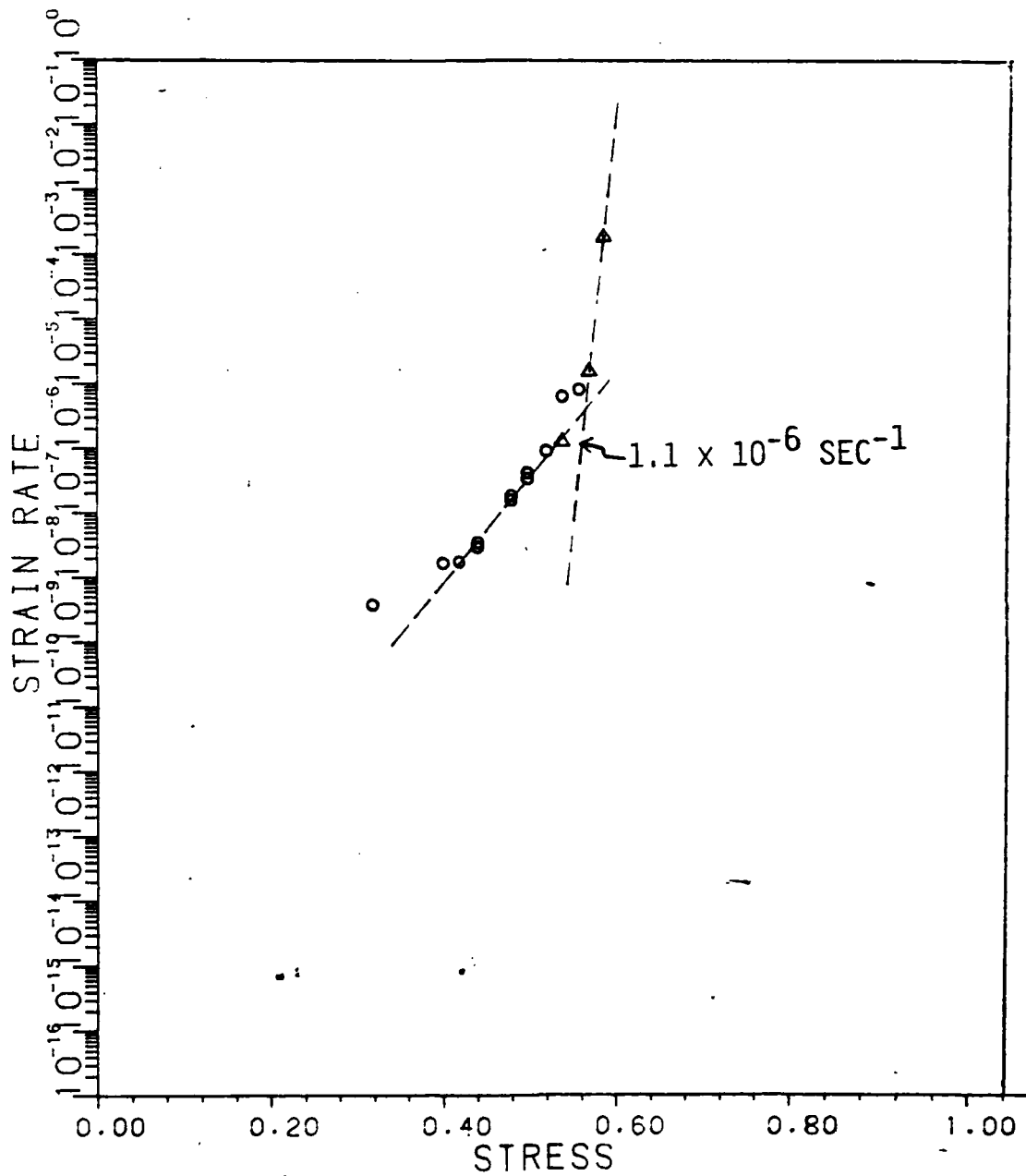


Figure 56. Experimental Data Base; IN 718, 1200°F

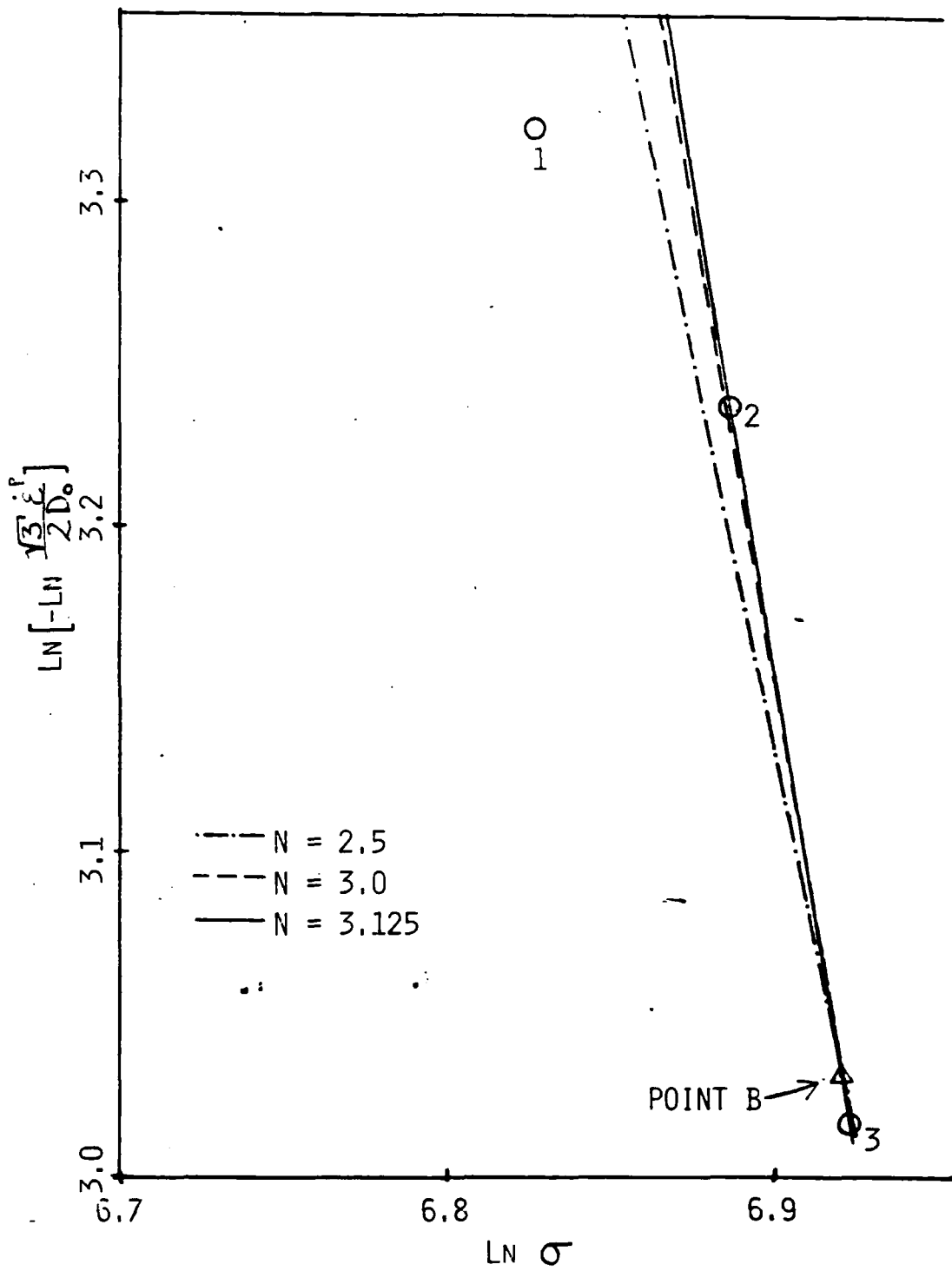


Figure 57. Determination of  $n$  and  $Z_1$

rate of  $1.3 \times 10^{-5} \text{ sec}^{-1}$  they are hardly discernable. Since these three coefficients appear only in the recovery term of Equation (15) these results indicate that recovery effects are not negligible at  $\dot{\epsilon} = 1.1 \times 10^{-6} \text{ sec}^{-1}$ .

Working with the remaining two data points, the value of  $n$  was computed in a variety of ways. First, working mathematically, a value of  $n = 3.211$  was computed using the coordinates of the two points. In order to illustrate the limitations on accuracy imposed by the graphical technique that would have been used had more than two appropriate data points been available, a second value was computed. Coordinates of two points (other than the data points) were picked off a line drawn through the data, and they indicated a value of  $n = 3.125$ . Because  $n = 3.0$  is a nice integer value, the line representing it was also drawn; it appears to also be fairly representative of the data. As a lower limit, the line representing  $n = 2.5$  was also drawn. These four values represent the range of  $n$  values to be considered.

Values for  $Z_1$  were then calculated. All of the aforementioned lines were drawn through a single point B (whose coordinates are (6.92, 3.03)) in Figure 57. Using this point, the various values for  $n$  and Equation (16) lead to the following values for  $Z_1$ :

TABLE VII  
Values Computed for  $n$  and  $Z_1$

$n$	$Z_1$ (MPa)	$Z_1$ (KSI)
3.211	1732.871	251.329
3.125	1756.858	254.808
3.0	1794.672	260.293
2.5	1992.878	289.040

One consequence of the use of point B should be mentioned. It is only at the strain rate indicated by  $\ln(-\ln(\frac{\sqrt{3}\dot{\epsilon}P}{2D_0})) = 3.03$  that the saturation stresses will be the same for all the values of n. It is partly because of this fact that the saturation stress are not the same in the stress-strain curves where n is varied (e.g. Figure 41).

## APPENDIX C

### Determination of $m$ and $Z_0$

In the absence of thermal recovery of work hardening, the governing equation

$$\dot{Z} = m(Z_1 - Z)\dot{\sigma} \epsilon^p - AZ_1 \left[ \frac{Z - Z_2}{Z_1} \right]^r \quad (15)$$

can be written as a first-order linear differential equation:

$$dZ = m (Z_1 - Z) dW_p \quad (22)$$

This can be integrated, with the initial condition of  $Z = Z_0$  at  $W_p = 0$ :

$$\frac{dZ}{Z_1 - Z} = m dW_p$$

$$\ln (Z_1 - Z) = \ln (Z_1 - Z_0) - mW_p \quad (23)$$

Appropriate high strain rate data, graphed on  $\ln (Z_1 - Z)$  versus  $W_p$  axes, may be linearly approximated to determine  $m$  from the slope of the line and  $Z_0$  from the y-intercept.

The data used for this procedure came from a single high strain rate tensile test and is presented in Figure 58. This data was chosen because the strain rate was high enough that recovery effects would most likely be negligible, and the data maintained a nice, smooth character across a wide range of strains.

The elastic modulus [10] was first drawn on the figure. It happens that, although the data is reasonably accurate in the inelastic region, the accuracy in the elastic region is not good. Using the elastic

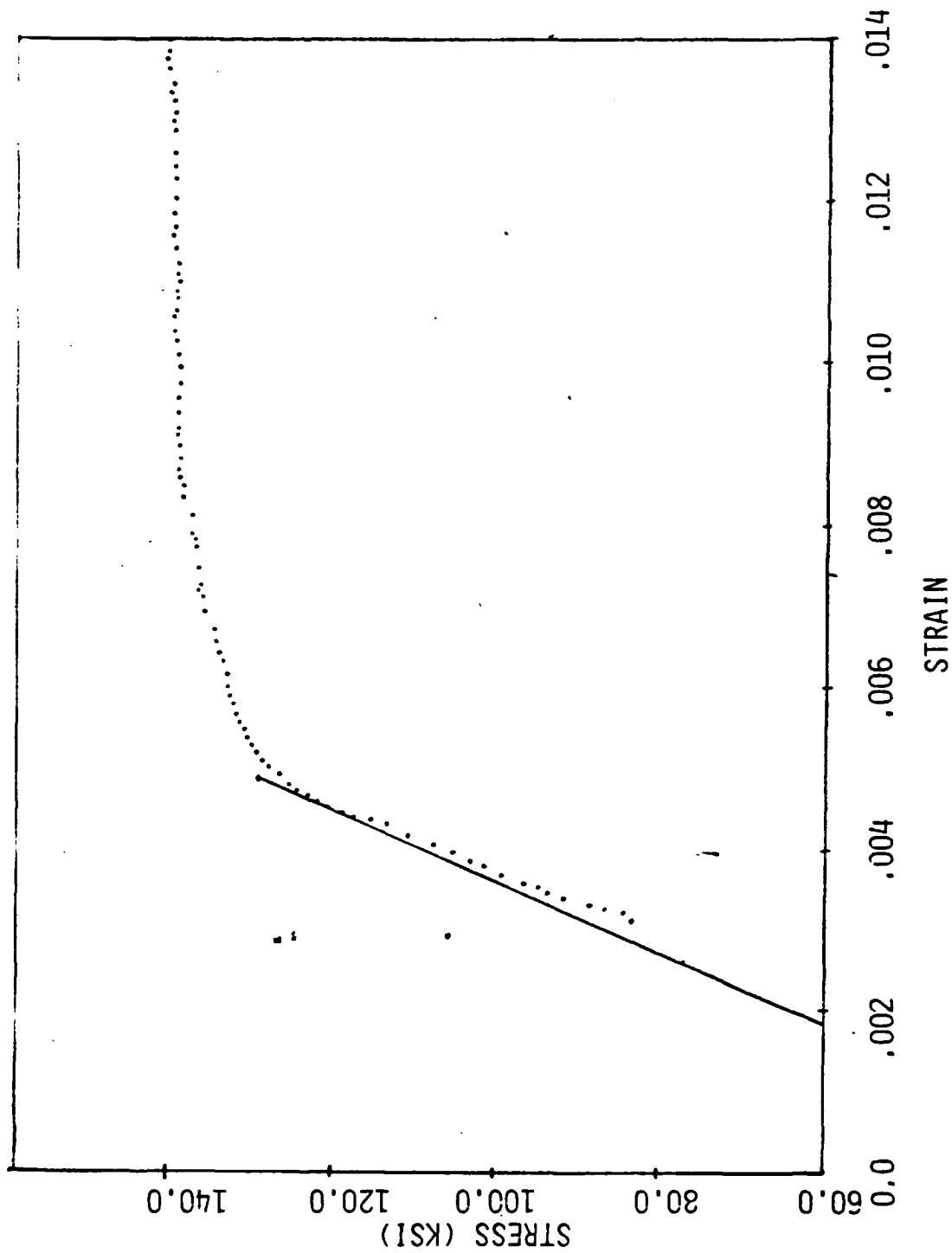


Figure 58. Experimental Stress-Strain Curve, IN 718, 1200°F

modulus as a more reliable description of the material's elastic behavior, the modulus was drawn on the figure, tangential to the curve of the data. The origin of the axes was then translated a negative 0.000575 units along the x-axis. This allowed the curve to indicate zero strain at a condition of zero stress.

Coordinates of selected data points were then read off the figure. The following table contains the information as digitized at this point:

TABLE VIII  
Experimental Data From Figure 58

Point No.	Stress(y)	Strain(x)	Strain plus "offset" strain
0	122.6 KSI	.00465	.005225
1	126 KSI	.00492	.005495
2	128 KSI	.00506	.005635
3	130 KSI	.00535	.005925
4	132 KSI	.00587	.006445
5	134 KSI	.00654	.007115
6	136 KSI	.00725	.007825
7	138 KSI	.0085	.009075
8	138.6 KSI	.00955	.010125
9	139 KSI	.01114	.011715
10	139.5 KSI	.012985	.01356

Computation of the plastic work  $W_p$  requires that plastic strains be derived from the total strains indicated from Figure 58. Using Hooke's Law, plastic strains may be computed from the equation



$$\epsilon^P = \epsilon - \frac{\sigma}{E} \quad (33)$$

The resulting values were then plotted against stress  $\sigma$ , and a numerical integration technique employed to evaluate the area under the curve.

TABLE IX  
Computation of Plastic Strain

Point No.	Total strain	Elastic strain	Plastic strain
0	.005225	122.6/23.6x10 <sup>3</sup>	3.01 x 10 <sup>-5</sup>
1	.005495	126/23.6x10 <sup>3</sup>	1.56 x 10 <sup>-4</sup>
2	.005635	128/23.6x10 <sup>3</sup>	2.11 x 10 <sup>-4</sup>
3	.005925	130/23.6x10 <sup>3</sup>	4.17 x 10 <sup>-4</sup>
4	.006445	132/23.6x10 <sup>3</sup>	8.52 x 10 <sup>-4</sup>
5	.007115	134/23.6x10 <sup>3</sup>	1.44 x 10 <sup>-3</sup>
6	.007825	136/23.6x10 <sup>3</sup>	2.06 x 10 <sup>-3</sup>
7	.009075	138/23.6x10 <sup>3</sup>	3.23 x 10 <sup>-3</sup>
8	.010125	138.6/23.6x10 <sup>3</sup>	4.25 x 10 <sup>-3</sup>
9	.011715	139/23.6x10 <sup>3</sup>	5.83 x 10 <sup>-3</sup>
10	.01356	139.5/23.6x10 <sup>3</sup>	7.65 x 10 <sup>-3</sup>

The plastic strain indicated for the point #0 was supposed to be zero, and is included here to indicate the limits on accuracy imposed by the method employed. Linearly interpolating between the points of Figure 12, and extrapolating to find a point where plastic strain  $\epsilon^P$  is zero, the values for plastic work  $W_p$  were then computed. The general form of the equation used is

$$W_p^n = W_p^{n-1} + \sigma^{n-1} (\epsilon^{p(n)} - \epsilon^{p(n-1)}) + \frac{1}{2}(\epsilon^{p(n)} - \epsilon^{p(n-1)})(\sigma^n - \sigma^{(n-1)}) \quad (34)$$

$$\begin{aligned} W_p^0 &= 0 + 121.79(.0000301 - 0) + \frac{1}{2}(.0000301 - 0)(122.6 - 121.79) \\ &= 0 + .00367 + \frac{1}{2}(.0000301)(122.6 - 121.79) \\ &= .00368 \end{aligned}$$

$$\begin{aligned} W_p^1 &= W_p^0 + 122.6(.000156 - .0000301) + \frac{1}{2}(.000156 - .0000301)(126 - 122.6) \\ &= .00368 + .0154 + .000214 \\ &= .01933 \end{aligned}$$

$$\begin{aligned} W_p^2 &= W_p^1 + 126(.000211 - .000156) + \frac{1}{2}(.000211 - .000156)(128 - 126) \\ &= .01933 + .00696 + .0000553 \\ &= .02635 \end{aligned}$$

$$\begin{aligned} W_p^3 &= W_p^2 + 128(.000417 - .000211) + \frac{1}{2}(.000417 - .000211)(130 - 128) \\ &= .02635 + .026327 + .000205 \\ &= .05282 \end{aligned}$$

$$\begin{aligned} W_p^4 &= W_p^3 + 130(.000852 - .000417) + \frac{1}{2}(.000852 - .000417)(132 - 130) \\ &= .05282 + .05658 + .000435 \\ &= .1098 \end{aligned}$$

$$\begin{aligned} W_p^5 &= W_p^4 + 132(.00144 - .000852) + \frac{1}{2}(.00144 - .000852)(134 - 132) \\ &= .1098 + .07725 + .000586 \\ &= .1877 \end{aligned}$$

$$\begin{aligned} W_p^6 &= W_p^5 + 134(.00206 - .00144) + \frac{1}{2}(.00206 - .00144)(136 - 134) \\ &= .1877 + .0838 + .000625 \\ &= .2721 \end{aligned}$$

$$\begin{aligned}
 W_p^7 &= W_p^5 + 136(.00323 - .00206) + \frac{1}{2}(.00323 - .00206)(138-136) \\
 &= .2721 + .1585 + .00117 \\
 &= .4317
 \end{aligned}$$

$$\begin{aligned}
 W_p^8 &= W_p^7 + 138(.00425 - .00323) + \frac{1}{2}(.00425 - .00323)(138.6-138) \\
 &= .4317 + .1414 + .000307 \\
 &= .5734
 \end{aligned}$$

$$\begin{aligned}
 W_p^9 &= W_p^8 + 138.6(.00583 - .00425) + \frac{1}{2}(.00583 - .00425)(139-138.6) \\
 &= .5734 + .218 + .000315 \\
 &= .7918
 \end{aligned}$$

$$\begin{aligned}
 W_p^{10} &= W_p^9 + 139(.00765 - .00583) + \frac{1}{2}(.00765 - .00583)(139.5-139) \\
 &= .7918 + .2535 + .000456 \\
 &= 1.0457
 \end{aligned}$$

Thus the x-coordinates of Equation (23) were computed. Determination of the y-coordinates begins with the evaluation of the equation

$$z = \sigma \left[ \frac{2n}{n+1} \ln \frac{2D_o}{\sqrt{3}\epsilon^p} \right]^{\frac{1}{2}n} \quad (24)$$

which requires that plastic strain rates be determined at each data point. The intervals between the points were numbered (0) through (10). Since numerical methods were used to determine elastic stress rates (from changes in the stress over time intervals), strain rates for the intervals were computed and the values of two adjoining intervals averaged to arrive at an appropriate value for the points.

Plastic strain rates were determined according to the following relationships:

$$\dot{\epsilon} = 1.3 \times 10^{-5} = \dot{\epsilon}^p + \dot{\epsilon}^e \quad (35)$$

$$\dot{\epsilon}^e = \frac{\dot{\sigma}}{E} = \frac{\Delta\sigma}{\Delta t} \frac{1}{E} \quad (36)$$

Since the total strain rate is constant, t can be computed for each interval using the change in total strain.

TABLE X

Determination of the Elastic Strain Rate  $\dot{\epsilon}^e$

Interval	$\Delta\epsilon$	$\Delta t$ (sec)	$\Delta\sigma$ (KSI)	$\frac{\Delta\sigma}{\Delta t}$ $\frac{\text{KSI}}{\text{SEC}}$	$\dot{\epsilon}^e$ ( $\text{sec}^{-1}$ )
0	.000030085	2.314	.8123	.351	$1.49 \times 10^{-5}$
1	.000125932	9.687	3.4	.351	$1.49 \times 10^{-5}$
2	.000055254	4.2503	2.0	.471	$1.99 \times 10^{-5}$
3	.000205254	15.789	2.0	.127	$5.37 \times 10^{-6}$
4	.000435255	33.481	2.0	.0597	$2.53 \times 10^{-6}$
5	.000585254	45.019	2.0	.0444	$1.88 \times 10^{-6}$
6	.000625254	48.096	2.0	.0416	$1.76 \times 10^{-6}$
7	.001165254	89.635	2.0	.0223	$9.45 \times 10^{-7}$
8	.001024577	78.814	0.6	.00761	$3.23 \times 10^{-7}$
9	.001573050	121.004	0.4	.00331	$1.40 \times 10^{-7}$
10	.001823814	140.293	0.5	.00356	$1.51 \times 10^{-8}$

Values for the plastic strain rates over the intervals can be easily computed, as the total strain rate is constant and the elastic component has now been calculated. The plastic strain rates at the points were then determined by averaging the rates over the intervals

adjacent to the point. The results are as follows:

TABLE XI  
Determination of Plastic Strain Rate  $\dot{\epsilon}^p$

Interval	$\dot{\epsilon}^p$ (sec <sup>-1</sup> )	Point	$\dot{\epsilon}^p$ (sec <sup>-1</sup> )	Stress(KSI)	Stress(MPa)
0	$-1.87 \times 10^{-6}$	0	$-1.87 \times 10^{-6}$	122.6	845.305
1	$-1.87 \times 10^{-6}$	1	$-4.41 \times 10^{-6}$	126	868.748
2	$-6.94 \times 10^{-6}$	2	$3.47 \times 10^{-7}$	128	882.537
3	$7.63 \times 10^{-6}$	3	$9.05 \times 10^{-6}$	130	896.327
4	$1.05 \times 10^{-5}$	4	$1.08 \times 10^{-5}$	132	910.117
5	$1.11 \times 10^{-5}$	5	$1.12 \times 10^{-5}$	134	923.906
6	$1.12 \times 10^{-5}$	6	$1.16 \times 10^{-5}$	136	937.696
7	$1.21 \times 10^{-5}$	7	$1.24 \times 10^{-5}$	138	951.933
8	$1.27 \times 10^{-5}$	8	$1.28 \times 10^{-5}$	138.6	954.933
9	$1.29 \times 10^{-5}$	9	$1.29 \times 10^{-5}$	139	958.380
10	$1.28 \times 10^{-5}$	10	$1.28 \times 10^{-5}$	139.5	961.828

Notice that the plastic strain rates over intervals (0), (1), and (2) turned out to have negative values. It would appear that the points defining these intervals are sufficiently close to the elastic region that graphical methods are not accurate enough to allow adequate determination of the strains and stresses there. Because of the negative values, the data corresponding to points 0 and 1 cannot be graphed, and the data corresponding to point 2 is highly suspect (and will be ignored when the data is graphed) because one of the neighboring intervals had a negative plastic strain rate.

At this point,  $W_p$  has been determined and the groundwork has been laid to allow the determination of  $Z$  and  $\ln(Z_1 - Z)$ . Calculation of  $Z$  adds some complexity to the procedure in that there are still four values of  $n$  under consideration. The following four data sets contain the information for each value of  $n$  and  $Z_1$ . The variable  $Z$  was evaluated using Equation (24).

TABLE XII

Computation of  $\ln(Z_1 - Z)$ ;  $n = 2.5, Z_1 = 1992.878$  MPa

Point	$\left[ \frac{2n}{n+1} \ln \frac{2D_o}{\sqrt{3E}P} \right]^{1/2n}$	Z (MPa)	$\ln(Z_1 - Z)$
2	2.1036	1856.489	4.916
3	2.0537	1840.771	5.025
4	2.0508	1866.509	4.839
5	2.0503	1894.267	4.591
6	2.0496	1921.916	4.262
7	2.0486	1949.256	3.776
8	2.0481	1955.822	3.612
9	2.0480	1962.778	3.405
10	2.0480	1969.846	3.137

TABLE XIII

Computation of  $\ln(Z_1 - Z)$ ;  $n = 3.0$ ,  $Z_1 = 1794.672$  MPa

Point	$\left[ \frac{2n}{n+1} \ln \frac{2D_o}{\sqrt{3}\epsilon P} \right]^{1/2n}$	Z (MPa)	$\ln (Z_1 - Z)$
2	1.8735	1653.474	4.950
3	1.8364	1646.048	5.001
4	1.8343	1669.447	4.830
5	1.8339	1694.353	4.608
6	1.8334	1719.177	4.324
7	1.8327	1743.771	3.930
8	1.8323	1749.718	3.806
9	1.8322	1755.957	3.656
10	1.8322	1762.279	3.478

TABLE XIV

Computation of  $\ln(Z_1 - Z)$ ;  $n = 3.125$ ,  $Z_1 = 1756.858$  MPa

Point	$\left[ \frac{2n}{n+1} \ln \frac{2D_o}{\sqrt{3}E^p} \right]^{\frac{1}{2}n}$	Z (MPa)	$\ln (Z_1 - Z)$
2	1.8300	1615.062	4.954
3	1.7952	1609.095	4.996
4	1.7932	1632.045	4.827
5	1.7928	1656.408	4.610
6	1.7924	1680.694	4.333
7	1.7917	1704.764	3.953
8	1.7913	1710.593	3.834
9	1.7912	1716.695	3.693
10	1.7913	1722.875	3.526



TABLE XV

Computation of  $\ln(Z_1 - Z)$ ;  $n = 3.211$ ,  $Z_1 = 1732.871$  MPa

Point	$\left[ \frac{2n}{n+1} \ln \frac{2D_o}{\sqrt{3}\epsilon^P} \right]^{\frac{1}{2}n}$	Z (MPa)	$\ln (Z_1 - Z)$
2	1.8025	1590.744	4.957
3	1.7691	1585.683	4.992
4	1.7672	1608.346	4.825
5	1.7668	1632.365	4.610
6	1.7664	1656.310	4.338
7	1.7657	1680.048	3.967
8	1.7654	1685.802	3.852
9	1.7653	1691.817	3.715
10	1.7653	1697.908	3.554

This data is presented in graphical form in Figures 13 through 16. According to Equation (23), the data should have indicated a straight line that would allow determination of  $m$  and  $Z_0$ . In each case, however, the data appeared to follow more of a bi-linear distribution than a linear one. When the data point 2 (which contains some influence from that negative strain rate) is ignored, the first five points suggest one linear approximation and the last four points suggest another. It is perhaps a curious coincidence that the distribution is bi-linear; the failure of the data to be linear could be due to the inadequacy of the Bodner model or simply due to scatter of the experimental data. Whatever the cause, one single straight line was not indicated by the data, so a slight modification to the procedure was indicated.

In each case, three straight lines were taken from the figure. One straight line, drawn through the first five data points, indicated what is referred to as the "front" values of  $m$  and  $Z_0$ . One straight line, drawn through the last four data points, indicated what is referred to as the "back" values of  $m$  and  $Z_0$ . And an approximation of a straight line through all the data provided what is called the "mean" values of  $m$  and  $Z_0$ .

The following are the four data sets at the conclusion of this procedure:

Set #1:  $n = 2.5$

$$Z_1 = 1992.878 \text{ MPa}$$

"front"

$$m = .483 \text{ MPa}^{-1}$$

$$Z_0 = 1811.606 \text{ MPa}$$

"back"

$$m = .15 \text{ MPa}^{-1}$$

$$Z_0 = 1924.161 \text{ MPa}$$

"mean"

$$m = .242 \text{ MPa}^{-1}$$

$$Z_0 = 1866.408 \text{ MPa}$$

Set #2: n = 3.0

$$Z_1 = 1794.672 \text{ MPa}$$

"front"

$$m = .417 \text{ MPa}^{-1}$$

$$Z_0 = 1622.24 \text{ MPa}$$

"back"

$$m = .104 \text{ MPa}^{-1}$$

$$Z_0 = 1725.264 \text{ MPa}$$

"mean"

$$m = .219 \text{ MPa}^{-1}$$

$$Z_0 = 1669.461 \text{ MPa}$$

Set #3: n = 3.125

$$Z_1 = 1756.858 \text{ MPa}$$

"front"

$$m = .4 \text{ MPa}^{-1}$$

$$Z_0 = 1586.143 \text{ MPa}$$

"back"

$$m = .0985 \text{ MPa}^{-1}$$

$$Z_0 = 1686.753 \text{ MPa}$$

"mean"

$$m = .18 \text{ MPa}^{-1}$$

$$Z_0 = 1637.754 \text{ MPa}$$

Set #4: n = 3.211

$$Z_1 = 1732.871 \text{ MPa}$$

"front"

$$m = .4 \text{ MPa}^{-1}$$

$$Z_0 = 1562.155 \text{ MPa}$$

"back"

$$m = .0938 \text{ MPa}^{-1}$$

$$Z_0 = 1663.463 \text{ MPa}$$

"mean"

$$m = .185 \text{ MPa}^{-1}$$

$$Z_0 = 1608.284 \text{ MPa}$$

## APPENDIX D

### Computer Programs

This appendix contains the three computer codes used in the course of this work. All three use the Bodner constitutive relations to predict material behavior for uniaxial loading conditions. The two programs called BODNER and CYBODR were written by A. M. Rajendran of the University of Dayton Research Institute.

#### Program BODNER

This program is used to generate stress-strain curves (e.g. Figure 1) and creep curves (e.g. Figure 22). It is written in FORTRAN 4; it utilizes an external data file (TAPE5) for input and creates two output files (TAPE6 and TAPE7). The file TAPE6 contains the incremental values of the program parameters and is formatted in a readable fashion. TAPE7 contains plotting data in x-y pairs (strain = x, stress = y for strain rate controlled runs; time = x, strain = y for stress rate controlled runs).

The format for the input file TAPE5 is as follows:

line 1: Bodner model, material coefficients, free format, using real values

$E, Z_0, Z_1, Z_2, m, A, r, n$

line 2: test control parameter, integer value (0, 1 or 2)

0 implies strain rate controlled run

1 implies stress rate controlled run

2 implies run over

line 3: number of times the controlling load (strain rate or stress rate) changes; integer value

line 4: test conditions, free format, using real values

Rate, Time, Time step, Print interval

where rate = stress or strain rate in this part of the test

time = time when this test condition terminates, measured from the start of all loading

time step = time increment used for calculations (for the stress-strain curves used in this work, the time step was 0.01 sec)

print interval = time interval between printed output values

Repeat line 4 until there are the same number of test conditions specified as there are load changes indicated in line 3 (i.e. if line 3 reads "3" there should be three line 4's following it.

last line: test termination parameter; integer value of 2, free format

#### Program PLOT

This program is used to generate strain rate versus stress curves (e.g. Figure 6). It is written in FORTRAN 5. Values for the variables are set by modifying the program statements directly. The dimensionless forms of the coefficients are used. Values for  $m$  times  $Z_1$ ,  $n$ ,  $AVD_0$  ( $A/D_0$ ),  $r$ , and  $Z_2/Z_1$  must be established. The form listed here generates a family of curves, one for each different value of  $Z_2/Z_1$ .

Output is into a file called TAPE5; x-y plotting pairs for non-dimensionalized strain rate versus stress curves are written in free format onto TAPE5.

Program CYBODR

This program is used to generate stress-strain curves for cases involving cyclic loading (e.g. Figure 32). It is written in FORTRAN 4 and is meant to be run interactively. The Bodner material coefficients can be changed either before compilation (by modifying the code) or during execution when terminal inputs are solicited. The variable  $q$  can only be changed by modifying it in the text of the code. This is a user-friendly program requiring no special instructions prior to operation. Output is to TAPE6 in a formatted-to-read record of time steps and incremental variable values, and to TAPE7 as free-formatted  $x$ - $y$  pairs.

PROGRAM BODNER (INPUT,OUTPUT,TAPES,TAPE6,TAPE7)

.... BODNERS MODEL IS A UNIFIED THEORY WITH ONE  
STATE VARIABLE KNOWN AS THE HARDNESS PARAMETER,Z...

.... THIS CODE USES A FIRST ORDER EULER FORWARD  
INTEGRATION SCHEME IN ORDER TO COMPARE IT TO  
OTHER THEORIES OF THE SAME TYPE.....

COMMON/A/E,Z0,Z1,ZI,RM,A,R,RN,D0,UP,EXLMT,EXUPLMT

....READ IN THE BODNER CONSTANTS AS SHOWN.....

REWIND 5  
REWIND 6  
REWIND 7

EXLMT=1.0 8 EXUPLMT= 70.0

READ(5,\*) E,Z0,Z1,ZI,RM,A,R,RN  
UP=0.0  
SIG=0.0  
EPLAS=0.0  
STRAIN=0.0  
D0=1.E06  
T=0.0

....UP IS THE PLASTIC WORK INITIALLY  
....SIG IS THE STRESS  
....EPLAS IS THE PLASTIC  
....STRAIN IS TOTAL STRAIN = ELASTIC + INELASTIC COMPONENTS  
....D0 IS A BODNER CONSTANT  
....T IS THE CURRENT TIME

$Z = Z1 - (Z1 - Z0) \times \exp(-RM \times UP)$

....THE ABOVE Z EQUATION IS USED TO DETERMINE THE FIRST  
VALUE OF Z ONLY.

101 WRITE(6,101) E,Z0,Z1,ZI,RM,A,R,RN  
FORMAT(10X,2X,3E-1,E11.4,2X,2Z0-1,F6.2,2X,2Z1-1,F7.2,3X,2ZI-1,  
1 F6.2,2X,2M-1,F5.2,2X,2A-1,E10.3,2X,2R-1,F5.2,2X,2SMALL N-1,  
1F4.2,//)

17 CONTINUE  
READ(5,\*) M  
M=0 DENOTES STRAIN CONTROL, KNOWN STRAIN RATE OR STRAIN/TIME CURVE  
M=1 DENOTES: STRESS CONTROL, KNOWN STRESS/TIME (PIECEWISE LINEAR) CURVE  
M=2 INDICATES A JUMP OUT OF THE LOOP TO STOP.

IF(M.EQ.0) GO TO 15  
IF(M.EQ.1) GO TO 16  
IF(M.EQ.2) GO TO 999

15 CONTINUE  
CALL EPSLON(T,SIG,STRAIN,Z,EPLAS)  
GO TO 17  
16 CONTINUE  
CALL STRESS(T,SIG,STRAIN,Z,EPLAS)  
GO TO 17  
999 CONTINUE  
END

```

SUBROUTINE EPSLON(T,SIG,STRAIN,Z,EPLAS)
COMMON/A,E,Z0,Z1,ZI,RM,A,R,RN,D0,UP,EXLMT,EXUPLMT
WRITE(6,150)
150 FORMAT(10X,1X,THIS SECTION HAS M=0,FOR STRAIN CONTROL,WHERE THE S
I TRAIN/TIME CURVE IS IMPOSED.,//)
C
READ(5,*) N
WRITE(6,102) N
102 FORMAT(10X,1X,IMPOSED STRAIN RATE CHANGES,12,1X, TIMES,/,)
C
...N IS THE NUMBER OF TIMES THE STRAIN RATE CHANGES,
... NOT COUNTING THE ORIGIN POINT.
C
SSC=50.
ESC=0.5
WRITE(6,103)
103 FORMAT(15X,1X,8X,DELTA T,10X,STRESS,6X,STRAIN RATE,6X,
1X,STRAIN,5X,PLASTIC,12X,2X,/)
DO 25 I=1,N
C
READ(5,*) RATE,TIME,DELTAT,PRINT
C
C
C
....RATE = STRAIN RATE IN THIS PIECEWISE LINEAR REGION
....TIME = TIME WHEN RATE FINISHES AND CHANGES TO THE NEXT RATE
....DELTAT = TIME INCREMENT THAT THE RATE IS DIVIDED INTO
....PRINT = AT WHAT TIME INTERVALS A VALUE WILL BE PRINTED
C
P=0.0
CONST = DELTAT*2.0/SQRT(3.0)*D0
10 CONTINUE
T = T + DELTAT
P=P+DELTAT
IF(ABS(SIG).LE.EXLMT) GO TO 5
X=-((RN+1.)/(2.*RN))*(Z/ABS(SIG))*(2.*RN)
IF(ABS(X).GE.EXUPLMT) GO TO 5
CONTRB = SIGN(CONST*EXP(X),SIG)
GO TO 6
5 CONTINUE
CONTRB = 0.0
6 CONTINUE
EPLAS = EPLAS + CONTRB
UPDOT=SIG*(CONTRB)/DELTAT
SIG=SIG+EX*(DELTAT*RATE)-EX*(CONTRB)
STRAIN=SIG/E+EPLAS
ZDOT=RN*(Z1-Z)*UPDOT-Z1*X*((Z-Z1)/Z1)*R
Z=Z+ZDOT*DELTAT
IF (P.LT.PRINT) GO TO 113
WRITE(6,104) T,DELTAT,SIG,RATE,STRAIN,EPLAS,Z
104 WRITE(7,*) STRAIN,SIG
FORMAT(1X,F8.3,5X,F8.4,3X,5E14.4)
SX1=SIG/SSC
EPX1=100.*STRAIN/ESC
P=0.0
113 IF (T.LT.TIME) GOTO 10
24 T=TIME
25 CONTINUE
WRITE(7,*) 999,999
RETURN
END
C
C

```



```

SUBROUTINE STRESS(T,SIG,STRAIN,Z,EPLAS)
COMMON/A,E,Z0,Z1,Z1,RN,A,R,RN,D0,UP,EXLMT,EXUPLMT
WRITE(6,151)
151 FORMAT(10X,1X,THIS SECTION HAS N=1,FOR STRESS CONTROL,WHERE STRES
IS/TIME CURVE IS IMPOSED.,/)
C
READ(5,*) N
WRITE(6,112) N
112 FORMAT(10X,1X,IMPOSED STRESS RATE CHANGES,I2,1X,XTIMES.,/)
SSC=50.
ESC=0.5
WRITE(6,153)
153 FORMAT(15X,1X,9X,DELTA T,10X,STRESS,6X,STRESS RATE,6X,STRA
1IN X,5X,PLASTIC,12X,2X,/)
C
DO 28 I=1,N
READ(5,*) RATE,TIME,DELTAT,PRINT
CONST=DELTAT*2.0/SQRT(3.0)*D0
P=0.0
110 CONTINUE
T=T+DELTAT
P=P+DELTAT
IF(ABS(SIG).LE.EXLMT) GO TO 105
X=-((RN+1.)/(2.*RN))*Z/ABS(SIG)*X(2.*RN)
IF(ABS(X).GE.EXUPLMT) GO TO 105
CONTRB=SIGN(CONST*EXP(X),SIG)
GO TO 106
105 CONTINUE
CONTRB=0.0
106 CONTINUE
EPLAS=EPLAS+CONTRB
STRAIN=STRAIN+DELTAT*RATE/E+CONTRB
UPDOT=SIG*CONTRB/DELTAT
SIG=EXP(STRAIN-EPLAS)
ZDOT=RN*(Z1-Z)*UPDOT-Z1*X*((Z-Z1)/Z1)*X
Z=Z+ZDOT*DELTAT
PP=P+.00000001
IF(PP.LT.PRINT) GO TO 152
WRITE(6,107) T,DELTAT,SIG,RATE,STRAIN,EPLAS,Z
WRITE(7,*) T,STRAIN
107 FORMAT(10X,1X,F8.3,5X,F8.4,3X,SE14.4)
SX1=SIG/SSC
EPX1=100.*STRAIN/ESC
P=0.0
152 CONTINUE
TTT=T+.000000001
IF(TTT.LT.TIME) GO TO 110
124 T=TIME
28 CONTINUE
RETURN
END

```

```

PROGRAM PLOT
X
X
COMMON/VALUE/MZ1,AUD0,Z2UZ1,N,R,X,L
REAL MZ1,AUD0,Z2UZ1,N,XP,DUMMY,F,XARRAY,YARRAY,R
INTEGER L
DIMENSION DUMMY(8),F(2),XARRAY(54),YARRAY(54)
X
X
XXXXXXXXXXXXXXXXXXXXX
X CREATE SOME STARTING PLACE FOR X IN THE
X ITERATIVE SCHEME TO FOLLOW
X
XXXXXXXXXXXXXXXXXXXXX
X
X   X = .5
X
XXXXXXXXXXXXXXXXXXXXX
X INITIALIZE NOMINAL VALUES OF THE
X "BACKGROUND" COEFFICIENTS
X
XXXXXXXXXXXXXXXXXXXXX
X
X   MZ1 = 747.859822
X   N = 3.0
X   AUD0 = .000000003
X   R = 7.0
X   DO 200 K=1,5
X
XXXXXXXXXXXXXXXXXXXXX
X INITIALIZE THE COEFFICIENT OF INTEREST
X
XXXXXXXXXXXXXXXXXXXXX
X
X   IF (K .EQ. 1) THEN
X     Z2UZ1 = 0.3
X   ELSE IF (K .EQ. 2) THEN
X     Z2UZ1 = 0.35
X   ELSE IF (K .EQ. 3) THEN
X     Z2UZ1 = 0.4
X   ELSE IF (K .EQ. 4) THEN
X     Z2UZ1 = 0.45
X   ELSE IF (K .EQ. 5) THEN
X     Z2UZ1 = 0.5
X     R = 7.3
X   ENDIF
X
X   Y = 1.220703125E-16
X   YARRAY(1) = Y
X
X
X   CALL CALC (Y)
X
X   XARRAY(1) = X
X
X   DO 100 I=1,53
X     L = I + 1
X     Y = 2. * Y
X     CALL CALC(Y)
X     XARRAY(L) = X
X     YARRAY(L) = Y
100 CONTINUE
X
X   DO 150 ID=1,54
X     WRITE (5,X) XARRAY(ID),YARRAY(ID)
150 CONTINUE
X
X   200 CONTINUE
X
X
X   999 FORMAT (F15.13)
X
X   END

```

```

SUBROUTINE CALC(Y)
COMMON/VALUE/MZ1,AUD0,Z2UZ1,N,R,X,L
*
REAL X,Y,MZ1,AUD0,Z2UZ1,N,DUMMY,F,XP,R
*
INTEGER M
*
DIMENSION DUMMY(8),F(2)
*
*
DUMMY(1) = (2. * N) / (N + 1.)
*
DO 100 J=1,1
DUMMY(2) = LOG(2./((SQRT(3.))*Y))
ALPHA = (DUMMY(1) * DUMMY(2))**((1./(2.*N))
DUMMY(3) = MZ1 * (1.-(ALPHA * X)) * X * Y
DUMMY(4) = AUD0 * ((ALPHA * X) - Z2UZ1) ** R
F(1) = DUMMY(3) - DUMMY(4)
XP = 1.1 * X
*
DO 50 K=1,50
N = L - 1
IF (N .GE. 39) THEN
X = 1./ ALPHA
GOTO 60
ELSE
DUMMY(5) = MZ1 * (1. -(ALPHA * XP)) * XP * Y
DUMMY(6) = AUD0 * ((ALPHA * XP) - Z2UZ1) ** R
F(2) = DUMMY(5) - DUMMY(6)
DUMMY(7) = (F(2) * (X - XP))/(F(1) - F(2))
DUMMY(8) = XP - DUMMY(7)
F(1) = F(2)
X = XP
XP = DUMMY(8)
IF (ABS(F(1)).LT.1.E-15) GOTO 60
ENDIF
50 CONTINUE
PRINT *, 'ROUTINE DID NOT CONVERGE'
60 CONTINUE
100 CONTINUE
RETURN
END

```

PROGRAM CYBODR (INPUT,OUTPUT,TAPES,TAPE6,TAPE7)

THIS PROGRAM SOLVES BODNERS LATEST UNIFIED THEORY FOR ANISOTROPIC PLASTIC FLOW. THE STATE VARIABLE PARAMETER Z HAS BEEN SPLIT INTO Z TENSION AND Z COMPRESSION. BOTH VALUES OF Z ARE CONTINUOUSLY COMPUTED WHETHER THE LOADING IS IN POSITIVE OR NEGATIVE DIRECTION, IRRESPECTIVELY.

CYCLIC ANALYSIS IS CARRIED OUT WITH TIME STEP AUTOMATICALLY SELECTED BY THE PROGRAM. IT IS AN INTERACTIVE PROGRAM FOR DATA INPUT. THE NUMBER OF CYCLES ANALYSIS TO BE CARRIED OUT MUST BE TEN.

```

XXXXXXXXXXXXXXXXXXXXXXXXXXXXXXXXXXXXXXXXXXXX
X
X   DEVELOPED BY   A . M . RAJENDRAN
X   SERVICE LIFE MANAGEMENT SECTION,
X   UNIVERSITY OF DAYTON RESEARCH INSTITUTE.
X
XXXXXXXXXXXXXXXXXXXXXXXXXXXXXXXXXXXXXXXXXXXX
    
```

```

REAL M,MBAR,N
COMMON / MATCONS/ E,Z0,Z1,Z2,Z3,M,MBAR,N,A,R,D0,Q
COMMON / LIMITS / EXLMT,EXUPLMT,TOLR
    
```

```

DATA E/162.5E3/,Z0/1622./,Z1/1795./,Z2/718./,Z3/0.0/,
+M/.41667/,MBAR/0.0/,N/3.0/,A/1.5E-03/,R/7.0/,D0/1.E+06/
    
```

```

Q = -.50
REWIND 6
REWIND 5
WRITE(6,1001)
WRITE 1001
1001 FORMAT(//5X,60(1H#)/5X,1H#,58X,1H#/5X,1H#,14X,1CYCLIC #,
+*STRESS-STRAIN RESPONSE*,15X,1H#/5X,1H#,58X,1H#/5X,1H#,4X,
+*CALCULATED FROM BODNER-PARTON CONSTITUTIVE MODELS*,5X,1H#/
+5X,1H#,7X,*FOR ISOTROPIC/ANISOTROPIC MATERIAL BEHAVIOR*,8X,1H#/
+5X,1H#,58X,1H#/5X,60(1H#))
CALL PRINT
WRITE 1003
1003 FORMAT(//15X,*MATERIAL CONSTANT CHANGES NEEDED?*/16X,
+*(Y/N) ==> #)
20 READ 130, I
130 FORMAT(A1)
IF( I.EQ.'N') GO TO 250
IF(I.EQ.'Y')GO TO 50
WRITE 1000
1000 FORMAT(//15X,5(1H#),* INVALID RESPONSE *,5(1H#)/18X,
+*PLEASE ENTER 'Y' = YES*/31X,*'N' = NO*/28X,*--> #)
GO TO 20
50 WRITE 1002
1002 FORMAT(//5X,17(1H#),* ENTER MATERIAL CONSTANTS *,17(1H#)//
+8X,*NOTE: IF THE CURRENT VALUE OF A PARTICULAR CONSTANT IS*,
+//12X,*ACCEPTABLE, ENTER A ZERO IN THE FIELD AND RETURN*)
WRITE 134
134 FORMAT(/5X,60(1H#)//18X,*E = #)
CALL INPUT(E)
WRITE 135
135 FORMAT(17X,*Z0 = #)
CALL INPUT(Z0)
WRITE 136
136 FORMAT(17X,*Z1 = #)
CALL INPUT(Z1)
WRITE 137
137 FORMAT(17X,*Z2 = #)
CALL INPUT(Z2)
WRITE 138
138 FORMAT(17X,*Z3 = #)
CALL INPUT(Z3)
WRITE 139
139 FORMAT(18X,*M = #)
CALL INPUT(M)
WRITE 140
140 FORMAT(15X,*MBAR = #)
    
```

```

CALL INPUT(MBAR)
WRITE 141
141 FORMAT(18X,1A = 1)
CALL INPUT(A)
WRITE 142
142 FORMAT(18X,1R = 1)
CALL INPUT(R)
WRITE 143
143 FORMAT(18X,1Q = 1)
CALL INPUT(Q)
C
200 CONTINUE
CALL PRINT
C
C
C   VERIFY CONSTANT DATA INPUT
C
C   WRITE 144
144 FORMAT(//5X,1ARE THE PRINTED VALUES FOR THE MATERIAL CONSTANTS1,
+1 ACCEPTABLE?1//16X,1(Y/N) --) 1)
220 READ 130,1
IF(1.EQ.'N')GO TO 50
IF(1.EQ.'Y')GO TO 250
WRITE 1000
GO TO 220
250 EXLMT=1.0 1 EXUPLMT= 70.0 1 TOLR=1.E-15
C
C
C   WRITE 1005
1005 FORMAT(//5X,22(1H1),1 CYCLE CONTROL 1,23(1H1)//15X,
+1ENTER1,7X,1'1' = STRAIN1/27X,1'2' = STRESS1//24X,1--) 1)
READ 1,1PROB
CALL INCNTL (1PROB,E)
STOP
END
C
C
C
C   SUBROUTINE ZDOT(ZT,ZC,UDRCT,UPDOT,DELTAT)
REAL M,MBAR,N
COMMON / MATCONS / E,Z0,Z1,Z2,Z3,M,MBAR,N,A,R,D0,Q
COMMON / LIMITS / EXLMT,EXUPLMT,TOLR
IF(UDRCT.GT.TOLR) ZEFF=ZT
IF(UDRCT.LT.TOLR) ZEFF=ZC
HARD1=M*(Z1-ZEFF)*UPDOT
PPPPP=ABS((ZEFF-Z2)/Z1)
ZZDOT = HARD1-A*Z1*(PPPPP)*1R
ZTDOT = (Q+(1.0-Q)*UDRCT)*ZZDOT
ZCDOT = (Q-(1.0-Q)*UDRCT)*ZZDOT
ZT=ZT+ZTDOT*DELTAT
ZC=ZC+ZCDOT*DELTAT
RETURN
10 WRITE(6,1000)CH1,CH2
WRITE 1000,CH1,CH2
1000 FORMAT(//5X,22(1H1),1 END OF PROGRAM 1,22(1H1)//10X,
+1THE EXPONENT OF THE RECOVERY TERMS HAVE BECOME1/10X,
+1NEGATIVE IN SUBROUTINE 'ZDOT'1//16X,1CH1 = 1,E15.4/16X,
+1CH2 = 1,E15.4,/)
STOP
END
C
C
C
C   SUBROUTINE INPUT ( CNST )
READ 1, CNSTMAT
IF(CNSTMAT.LE. 0.000001) RETURN
CNST = CNSTMAT
RETURN
END
C
C
C   SUBROUTINE PRINT
REAL M,MBAR,N
COMMON / MATCONS / E,Z0,Z1,Z2,Z3,M,MBAR,N,A,R,D0,Q
COMMON / LIMITS / EXLMT,EXUPLMT,TOLR
WRITE 100,E,Z0,Z1,Z2,Z3,M,MBAR,N,A,R,D0,Q
WRITE(6,100)E,Z0,Z1,Z2,Z3,M,MBAR,N,A,R,D0,Q
100 FORMAT(//5X,13(1H1),1 CURRENT MATERIAL CONSTANT VALUES 1,
+13(1H1)//18X,1E = 1,F15.4/17X,1Z0 = 1,F15.4/17X,1Z1 = 1,F15.4/
+17X,1Z2 = 1,F15.4/17X,1Z3 = 1,F15.4/18X,1M = 1,F6.3/15X,1MBAR = 1,
+1F6.3/18X,1N = 1,F6.3/18X,1A = 1,F6.4/18X,1R = 1,F6.3/17X,1D0 = 1,
+1F7.1/18X,1Q = 1,F6.3/)

```

```

RETURN
END
C
C
SUBROUTINE INCNTL ( IPROB,E )
WRITE 100
100 FORMAT(///15X, 'TOTAL NUMBER OF CYCLES'//24X, I--> )
READ 1, NDCYCLE
WRITE 120
120 FORMAT(///15X, 'MAXIMUM AND MINIMUM STRAIN OR STRESS'//24X, I--> )
READ 1, SMAX, SMIN
WRITE 140
140 FORMAT(///15X, 'NUMBER OF CYCLES PER MINUTE'//24X, I--> )
READ 1, CPM
CPS=CPM/60.0
PERIOD = 1.0 / CPS
RATE = ( SMAX + SMIN ) / PERIOD * 2.0
TOTCY = NDCYCLE
TMAX = PERIOD * TOTCY
IF(IPROB.EQ.2) TSTEP=0.0001*E/RATE
IF(IPROB.EQ.1) TSTEP=0.0001/RATE
C
C
CALL STRSTN (IPROB,ZT,ZC,RATE,TSTEP,TMAX,PERIOD,SMAX,SMIN)
C
C
RETURN
END
C
C
SUBROUTINE RATECHG ( RATE,T,TSTEP,PERIOD,TCHECK,IDENT ,DTOLD
+ SMAX,SMIN,PCHECK )
TOLR=1.0E-15
IF(T.LE.TOLR) RETURN
TTT=TCHECK-TOLR
TEMP=ABS(RATE)
IF(IDENT.EQ.1) PCHECK=SMAX/TEMP
IF(IDENT.EQ.2) PCHECK=SMAX/TEMP
IF(IDENT.EQ.3) PCHECK=SMIN/TEMP
IF(IDENT.EQ.4) PCHECK=SMIN/TEMP
IF(TTT.LT.PCHECK) RETURN
TSTEP=DTOLD
TCHECK = 0.0
WRITE(6,1111)
1111 FORMAT(5X, '999 999 999 999 999 999 999 999 999 999 ', )
GO TO ( 1,2,3,4 ), IDENT
1 RATE=-RATE
IDENT=2
RETURN
2 IDENT=3
RETURN
3 RATE=-RATE
IDENT=4
RETURN
4 IDENT=1
RETURN
END
C
C
SUBROUTINE STRSTN ( IPROB,ZT,ZC,RATE,TSTEP,TMAX,PERIOD,SMAX,SMIN )
REAL M,MBAR,N
COMMON / MATCONS/ E,Z0,Z1,Z2,Z3,M,MBAR,N,A,R,D0,G
COMMON / LIMITS / EXLMT,EXUPLMT,TOLR
INITIALIZE THE VARIABLES
ZT=Z0 $ ZC=Z0 $ DTOLD=TSTEP $ ISTOP=1 $ EPINCR=0.0
UP= 0.0 $ SIG = 0.0 $ EPLAST = 0.0 $ ETOT = 0.0
T = 0.0 $ IDENT = 1 $ TCHECK = 0.0 $ TPRINT = 0.0
PCHECK=SMAX/RATE
C
C
PRINT HEADING
WRITE (6,200)
200 FORMAT(///5X,95(1H2)//
+10X,'TIME' 5X,'TIME STEP' 6X,'STRAIN' 10X,'STRESS'
+5X,'INELASTIC STRAIN' 3X,'TENSION' 5X,'COMPRESSION'//
+5X,95(1H2)//)

```

```

PRINT= PERIOD /200.0
10 CONTINUE
CALL RATECHG ( RATE, T, TSTEP, PERIOD, TCHECK, IDENT, DTOLD,
+SMAX, SMIN, PCHECK)
CALL TIMECHG(EPINCR, IDENT, TSTEP, ISTOP)
CALL TIMEADJ(PERIOD, TSTEP, TCHECK, DTOLD, IADJ, PCHECK)
CONST= TSTEP * 2. / SQRT ( 3.0 ) * D0
T=T+TSTEP
TCHECK=TCHECK+TSTEP
TPRINT=TPRINT+TSTEP
IF(ABS(SIG).LE.EXLMT) GO TO 100
IF(UDRCT.GT.TOLR) Z-ZT
IF(UDRCT.LT.TOLR) Z-ZC
X=-((M+1.)/(2.*N))*(((Z/ABS(SIG))*2)*N)
IF(ABS(X).GE.EXUPLMT) GO TO 100
EPINCR=SIGN(CONST * EXP(X), SIG)
GO TO 110
100 CONTINUE
EPINCR=0.0
110 CONTINUE
EPLAST=EPLAST+EPINCR
UPDOT=SIG*EPINCR/TSTEP
GO TO (120, 130), IPR0B
120 SIG=SIG+EX(TSTEP*RATE-EPINCR)
ETOT=SIG/E+EPLAST
GO TO 140
130 ETOT=ETOT+TSTEP*RATE/E+EPINCR
SIG=EX(ETOT-EPLAST)
140 CONTINUE
UDRCT=SIG/ABS(SIG)
CALL ZDOT(ZT, ZC, UDRCT, UPDOT, TSTEP)
TTT=TPRINT+TOLR
IF(IADJ.EQ.1) GO TO 145
IF(TTT.LT.PRINT) GO TO 150
145 CONTINUE
WRITE(7, 222) T, TSTEP, ETOT, SIG, EPLAST, ZT, ZC
WRITE (5, *) ETOT, SIG
222 FORMAT(5X, 7(E12.5, 4X))
TPRINT = 0.0
150 CONTINUE
TTT=T+TOLR
IF(TTT.LT.TMAX) GO TO 10
RETURN
END
SUBROUTINE TIMECHG(A, IDENT, TSTEP, ISTOP)
TOLR=1.0E-06
CR=ABS(A)
GO TO (10, 20, 10, 20), IDENT
10 IF(CR .LE. TOLR) RETURN
IF(ISTOP .EQ. 2) RETURN
TSTEP=TSTEP/10.0
ISTOP=2
RETURN
20 IF(CR.GE.TOLR) RETURN
IF(ISTOP .EQ. 3) RETURN
TSTEP=TSTEP*10.0
ISTOP=3
RETURN
END

```

C  
C  
C  
C

```

SUBROUTINE TIMEADJ(PERIOD, TSTEP, TCHECK, DTOLD, IADJ, PCHECK)
DT1=PCHECK-TCHECK
IADJ=0
IF(DT1 .GE. TSTEP) RETURN
IADJ=1
DTOLD=TSTEP
TSTEP=DT1
RETURN
END

```

## Bibliography

1. Bodner, S. R. "Representation of Time Dependent Mechanical Behavior of Rene 95 By Constitutive Equations," Technical Report AFML-TR-79-4116, August 1979.
2. Keck, J. E. "The High Temperature Viscoplastic Fatigue Behavior of a Compact Tension Specimen Using the Bodner-Partom Flow Law," Master of Science Thesis, Department of Aeronautics and Astronautics, Air Force Institute of Technology, 82/GAE/17, 1982.
3. Hinnerichs, T., Nicholas, T., and Palazotto, A. "A Hybrid Experimental-Numerical Procedure for Determining Creep Crack Growth Rates," Journal of Fracture Mechanics, Vol. 16, No. 2, pp 265-277, 1982.
4. Stouffer, D. C. and Bodner, S. R. "A Constitutive Model for the Deformation Induced Anisotropic Plastic Flow of Metals," International Journal of Engineering Science, Vol. 17, pp 757-764, 1979.
5. Hertzberg, R. W. Deformation and Fracture Mechanics of Engineering Materials, John Wiley & Sons, Inc., 1976.
6. Stouffer, D. C., Papernik, L., and Bernstein, H. L. "Prediction of the Mechanical Response of a High-Temperature Superalloy-Rene 95," Technical Report AFWAL-TR-80-4184, September 1980.
7. Bodner, S. R., Partom, I., and Partom, Y. "Uniaxial Cyclic Loading of Elastic-Viscoplastic Materials," Journal of Applied Mechanics, ASME Paper No. 79-WA/APM-30.
8. Zaphir, Z. and Bodner, S. R. "Implementation of Elastic-Viscoplastic Constitutive Equations Into 'NONSAP' With Applications to Fracture Mechanics," Proceedings ADINA Conference, MIT Report 82448-9, August 1979.
9. Stouffer, D. C. "A Constitutive Representation for IN 100," Technical Report AFWAL-TR-81-4039, June 1981.
10. Domas, P. A. et al. "Benchmark Notch Test for Life Prediction," NASA CR-165571, NASA-Lewis Research Center, June 1982.
11. Barrett, C. R., Nix, W. D., and Teletman, A. S. The Principles of Engineering Materials, Prentice-Hall, Inc, Englewood Cliffs, New Jersey, 1973.
12. Gilman, J. J. "Dynamical Behavior of Dislocations," Mechanical Behavior of Materials Under Dynamic Loads, ed. by U.S. Lindholm, Springer-Verlag New York Inc., 1968.
13. Gilman, J. J. "The Plastic Resistance of Crystals," Australian Journal of Physics, Vol 13, pp 327-346, 1960.



14. Gilman, J. J. Micromechanics of Flow in Solids, McGraw-Hill Book Company, 1969.
15. Gilman, J. J. and Johnston, W. G. "The Origin and Growth of Glide Bonds in Lithium Fluoride Crystals," Dislocations and Mechanical Properties of Crystals, ed. by J. C. Fisher et al, John Wiley & Sons, Inc., New York, 1957.
16. Eisenberg, M. A. and Yen, C. F. "Application of a Theory of Viscoplasticity to Uniaxial Cyclic Loading," Journal of Engineering Materials and Technology, Vol. 105, pp 106-112, April 1983.
17. Cernocky, E. P. "An Examination of Four Viscoplastic Constitutive Theories in Uniaxial Monotonic Loading," International Journal of Solids and Structures, Vol. 18, No. 11, pp 989-1005, 1982.
18. Merzer, A. and Bodner, S. R. "Analytical and Computational Representation of High Rate of Straining Behavior," Institute of Physics Conference Series No. 47, Chapter 1, 1979.
19. Merzer, A. and Bodner, S. R. "Analytical Formulation of a Rate and Temperature Dependent Stress-Strain Relation," Journal of Engineering Materials and Technology, Vol. 101, pp 254-257, July 1979.
20. Bodner, S. R. "Evolution Equations for Anisotropic Hardening and Damage of Elastic-Viscoplastic Materials," prepared for presentation at the Symposium on "Plasticity Today," Udine, Italy, June 1983; to appear in the Proceedings of the Symposium.
21. Bodner, S. R. "Constitutive Equations for Dynamic Material Behavior," Mechanical Behavior of Materials Under Dynamic Loads, ed. by U.S. Lindholm, Springer-Verlag New York Inc., 1968.
22. Bodner, S. R. and Partom, Y. "Constitutive Equations for Elastic-Viscoplastic Strain-Hardening Materials," Journal of Applied Mechanics, Vol. 42, pp 385-389, 1975.
23. Lin, H. C. and Wu, H. C. "Strain Rate Effect in the Endochronic Theory of Viscoplasticity," Journal of Applied Mechanics, Vol. 43, pp 92-96, 1976.
24. Cernocky, E. P. and Krempl, E. "A Non-Linear Uniaxial Integral Constitutive Equation Incorporating Rate Effects, Creep and Relaxation," International Journal of Non-Linear Mechanics, Vol. 14, pp 183-203, 1979.
25. Wu, H. C. and Yip, M. C. "Strain Rate and Strain Rate History Effects on the Dynamic Behavior of Metallic Materials," International Journal of Solids and Structures, Vol. 16, pp 515-536, 1980.

26. Bodner, S. R. and Partom, Y. "A Large Deformation Elastic-Viscoplastic Analysis of a Thick-Walled Spherical Shell," Journal of Applied Mechanics, Vol. 39., pp 751-757, 1972.
27. Malvern, L. E. "The Propagation of Longitudinal Waves of Plastic Deformation in a Bar of Material Exhibiting a Strain Rate Effect," Journal of Applied Mechanics, Vol. 18, pp 203-208, 1951.
28. Perzyna, P. "The Constitutive Equations for Rate Sensitive Plastic Materials," Quarterly of Applied Mathematics, Vol. 20, pp 321-332, 1963.
29. Mendelson, A. Plasticity: Theory and Application, The MacMillan Company, New York, 1968.

VITA

Rebecca L. Beaman was born in Albany, Oregon on 10 May 1957. She graduated from Charles A. Sprague High School in Salem, Oregon in 1975. She received a B.A. in General Science in 1979 from the Honors College of the University of Oregon. In 1980 she joined the Air Force and earned a commission as a second lieutenant through Officer Training School. She then entered the School of Engineering, Air Force Institute of Technology and earned a B.S. in Aeronautical Engineering in 1982. Upon graduation she was assigned to Aeronautical Systems Division as a structural vibration and loads engineer.

Permanent address: 742 Red Hill Dr. SE  
Salem, OR 97302

## REPORT DOCUMENTATION PAGE

1a. REPORT SECURITY CLASSIFICATION <b>UNCLASSIFIED</b>		1b. RESTRICTIVE MARKINGS	
SECURITY CLASSIFICATION AUTHORITY		3. DISTRIBUTION/AVAILABILITY OF REPORT  Approved for public release; distribution unlimited.	
2b. DECLASSIFICATION/DOWNGRADING SCHEDULE		4. PERFORMING ORGANIZATION REPORT NUMBER(S)  AFIT/GAE/AA/84M-1	
4. PERFORMING ORGANIZATION REPORT NUMBER(S)		5. MONITORING ORGANIZATION REPORT NUMBER(S)	
6a. NAME OF PERFORMING ORGANIZATION  School of Engineering	6b. OFFICE SYMBOL (If applicable)  AFIT/EN	7a. NAME OF MONITORING ORGANIZATION	
6c. ADDRESS (City, State and ZIP Code)  Wright-Patterson AFB, Ohio 45433		7b. ADDRESS (City, State and ZIP Code)	
8a. NAME OF FUNDING/SPONSORING ORGANIZATION	8b. OFFICE SYMBOL (If applicable)	9. PROCUREMENT INSTRUMENT IDENTIFICATION NUMBER	
8c. ADDRESS (City, State and ZIP Code)		10. SOURCE OF FUNDING NOS.	
11. TITLE (Include Security Classification)  See Box 19		PROGRAM ELEMENT NO.	TASK NO.
12. PERSONAL AUTHOR(S)  Rebecca L. Beaman, B.A., B.S., 1 Lt, USAF		PROJECT NO.	WORK UNIT NO.
13a. TYPE OF REPORT  MS Thesis	13b. TIME COVERED FROM _____ TO _____	14. DATE OF REPORT (Yr., Mo., Day)  1984 March	15. PAGE COUNT  144
16. SUPPLEMENTARY NOTATION		Approved for public release: LAW AFB 190-17. <i>John Wolaver</i> LYNN E. WOLAVER Dean for Research and Professional Development Air Force Institute of Technology (AFIT) Wright-Patterson AFB OH 45433	
17. COSATI CODES		18. SUBJECT TERMS (Continue on reverse if necessary and identify by block number)	
FIELD	GROUP	Plasticity, Cyclic Loading, Elasto-visco Plasticity.	
11	04		
19. ABSTRACT (Continue on reverse if necessary and identify by block number)			
Title: THE DETERMINATION OF THE BODNER MATERIAL COEFFICIENTS FOR IN 718 AND THEIR EFFECTS ON CYCLIC LOADING			
Thesis Chairman: Dr. Anthony N. Palazotto			
20. DISTRIBUTION/AVAILABILITY OF ABSTRACT  UNCLASSIFIED/UNLIMITED <input checked="" type="checkbox"/> SAME AS RPT. <input type="checkbox"/> DTIC USERS <input type="checkbox"/>		21. ABSTRACT SECURITY CLASSIFICATION  UNCLASSIFIED	
22a. NAME OF RESPONSIBLE INDIVIDUAL  Dr. Anthony N. Palazotto		22b. TELEPHONE NUMBER (Include Area Code)  513-255-3517	22c. OFFICE SYMBOL  AFIT/ENY

Development and use of new materials and technologies for use in high temperature environments are dependent on the availability of a material model appropriate for such applications. The Bodner-Partom constitutive model shows promising flexibility in modeling materials under such conditions. Evaluation of the model's adequacy and range of application has thus far been hampered by a lack of physical understanding of the model's coefficients and the lack of a systematic method for evaluating them.

This study uses experimental data for IN 718 at 1200°F to establish a systematic approach to the evaluation of the Bodner coefficients. Parametric studies were used to develop a comprehensive description of each coefficient and its impact on the material model. A simple extension of the Bodner constitutive equations to model cyclic loading situations was carried out.

Results show that systematic evaluation of the Bodner coefficients from experimental data is achievable although somewhat subjective in nature. Cyclic load studies revealed that the Bodner model is capable of modeling isotropic and directional hardening as well as strain softening.

REPROD

FILMED

MIAMI